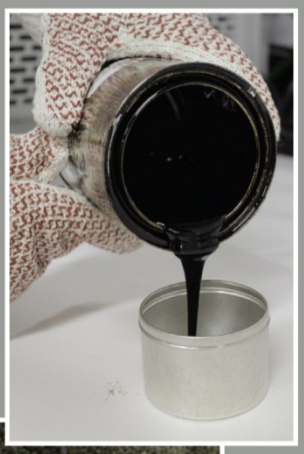

NCAT Report 12-08

FIELD AND LABORATORY STUDY OF HIGH-POLYMER MIXTURES AT THE NCAT TEST TRACK – INTERIM REPORT

By

Dr. David H. Timm
Mary M. Robbins
Dr. J. Richard Willis
Dr. Nam Tran
Adam J. Taylor

August 2012

National Center for Asphalt Technology
NCAT
at AUBURN UNIVERSITY

277 Technology Parkway ■ Auburn, AL 36830

Field and Laboratory Study of High-Polymer Mixtures at the NCAT Test Track

Interim Report

By
Dr. David H. Timm
Mary M. Robbins
Dr. J. Richard Willis
Dr. Nam Tran
Adam J. Taylor

National Center for Asphalt Technology
Auburn University

Sponsored by
Kraton Performance Polymers, Inc.

August 2012

ACKNOWLEDGEMENTS

This project was sponsored by Kraton Performance Polymers, LLC. The project team appreciates and thanks Kraton Performance Polymers, LLC for their sponsorship of this project. Robert Kluttz of Kraton Performance Polymers, LLC deserves special recognition for providing detailed technical and editorial review of this document.

DISCLAIMER

The contents of this report reflect the views of the authors who are responsible for the facts and accuracy of the data presented herein. The contents do not necessarily reflect the official views or policies of Kraton Performance Polymers, LLC. or the National Center for Asphalt Technology, or Auburn University. This report does not constitute a standard, specification, or regulation. Comments contained in this paper related to specific testing equipment and materials should not be considered an endorsement of any commercial product or service; no such endorsement is intended or implied.

TABLE OF CONTENTS

1. INTRODUCTION 1
   1.1. Background 1
   1.2. Objectives and Scope of Work 4
2. INSTRUMENTATION 4
3. MIX DESIGN, CONSTRUCTION AND INSTRUMENTATION INSTALLATION 5
   3.1. Mix Design 6
   3.2. Construction and Instrumentation Installation 7
4. LABORATORY TESTING ON BINDERS AND PLANT PRODUCED MIXTURES 20
   4.1. Compaction of Performance Testing Specimens from Plant-Produced Mixes 20
   4.2. Binder Properties 21
      4.2.1. Performance Grading (AASHTO M 320-10) 21
      4.2.2. Performance Grading (AASHTO MP 19-10) 21
   4.3. Dynamic Modulus Testing 22
   4.4. Beam Fatigue Testing 30
   4.5. Asphalt Pavement Analyzer (APA) Testing 34
   4.6. Flow Number 36
   4.7. Indirect Tension (IDT) Creep Compliance and Strength 38
   4.8. Energy Ratio 40
   4.9. Moisture Susceptibility 41
5. FALLING WEIGHT DEFLECTOMETER TESTING AND BACKCALCULATION 42
6. PAVEMENT RESPONSE MEASUREMENTS 51
   6.1. Seasonal Trends in Pavement Response 53
   6.2. Pavement Response vs. Temperature 56
   6.3. Pavement Responses Normalized to Reference Temperatures 61
      6.3.1. Longitudinal Strain Responses 62
      6.3.2. Transverse Strain Responses 63
      6.3.3. Aggregate Base Vertical Pressure Responses 64
      6.3.4. Subgrade Vertical Pressure Responses 64
   6.4. Pavement Response Over Time at 68F 65
7. PAVEMENT PERFORMANCE 68
8. KEY FINDINGS, CONCLUSIONS AND RECOMMENDATIONS 71

REFERENCES 73

APPENDIX A – MIX DESIGN AND AS BUILT AC PROPERTIES 76

APPENDIX B – SURVEYED PAVEMENT DEPTHS 83

APPENDIX C – BINDER GRADING 85

APPENDIX D – MASTER CURVE DATA 90

LIST OF TABLES

Table 3.1 Mix Design Gradations – Percent Passing Sieve Sizes 7
Table 3.2 Mix Design Parameters.....7
Table 3.3 Random Locations 8
Table 3.4 Subgrade Dry Unit Weight and Moisture Contents.....9
Table 3.5 Aggregate Base Dry Unit Weight and Moisture Contents 12
Table 3.6 Date of Paving 14
Table 3.7 Material Inventory for Laboratory Testing.....14
Table 3.8 Asphalt Concrete Layer Properties – As Built.....16
Table 4.1 Summary of G_{mm} and Laboratory Compaction Temperatures 20
Table 4.2 Grading of Binders.....21
Table 4.3 Non-Recoverable Creep Compliance at Multiple Stress Levels 22
Table 4.4 Requirements for Non-Recoverable Creep Compliance (AASHTO MP 19-10) 22
Table 4.5 Temperatures and Frequencies used for Dynamic Modulus Testing 23
Table 4.6 High Test Temperature for Dynamic Modulus Testing.....23
Table 4.7 Master Curve Equation Variable Descriptions 25
Table 4.8 Master Curve Coefficients – Unconfined 25
Table 4.9 Master Curve Coefficients – 20 psi Confinement 25
Table 4.10 Two-Sample t-test p-values ($\alpha = 0.05$) comparing Kraton Surface Mix to Control Surface Mix Dynamic Modulus – Raw Data.....27
Table 4.11 Two-Sample t-test p-values ($\alpha = 0.05$) comparing Kraton Intermediate/Base Mix to Control Intermediate/Base Mix Dynamic Modulus – Raw Data.....30
Table 4.12 Bending Beam Fatigue Results.....33
Table 4.13 Fatigue Curve Fitting Coefficients (Power Model Form) 34
Table 4.14 Predicted Endurance Limits.....34
Table 4.15 APA Test Results.....35
Table 4.16 Average Measured IDT Strength Data 38
Table 4.17 Failure Time and Critical Temperature 40
Table 4.18 Energy Ratio Test Results.....41
Table 4.19 Summary of TSR Testing 42
Table 5.1 FWD Sensor Spacing.....43
Table 5.2 FWD Drop Heights and Approximate Weights.....43
Table 6.1 Pavement Response vs. Temperature Regression Terms 59
Table 6.2 Predicted Fatigue Life at 68F.....63

LIST OF FIGURES

Figure 1.1 Typical Crack Propagation in a Toughened Composite (Scientific Electronic Library Online, 2010). 1
Figure 1.2 Dispersion of SBS Polymer in Asphalt at Different Loadings……...2
Figure 2.1 Gauge Array 5
Figure 3.1 Cross-Section Design: Materials and Lift Thicknesses....6
Figure 3.2 Random Location and Instrumentation Schematic....8
Figure 3.3 Subgrade Earth Pressure Cell Installation Prior to Final Covering....9
Figure 3.4 Final Survey of Subgrade Earth Pressure Cell 10
Figure 3.5 Subgrade and Aggregate Base....11
Figure 3.6 Surveyed Aggregate Base Thickness 12
Figure 3.7 Gauge Installation. (a) Preparing grid and laying out gauges; (b) Trench preparation; (c) Gauges placed for paving; (d) Placing protective cover material over each gauge; (e) Paving over gauges 13
Figure 3.8 Mixture Sampling for Lab Testing....15
Figure 3.9 N7 Measured and Predicted Cooling Curves (Lifts 1, 2 and 3) 17
Figure 3.10 S9 Measured and Predicted Cooling Curves (Lifts 1, 2 and 3)....17
Figure 3.11 Average Lift Thicknesses and Depth of Instrumentation....18
Figure 3.12 Temperature Probe Installation 19
Figure 3.13 Asphalt Strain Gauge Survivability....19
Figure 4.1 IPC Global Asphalt Mixture Performance Tester 23
Figure 4.2 Confined Dynamic Modulus Testing Results – 9.5 mm NMAS Mixtures 26
Figure 4.3 Unconfined Dynamic Modulus Testing Results – 9.5 mm NMAS Mixtures 27
Figure 4.4 Confined Dynamic Modulus Testing Results – 19 mm NMAS Mixtures 28
Figure 4.5 Unconfined Dynamic Modulus Testing Results – 19 mm NMAS Mixtures 29
Figure 4.6 Kneading Beam Compactor 31
Figure 4.7 IPC Global Beam Fatigue Testing Apparatus 31
Figure 4.8 Comparison of Fatigue Resistance for Mixtures....33
Figure 4.9 Asphalt Pavement Analyzer 35
Figure 4.10 Rate of Rutting Plot....36
Figure 4.11 Flow Number Test Results....37
Figure 4.12 Indirect Tension Critical Analysis Data 40
Figure 5.1 Dynatest Model 8000 FWD....43
Figure 5.2 Backcalculated AC Modulus vs. Date (Section-Wide Average)....44
Figure 5.3 Backcalculated Granular Base Modulus vs. Date (Section-Wide Average) 45
Figure 5.4 Backcalculated Subgrade Soil Modulus vs. Date (Section-Wide Average)....45
Figure 5.5 Backcalculated AC Modulus vs. Mid-Depth Temperature (RMSE<3%)....47
Figure 5.6 N7 Backcalculated AC Modulus vs. Mid-Depth Temperature RMSE Comparison....48
Figure 5.7 Backcalculated AC Modulus Corrected to Reference Temperatures....49
Figure 5.8 Backcalculated AC Modulus vs. Date at 68^{o}F (RMSE < 3%) 50

Figure 5.9 Backcalculated AC Modulus (N7) vs. Date at 68°F (No RMSE Restriction).....51
Figure 6.1 DaDISP Screen Capture of Pressure Measurements for Truck Pass.....52
Figure 6.2 DaDISP Screen Capture of Longitudinal Strain Measurements 53
Figure 6.3 DaDISP Screen Capture of Transverse Strain Measurements 53
Figure 6.4 Longitudinal Microstrain Under Single Axles 54
Figure 6.5 Transverse Microstrain Under Single Axles 55
Figure 6.6 Aggregate Base Pressure Under Single Axles.....55
Figure 6.7 Subgrade Pressure Under Single Axles.....56
Figure 6.8 Longitudinal Strain vs. Mid-Depth Temperature Under Single Axles.....57
Figure 6.9 Transverse Strain vs. Mid-Depth Temperature Under Single Axles.....57
Figure 6.10 Base Pressure vs. Mid-Depth Temperature Under Single Axles 58
Figure 6.11 Subgrade Pressure vs. Mid-Depth Temperature Under Single Axles 58
Figure 6.12 Longitudinal Strain vs. Mid-Depth Temperature
Under Single Axles (N7 – 2/17/2010 Cutoff).....59
Figure 6.13 Transverse Strain vs. Mid-Depth Temperature
Under Single Axles (N7 – 2/17/2010 Cutoff).....60
Figure 6.14 Aggregate Base Pressure vs. Mid-Depth Temperature
Under Single Axles (N7 – 2/17/2010 Cutoff).....60
Figure 6.15 Subgrade Pressure vs. Mid-Depth Temperature
Under Single Axles (N7 – 2/17/2010 Cutoff).....61
Figure 6.16 Longitudinal Strain Under Single Axles at Three Reference Temperatures.....62
Figure 6.17 Transverse Strain Under Single Axles at Three Reference Temperatures.....63
Figure 6.18 Base Pressure Under Single Axles at Three Reference Temperatures.....64
Figure 6.19 Subgrade Pressure Under Single Axles at Three Reference Temperatures 65
Figure 6.20 Longitudinal Microstrain Under Single Axles vs. Date at 68F 66
Figure 6.21 Transverse Microstrain Under Single Axles vs. Date at 68F 66
Figure 6.22 Base Pressure Under Single Axles vs. Date at 68F 67
Figure 6.23 Subgrade Pressure Under Single Axles vs. Date at 68F.....68
Figure 7.1 Measured Rut Depths 69
Figure 7.2 Measured IRI.....69
Figure 7.3 Roughness vs. Distance in Kraton Section.....70

1. INTRODUCTION

1.1 Background (excerpt from Timm et al., 2011)

Ever increasing traffic intensities and pavement loadings accompanied by depleted agency budgets demand that pavement structures achieve better performance more efficiently to reach an overall reduced life cycle cost. Polymer-modified asphalt (PMA) is a well-established product for improving the effectiveness of asphalt pavements. In particular, styrene-butadiene-styrene (SBS) polymers are commonly used to improve permanent deformation resistance and durability in wearing courses (von Quintus, 2005; Anderson, 2007). Use of SBS in intermediate and base courses has been limited due partly to the perception that base courses, with narrower temperature spans than surface courses, do not need modification. However, the ability of SBS polymers to resist fatigue cracking could, in theory, be used to reduce the overall cross-section of a flexible pavement. This is of particular importance for perpetual pavements that often feature high-modulus intermediate asphalt layers and fatigue-resistant bottom layers. There is a need for a material that has enhanced fatigue characteristics and can carry load in a more efficient manner through a reduced cross-section.

Thermoplastic rubbers are used in a variety of industries to toughen composites and plastics. The combination of low modulus, high elongation, high tensile strength and high fracture energy that rubbers typically exhibit are excellent for inhibiting crack initiation and propagation (Halper and Holden, 1988). Figure 1.1 depicts a micrograph of a propagating crack in a typical rubber-toughened composite.

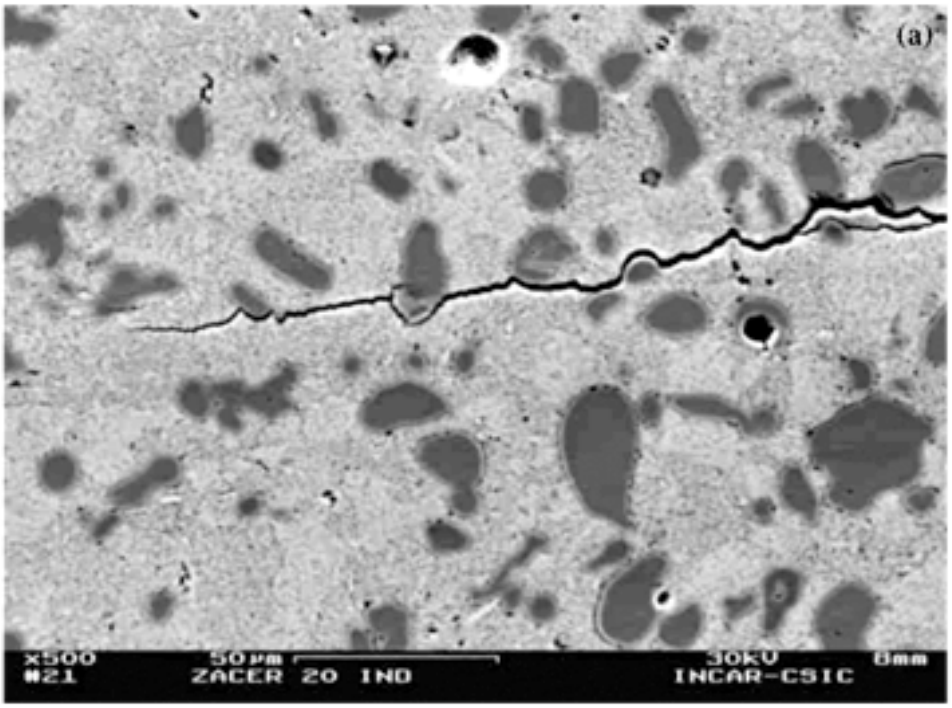

Figure 1.1 Typical Crack Propagation in a Toughened Composite (Scientific Electronic Library Online, 2010).

As a crack propagates through a composite material it follows the path of least resistance avoiding the rubbery tough phase and propagating through the weaker brittle phase. If the tough

rubbery phase now becomes the dominant phase, the propagating crack is trapped or "pinned" and cracking in the composite is greatly reduced. The polymer level needed to achieve this sort of phase inversion in a modified asphalt is a critical question. While an exact answer depends on the details of the physical and chemical interaction between a specific polymer and a specific asphalt, Figure 1.2 gives a general answer.

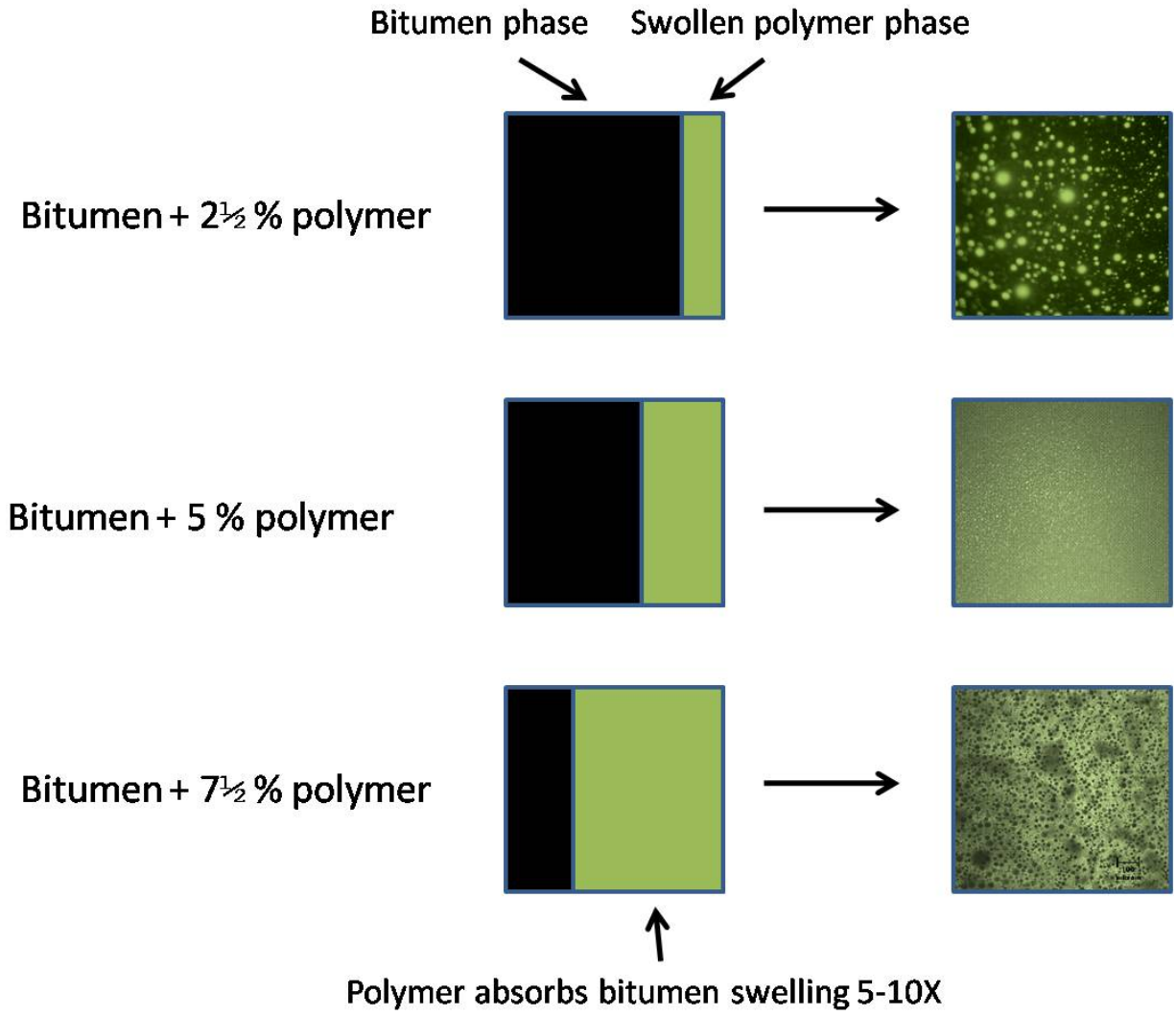

Figure 1.2 Dispersion of SBS Polymer in Asphalt at Different Loadings.

SBS polymers have a strong interaction with bitumen and absorb up to ten times their own volume of less polar asphalt components (Morgan and Mulder, 1995). For example, instead of having an asphalt modified with 4% of SBS, it is more appropriate to consider the modified binder as one that contains 25 – 40% of extended polymer on a volume basis. This is depicted in Figure 1.2 showing the relative proportions of swollen polymer and bitumen and actual micrographs showing the interdispersion of polymer and bitumen phases. At a typical modification polymer loading of 2.5 – 3% it is likely that the extended polymer is not yet continuously present in the binder. It will improve rutting resistance dramatically and it will also

improve the fatigue resistance substantially, but there will be a further, very significant improvement once the extended polymer is a fully continuous phase.

Thus, it is clear that higher polymer loadings have the potential to take cracking resistance to a much higher level than is normally achieved in polymer-modified asphalts. At the same time, one would also expect that the increase in elasticity, while keeping modulus more or less constant, should simultaneously give improvement in permanent deformation resistance. This strategy has been used in roofing applications for decades where SBS "mod bit" roofing membranes typically contain over 10% polymer based on asphalt and the modified asphalt itself functions as a major structural component of the roof assembly.

However, there is a challenge in formulating binders with such high polymer loadings for paving applications. At 7+% polymer in a stiff base asphalt, conventional SBS polymers will either give poor compatibility, poor workability at conventional mixing and compaction conditions, or both. Kraton Performance Polymers, LLC has developed PMA formulations that have a very high polymer content, 7-8%, yet have practical compatibility and viscosity for drum plant or pug mill production and for laydown and compaction. At this content, the polymer forms a continuous network in the asphalt turning it into an elastomer with substantially increased resistance to permanent deformation and fatigue cracking. Four-point bending beam fatigue testing on mixtures with these binders has shown well over an order of magnitude increase in fatigue life (van de Ven et al., 2007; Molenaar et al., 2008; Kluttz et al., 2009). In addition, 3D finite element modeling using the continuum damage Asphalt Concrete Response (ACRe) model developed by TU Delft (Scarpas and Blaauwendraad, 1998; Erkens, 2002) predicts improved resistance to permanent deformation and fatigue damage even with a 40% reduction in thickness (Halper and Holden, 1988; von Quintus, 2005; Anderson, 2007).

While the laboratory and simulation work done on this highly-polymer-modified (HPM) formulation were promising, field trials were necessary to fully understand the in-situ characteristics. From a structural design and analysis perspective, this is needed to evaluate whether HPM behaves like a conventional material under truck and falling weight deflectometer (FWD) loadings so that it can be modeled with conventional approaches (e.g., layered elasticity) within mechanics-based design frameworks. From a performance perspective, field trials were needed to evaluate whether the thickness reduction estimate is viable. To meet these needs, a full-scale experimental HPM section sponsored by Kraton Performance Polymers, LLC was constructed at the National Center for Asphalt Technology (NCAT) Test Track in 2009. A control section was constructed at the same time as part of a pooled fund group experiment. The sections were designed to provide comparisons between the HPM and control materials. The HPM section was designed to be thinner than the control section to investigate whether equal or better performance could be achieved cost effectively using HPM materials.

At the writing of this report in June 2011, approximately 8.9 million standard axle loads had been applied to the sections. Though some of the questions regarding longer-term performance will require further traffic and forensic investigation to fully answer, some of the issues mentioned above can now be directly addressed using data generated during construction, in the laboratory and under dynamic vehicle and falling weight deflectometer (FWD) loading.

1.2 Objectives and Scope of Work

The objective of this report was to document the findings from the Kraton and control sections at the Test Track after 22 months of testing. The findings include data obtained during construction, laboratory-determined mechanistic and performance properties, deflection testing, dynamic strain and pressure measurements in addition to preliminary performance results. This report will also serve as a reference document for subsequent documentation of these sections.

2. INSTRUMENTATION

Central to this investigation were the embedded earth pressure cells, asphalt strain gauges and temperature probes installed at different points in the construction process. The installation of the gauges will be discussed in the following section on construction while the gauges themselves are discussed in this section.

Figure 2.1 illustrates the gauge array used in this investigation. The instruments and arrangement were consistent with previous experiments at the Test Track (Timm et al., 2004; Timm, 2009) to provide continuity and consistency between research cycles. Within each section, an array of twelve asphalt strain gauges was used to capture strain at the bottom of the asphalt concrete. The gauges, manufactured by CTL, were installed such that longitudinal (parallel to traffic) and transverse (perpendicular to traffic) strains could be measured. Two earth pressure cells, manufactured by Geokon, were installed to measure vertical stress at the asphalt concrete/aggregate base interface. Temperature probes, manufactured by Campbell Scientific, were installed just outside the edge stripe to measure temperature at the top, middle and bottom of the asphalt concrete, in addition to 3 inches deep within the aggregate base. Full explanation regarding the sensors and arrangement has been previously documented (Timm, 2009).

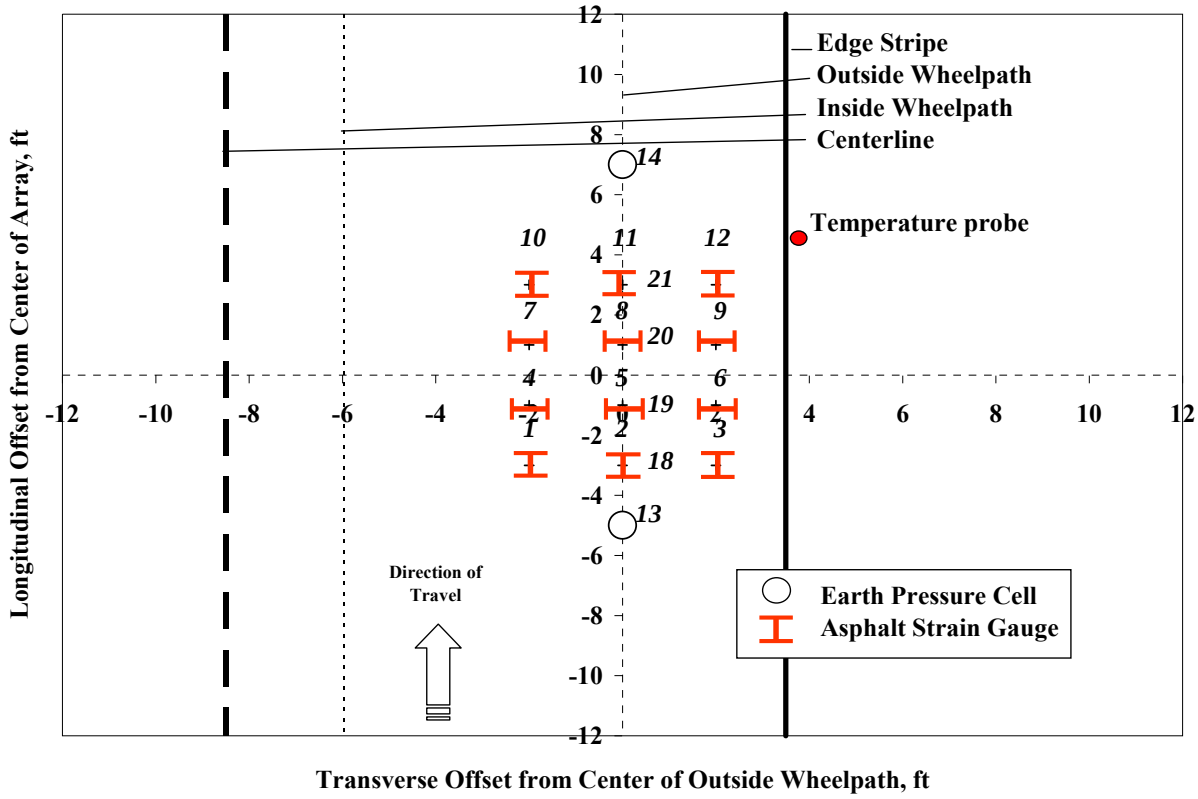

Figure 2.1 Gauge Array

3. MIX DESIGN, CONSTRUCTION AND INSTRUMENTATION INSTALLATION

This section documents the mix design, production and construction of the Kraton section, in addition to the control section, at the Test Track. Where appropriate, gauge installation procedures are also discussed. Figure 3.1 illustrates the as-designed pavement sections. The mix types and lift thicknesses are indicated in Figure 3.1 where the lifts are numbered top-to-bottom (e.g., 1 = surface mix).

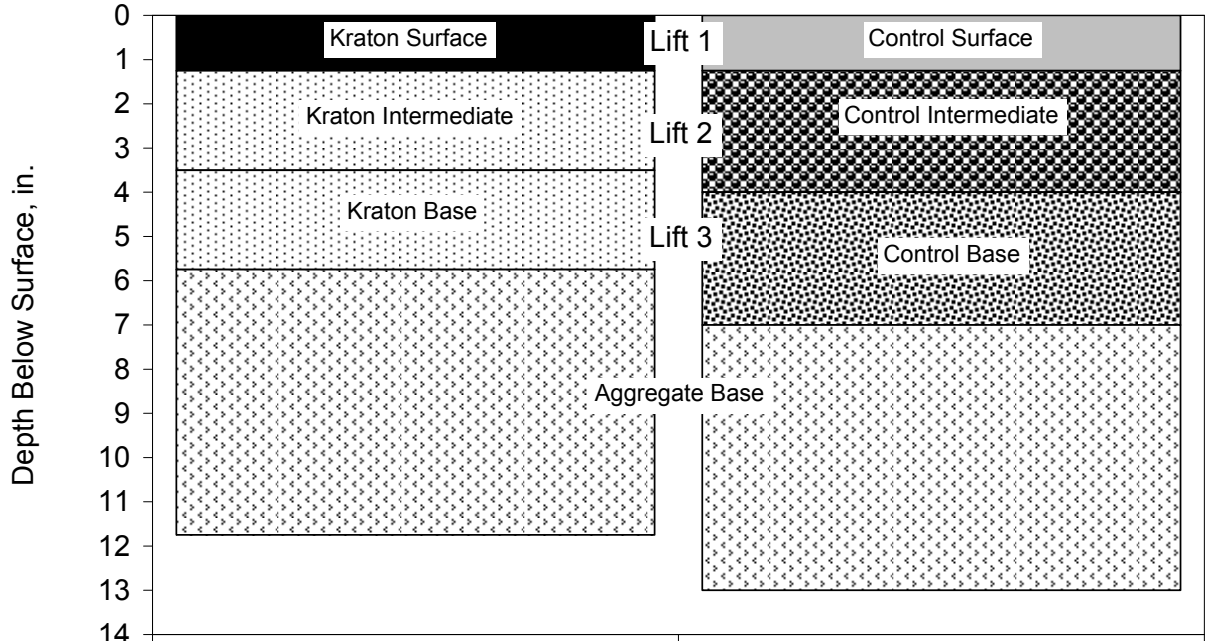

	Kraton	Control
Agg Base	6	6
Lift3	2.25	3
Lift2	2.25	2.75
Lift1	1.25	1.25

Figure 3.1 Cross-Section Design: Materials and Lift Thicknesses

3.1 Mix Design

A summary of the mix design results are provided here with more details available in Appendix A. In subsequent sections, details regarding the as-built properties of the mixtures are provided.

Two design gradations were used in this study. The surface layers utilized a 9.5 mm nominal maximum aggregate size (NMAS) while the intermediate and base mixtures used a 19 mm NMAS gradation. The aggregate gradations were a blend of granite, limestone and sand using locally available materials. Distinct gradations were developed for each control mixture (surface, intermediate and base) to achieve the necessary volumetric targets as the binder grade and nominal maximum aggregate size (NMAS) changed between layers. The Kraton gradations were very similar to the control mixtures. Table 3.1 lists the gradations by mixture type.

Table 3.1 Mix Design Gradations – Percent Passing Sieve Sizes

	Surface Layer		Intermediate Layer	Base Layer	
Sieve Size, mm	Control	Kraton	Control and Kraton	Control	Kraton
25	100	100	100	100	100
19	100	100	93	93	93
12.5	100	100	82	84	82
9.5	100	100	71	73	71
4.75	78	77	52	55	52
2.36	60	60	45	47	45
1.18	46	45	35	36	35
0.6	31	31	24	25	24
0.3	16	16	12	14	12
0.15	10	9	7	8	7
0.075	5.8	5.7	3.9	4.6	3.9

The mixtures were designed using the Superpave gyratory compactor (SGC) with 80 design gyrations. This level of compaction was determined through discussion and consensus with the representative sponsor groups. Table 3.2 lists the pertinent mix design parameters and resulting volumetric properties for each of the five mixtures. The control and Kraton mixtures had very similar volumetric properties despite the large difference in binder performance grade (PG) resulting from the additional polymer in the Kraton mixes.

Table 3.2 Mix Design Parameters

Mixture Type	Control			Kraton	
Lift (1=surface; 2=intermediate, 3=base)	1	2	3	1	2 & 3
Asphalt PG Grade	76-22	76-22	67-22	88-22	88-22
% Polymer Modification	2.8	2.8	0	7.5	7.5
Design Air Voids (VTM), %	4	4	4	4	4
Total Combined Binder (P_b), % wt	5.8	4.7	4.6	5.9	4.6
Effective Binder (P_{be}), %	5.1	4.1	4.1	5.3	4.2
Dust Proportion (DP)	1.1	0.9	1.1	1.1	0.9
Maximum Specific Gravity (G_{mm})	2.483	2.575	2.574	2.474	2.570
Voids in Mineral Aggregate (VMA), %	15.8	13.9	13.9	16.2	14.0
Voids Filled with Asphalt (VFA), %	75	71	71	75	72

3.2 Construction and Instrumentation Installation

At the Test Track, sections are designated according to their respective tangents (North = N; South = S) and section numbers (1 through 13 on each tangent). The Kraton section was placed in N7 while the control section was placed in S9. Section placement was based on availability of sections and for ease of construction.

Within each test section, prior to any construction activities, four random longitudinal stations (RL's) were established with three transverse offsets (outside wheelpath (OWP), inside wheelpath (IWP) and between wheelpath (BWP)) at each RL. These locations were numbered sequentially from 1 through 12 with each location corresponding to a particular RL and offset. Figure 3.2 shows these locations schematically. RL 1, 2 and 3 were randomly selected from 50-ft subsections within the center 150 ft of each section. Transition areas of 25 ft at either end of each section allow for mixture and elevation changes as needed. RL 4 was placed at the center of the instrumentation array within each section. Table 3.3 lists the random location stations for each section. These locations were important during construction in that they were the locations of nuclear density testing, and survey points for thickness. Once traffic began, they served as locations for frequent falling-weight deflectometer (FWD) testing and determination of transverse profiles.

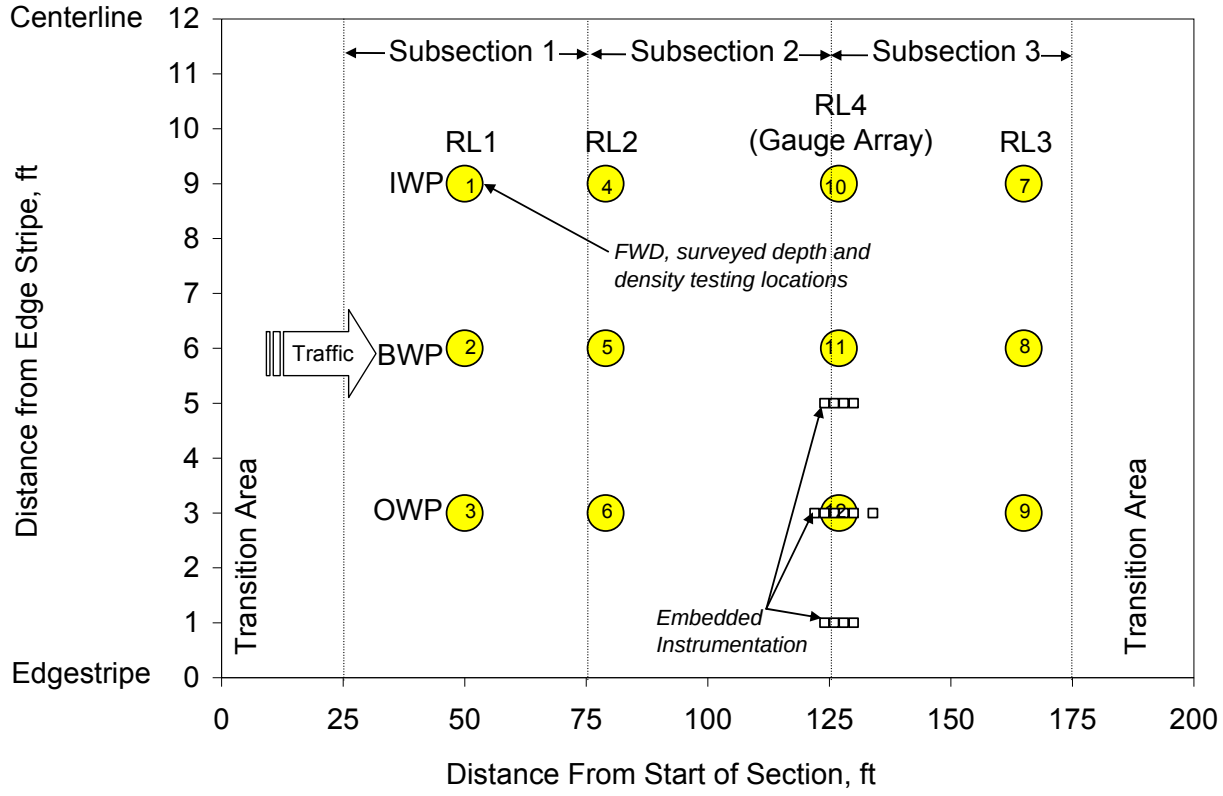

Figure 3.2 Random Location and Instrumentation Schematic

Table 3.3 Random Locations

Random Location	N7 (Kraton)	S9 (Control)
1	37	32
2	70	114
3	114	139
4 (center of gauges)	101	76

In each section, the subgrade was compacted to target density and moisture contents. The subgrade was consistent with the materials used in previous research cycles and has been well-

documented (Taylor and Timm, 2009). The subgrade was classified as an AASHTO A-4(0) metamorphic quartzite soil obtained on-site. Table 3.4 lists the average dry unit weight and moisture content achieved in each section.

Table 3.4 Subgrade Dry Unit Weight and Moisture Contents

Test Section	N7 (Kraton)	S9 (Control)
Average Dry Unit Weight, lb/ft^3	121.8	123.4
Average Moisture Content, %	9.38	9.2

After the subgrade had been brought to proper elevation, density and moisture content, the subgrade earth pressure cells were installed following previously-established procedures (Timm et al., 2004; Timm, 2009). Each gauge was installed such that it was nearly flush with the top of the subgrade, with sieved subgrade material below and on top of the gauge to prevent stress concentrations or damage from stone contact on the plate surface. Figure 3.3 shows an installed plate without the covering material, while Figure 3.4 shows the final surveyed elevation being determined with only the plate face uncovered. After the final survey, cover material was hand-placed on the gauge followed by construction of the aggregate base.

Figure 3.3 Subgrade Earth Pressure Cell Installation Prior to Final Covering

Figure 3.4 Final Survey of Subgrade Earth Pressure Cell

Following earth pressure cell installation, placement of the dense-graded aggregate base commenced. The aggregate base was consistent with that used in previous research cycles and has been well-documented (Taylor and Timm, 2009). The aggregate base was a crushed granite material often used in Alabama by the state department of transportation (ALDOT). Figure 3.5 illustrates the prepared subgrade with a portion of the aggregate base in place. A small amount of aggregate base was hand placed on the earth pressure cell to protect it from construction traffic until all the material was placed and compacted.

Figure 3.5 Subgrade and Aggregate Base

The design called for 6 inches of aggregate base to be placed in each section. Surveyed depths were determined at each of the 12 random locations in each section. Figure 3.6 summarizes the surveyed thicknesses at each location (values are tabulated in Appendix B). The random locations and offsets are noted in the figure and correspond to the numbering scheme in Figure 3.2. Overall, slightly less than 6 inches was placed in each section. The fact that 6 inches was not achieved uniformly is less important than knowing exactly what the thicknesses were for the purposes of mechanistic evaluation and backcalculation of FWD data. Each section was compacted to target density and moisture contents. Table 3.5 summarizes these data for each section.

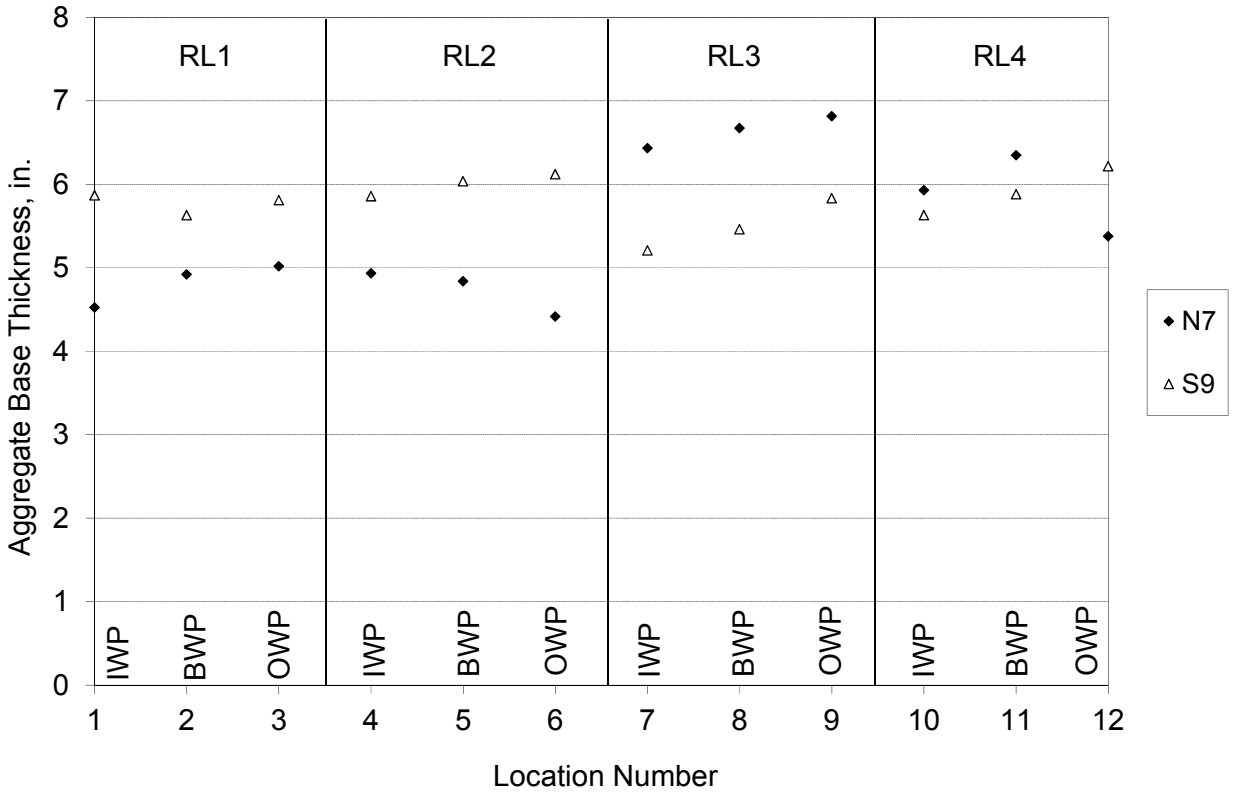

Figure 3.6 Surveyed Aggregate Base Thickness

Table 3.5 Aggregate Base Dry Unit Weight and Moisture Contents

Test Section	N7 (Kraton)	S9 (Control)
Average Dry Unit Weight, lb/ft^3	140.6	140.2
Average Moisture Content, %	4.1	5.0

Once the aggregate base was complete, work began on installing the asphalt strain gauges and aggregate base earth pressure cell. Again, previously-established procedures (Timm et al., 2004; Timm, 2009) were followed in lying out and installing the gauges. The sequence of photos in Figure 3.7 highlights the installation procedure; more detail can be found elsewhere (Timm et al., 2004; Timm, 2009).

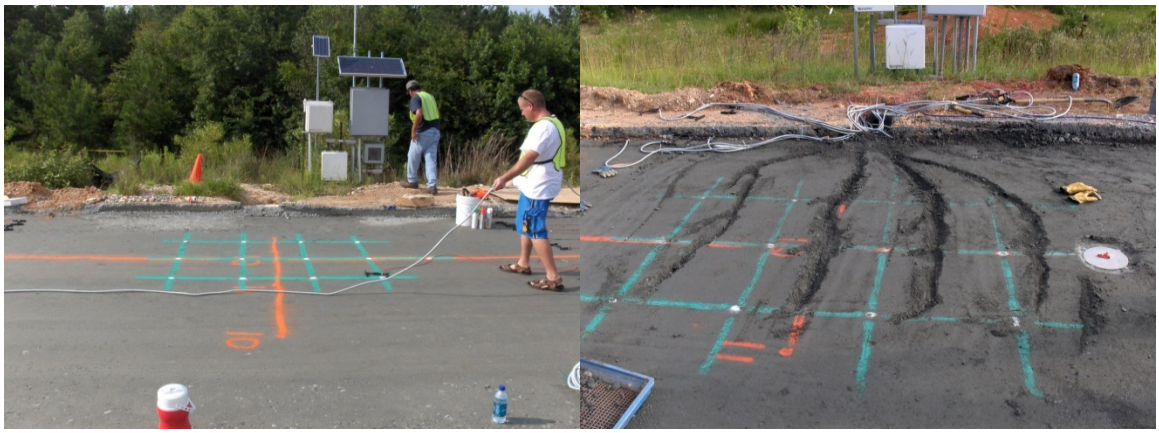

(a) (b)

(c) (d)

(e)

Figure 3.7 Gauge Installation: (a) Preparing grid and laying out gauges; (b) Trench preparation; (c) Gauges placed for paving; (d) Placing protective cover material over each gauge; (e) Paving over gauges

Table 3.6 lists the dates on which each pavement lift was constructed. The lifts are numbered from top to bottom of the pavement cross section. The gaps in paving dates for the control section reflect construction scheduling since many other sections were also paved during this reconstruction cycle.

Table 3.6 Date of Paving

	Test Section	
Asphalt Layer	N7 (Kraton)	S9 (Control)
Lift 1 (surface)	July 22, 2009	July 16, 2009
Lift 2 (intermediate)	July 21, 2009	July 14, 2009
Lift 3 (base)	July 20, 2009	July 3, 2009

Though the primary purpose of this experiment was to validate and understand the field performance of new paving technologies, a secondary objective was to characterize asphalt mixtures using these new technologies in the laboratory. To provide materials for testing in the laboratory, materials were sampled during the paving operation. Before construction, a testing plan was developed to determine the amount of material needed per mix design to complete its laboratory characterization. This testing plan was used to determine the number of 5-gallon buckets to be filled. The testing plan varied depending on the type of mix (base, intermediate or surface mix) and the sponsor's requests for particular tests. Table 3.7 provides the tally of buckets sampled for each mix associated with this project. Upon completion of material sampling, the mix was transferred to an off-site storage facility where it was stored on pallets. Also included in Table 3.7 are the sections and lifts that the bucket samples represented. Each unique binder was also sampled in the field during the paving operation. One 5-gallon bucket of each liquid binder was sampled from the appropriate binder tank at the plant during the mixture production run. At the end of each day, the binder was taken back to the NCAT laboratory for testing purposes.

Table 3.7 Material Inventory for Laboratory Testing

Mixture Description	Kraton Surface	Kraton Base	Control Surface	Control Intermediate	Control Base
Mixture Sampled	N7-1	N7-3	N5-1	S8-2	S8-3
Number of 5-Gallon Buckets	41	35	42	12	30
Section and Lifts Using Mix	N7-1	N7-2 N7-3	S9-1	S9-2	S9-3

Under ideal circumstances, mixture samples would have been taken from a sampling tower from the back of a truck. However, the amount of material needed to completely characterize each mixture made this sampling methodology impossible to achieve. Therefore, another sampling methodology was developed to ensure that mixture quality and quantity were maintained throughout the sampling process. When the mixtures arrived at the Test Track for paving, each truck transferred its material to the material transfer vehicle (MTV). After a sufficient amount of the mixture had been transferred into the paver, the MTV placed additional mix into the back of

a flatbed truck. The mixtures were then taken back to the parking lot behind the Test Track's on-site laboratory for sampling, loading into buckets and long-term storage on pallets (Figure 3.8).

a) Unloading Mix from Truck b) Sampling Mix

c) Loading Mix into Buckets d) Mix Storage

Figure 3.8 Mixture Sampling for Lab Testing

Table 3.8 contains pertinent as-built information for each lift in each section. As documented by Timm et al. (2011), the primary differences between S9 and N7 were the amount of polymer and overall HMA thickness. Section N7 contained 7.5% SBS polymer in each lift while S9 utilized more typical levels of polymer in the upper two lifts with no polymer in the bottom lift. The nominal binder PG grade of the HPM mixtures in N7 was PG 88-22. However, the formulation was designed to meet mixture toughness criteria (or damage resistance) as determined by beam fatigue and finite element modeling (Erkens, 2002; Kluttz et al., 2009) rather than a specific Superpave PG binder grade. The total HMA thickness in N7 was approximately 1.4 inches thinner than S9 to evaluate its ability to carry larger strain levels more efficiently.

The mixing and compaction temperatures listed in Table 3.8 were arrived at through discussions with the polymer supplier, plant personnel and the research team (Timm et al., 2011). Test mix was generated at the plant and test strips were paved to determine optimum compaction temperatures. As shown in Table 3.8, the HPM mixtures required higher mixing and generally higher compaction temperatures due to the increased polymer content.

Table 3.8 Asphalt Concrete Layer Properties – As Built (Timm et al., 2011)

Lift	1-Surface		2-Intermediate		3-Base	
Section	N7	S9	N7	S9	N7	S9
Thickness, in.	1.0	1.2	2.1	2.8	2.5	3.0
NMAS[a], mm	9.5	9.5	19.0	19.0	19.0	19.0
%SBS	7.5	2.8	7.5	2.8	7.5	0.0
PG Grade[b]	88-22	76-22	88-22	76-22	88-22	67-22
Asphalt, %	6.3	6.1	4.6	4.4	4.6	4.7
Air Voids, %	6.3	6.9	7.3	7.2	7.2	7.4
Plant Temp, ^{o}F[c]	345	335	345	335	340	325
Paver Temp, ^{o}F[d]	307	275	286	316	255	254
Comp. Temp, ^{o}F[e]	297	264	247	273	240	243

[a]Nominal Maximum Aggregate Size
[b]Superpave Asphalt Performance Grade
[c]Asphalt plant mixing temperature
[d]Surface temperature directly behind paver
[e]Surface temperature at which compaction began

Of particular interest in Table 3.8 were the measured temperatures behind the paver. In addition to initial temperature, temperatures were monitored over time for each paved lift. The purpose was to evaluate whether the Kraton system behaved in a fundamentally-different manner in terms of cooling rates relative to conventional AC.

The evaluation of temperature was made by measuring surface temperature approximately every three minutes after the mat was placed until final compaction was achieved. Simulations of mat cooling were then conducted using relevant input data such as time of day, paving date and ambient conditions. The simulations were conducted using the MultiCool software which was originally developed in Minnesota (Chadbourn et al., 1998) for cold weather conditions and adapted for multilayer conditions in California (Timm et al., 2001). Since MultiCool uses fundamental heat transfer equations coupled with assumed material properties, significant differences between the measured and predicted cooling rates would signify a material behaving in a fundamentally-different manner or having different heat-transfer properties.

Further details regarding the temperature investigation are documented elsewhere (Vargas and Timm, 2011), while the measured and simulated cooling curves are presented in Figures 3.9 and 3.10 for N7 and S9, respectively. Based on these data, it was concluded that MultiCool provided satisfactory predicted cooling curves for each material tested. In fact, the MultiCool predictions were somewhat better for the Kraton mixtures than the control mixtures. This indicates that the materials are cooling in a similar manner and can be simulated with confidence using the MultiCool software.

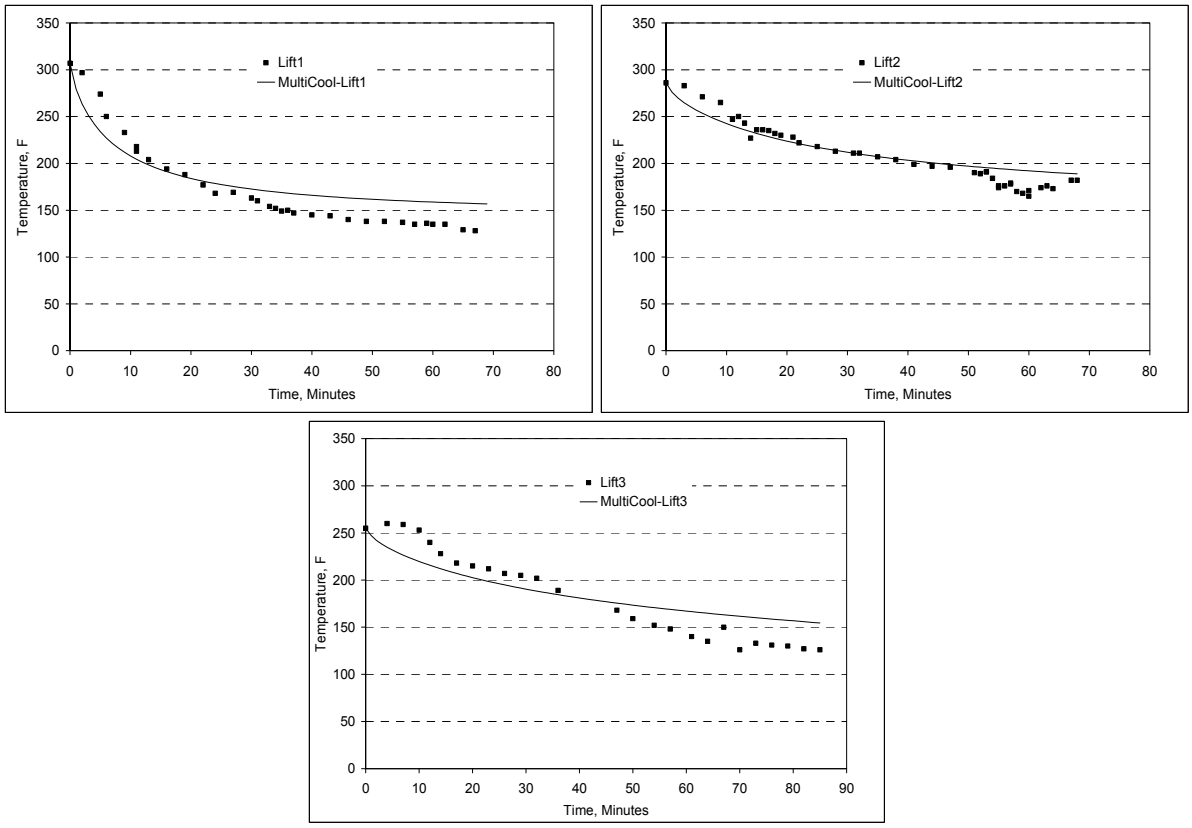

Figure 3.9 N7 (Kraton) Measured and Predicted Cooling Curves (Lifts 1, 2 and 3)

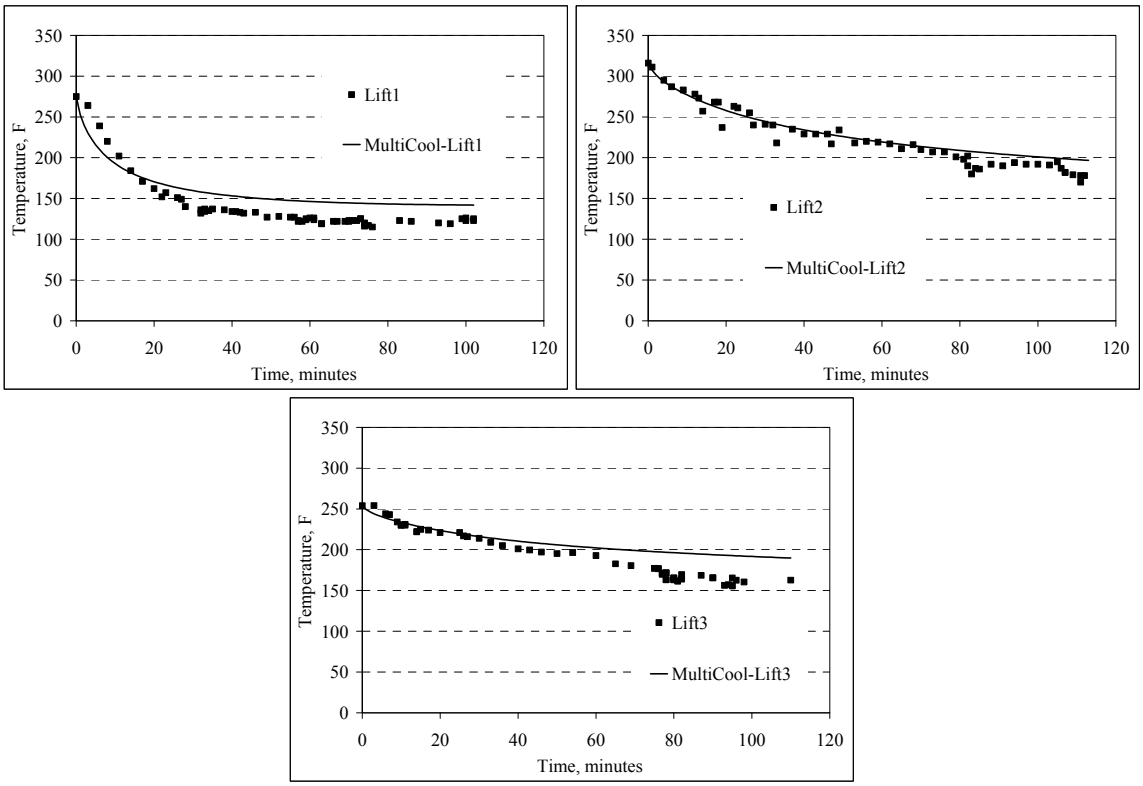

Figure 3.10 S9 (Control) Measured and Predicted Cooling Curves (Lifts 1, 2 and 3)

After paving each lift of AC, depths at the 12 locations (Figure 3.2) within each section were surveyed. This provided very specific lift thickness information in addition to overall pavement depth. Figure 3.11 summarizes these data by providing average depths for each lift of each section. The figure also indicates the three instrument types and their depth of installation. More detailed information is contained in Appendix B. Overall, the sections were constructed very close to their target AC thicknesses (5.75 inches for N7; 7 inches for S9).

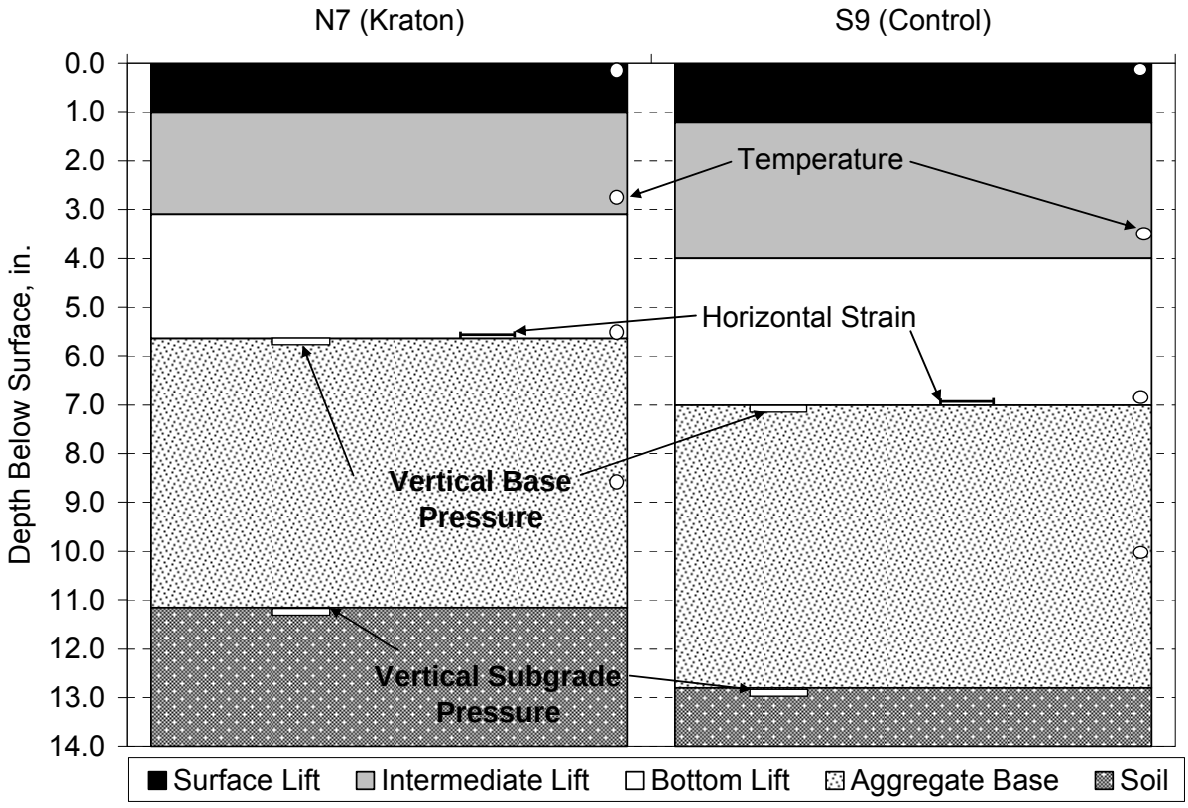

Figure 3.11 Average Lift Thicknesses and Depth of Instrumentation

Soon after paving was complete, temperature probes were installed in each section. The probes were installed as an array of four thermistors to provide temperature at the pavement surface, mid-AC, bottom-AC and 3 inches below AC. Figure 3.12 illustrates two parts of the probe installation. After the vertical hole had been drilled, the probes were coated in roofing asphalt and inserted into the hole. The cable was tacked to the bottom of the slot running to the edge of the pavement, then run through conduit into the data acquisition box.

Figure 3.12 Temperature Probe Installation

At the conclusion of construction, all gauges were checked for functionality. Figure 3.13 shows the survival rate for the strain gauges in each of the sections. The figure indicates that 75% (9 of 12) of the strain gauges survived construction in N7 while 83.3% (10 of 12) gauges survived in the control section (S9). However, when redundancy was considered, each section had at least one gauge survive in each of the three offsets (center-, right-, left-of-wheelpath) and directions (longitudinal and transverse). All the pressure plates survived the construction process.

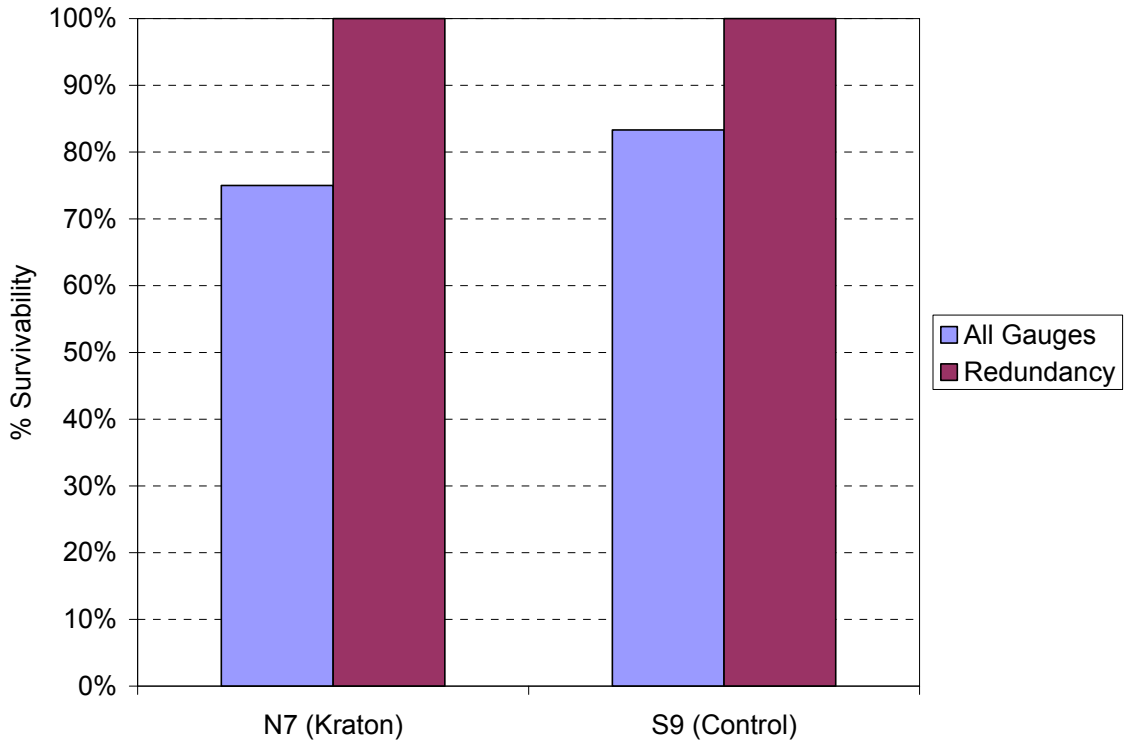

Figure 3.13 Asphalt Strain Gauge Survivability

4. LABORATORY TESTING ON BINDERS AND PLANT PRODUCED MIXTURES

During production of the mixtures, as described previously, samples of binder and mix were obtained for laboratory testing and characterization. The following subsections detail the tests conducted and results for each mixture and binder.

4.1 Compaction of Performance Testing Specimens from Plant-Produced Mixes

For the 2009 research cycle at the Test Track, a large amount of plant-produced mix was sampled in order to perform a wide range of laboratory performance tests. These mixtures were sampled in 5-gallon buckets and sent to the NCAT laboratory for sample fabrication and testing.

The first step in the sample fabrication process was to verify the maximum theoretical specific gravity (G_{mm}) of each mix in accordance with the AASHTO T209-09 procedure. During construction of the Test Track, this test was performed on each mix as the mix was constructed. The results of these tests are collectively termed "QC G_{mm}". The test was also performed on the re-heated mix in the NCAT lab. For each Kraton/control mixture, the QC G_{mm} value and the NCAT lab G_{mm} fell within the variability allowed by the multi-laboratory precision statement in section 13 of AASHTO T209-09; hence, the QC G_{mm} value was used for sample fabrication.

A summary of the G_{mm} values used for performance sample fabrication can be found in Table 4.1. The Kraton test section (N7) was constructed in three lifts. The base lift and intermediate lift were constructed from the same 19 mm NMAS mix design. For the purposes of laboratory testing, these mixes were treated as the same. The testing on this mix design was performed on mix sampled from the lower lift (lift 3).

Table 4.1 Summary of G_{mm} and Laboratory Compaction Temperatures

Mix Description	Lab Compaction Temp, F	QC G_{mm}	Lab G_{mm}	G_{mm} Difference	G_{mm} for Lab Samples
Kraton Base and Intermediate	315	2.545	2.535	0.010	2.545
Kraton Surface	315	2.468	2.464	0.004	2.468
Control Base	290	2.540	2.538	0.002	2.540
Control Intermediate	310	2.556	2.543	0.013	2.556
Control Surface	310	2.472	2.464	0.008	2.472

For sample fabrication, the mix was re-heated in the 5-gallon buckets sampled during production at approximately 20°F above the documented lay-down temperature for the Test Track. When the mix was sufficiently workable, the mix was placed in a splitting pan. A quartering device was then used to split out appropriately-sized samples for laboratory testing. The splitting was done in accordance with AASHTO R47-08. The individual samples of mix were then returned to an oven set to 10-20°F above the target compaction temperature. Once a thermometer in the loose mix reached the target compaction temperature, the mix was compacted into the appropriately-sized performance testing sample. No short-term mechanical aging (AASHTO R30-02) was conducted on the plant-produced mixes from the test track since these mixes had already been short-term aged during the production process. More discussion of sample properties will be provided (sample height, target air voids, etc.) when the individual performance tests are discussed. A summary of the target compaction temperatures for this project are provided in Table 4.1.

4.2 Binder Properties

Ideally, all binders were to be sampled at the plant. This was the case for every binder except the virgin asphalt (PG 76-22) used in the surface mixture of S9. The wrong binder was sampled at the plant during construction, so this binder was extracted from the surface mixture and the recovered material was tested. All the binders used in the two sections were tested in the NCAT binder laboratory to determine the performance grade (PG) in accordance with AASHTO M 320-10 and the performance grade using Multiple Stress Creep Recovery (MSCR) in compliance with AASHTO MP 19-10. Testing results are described in the following subsections.

4.2.1 Performance Grading (AASHTO M 320-10)

The binders were tested and graded according to AASHTO M 320-10. Detailed results are presented in Appendix C. Table 4.2 summarizes the true grade and performance grade of each binder. The results confirmed that all the binders used in the construction of the two sections were as specified in the mix designs.

Table 4.2 Grading of Binders

Mixture	True Grade	Performance Grade
All Lifts of N7 (Kraton)	93.5 – 26.4	88 – 22
Base Lift of S9 (Control)	69.5 – 26.0	64 – 22
Intermediate Lift of S9 (Control)	78.6 – 25.5	76 – 22
Surface Lift of S9 (Control)	81.7 – 24.7	76 – 22

Note: The binder used in the base lift of Section S9 was graded as PG 67-22 in the southeast.

It should be noted that while the binder used in N7 had a high temperature performance grade of 88^{o}C and rotational viscosity of 3.6 Pa·S, its workability and compactability were similar to those of a PG 76-22 binder both in the laboratory and in the field.

4.2.2 Performance Grading (AASHTO MP 19-10)

To determine the performance grade in accordance with AASHTO M 19-10, the MSCR test (AASHTO TP 70-09) was conducted at 64^{o}C, which was determined based on the average 7-day maximum pavement design temperature for the Test Track location. The MCSR results were used to determine the non-recoverable creep compliance for all the binders. The same rolling thin film oven (RTFO) aged specimen utilized in the Dynamic Shear Rheometer (DSR) test according to AASHTO T 315-10 was also used in the MSCR test. Table 4.3 summarizes the MSCR testing results. Table 4.4 shows the acceptable non-recoverable creep compliance at 3.2 kPa and percent differences for varying levels of traffic as specified in AASHTO MP 19-10. Based on the MSCR test results, the virgin binders used in the three layers of Section S9 were graded as PG 64-22 "H". According to AASHTO MP 19-10, high grade "H" is for traffic levels of 10 to 30 million ESALs or slow moving traffic (20 to 70 km/h). The highly polymer-modified binder used in Section N7 was not graded because the percent difference in non-recoverable creep compliance between 0.1 kPa and 3.2 kPa (J_{nrdiff}) was greater than the maximum J_{nrdiff} specified in AASHTO MP 19-10.

Table 4.3 Non-Recoverable Creep Compliance at Multiple Stress Levels

Mixture	Test Temperature	$J_{nr0.1}$ (kPa^{-1})	$J_{nr3.2}$ (kPa^{-1})	J_{nrdiff} (%)	Performance Grade
All Lifts of N7	64°C	0.004	0.013	200.7	Not Graded
Base Lift of S9	64°C	1.68	1.95	16.1	64-22 H
Intermediate Lift of S9	64°C	0.84	1.15	36.9	64-22 H
Surface Lift of S9	64°C	0.98	1.37	39.8	64-22 H

Note: Jnr0.1 = average non-recoverable creep compliance at 0.1 kPa;
Jnr3.2 = average non-recoverable creep compliance at 3.2 kPa;
Jnrdiff = percent difference in non-recoverable creep compliance between 0.1 kPa and 3.2 kPa.

Table 4.4 Requirements for Non-Recoverable Creep Compliance (AASHTO MP 19-10)

Traffic Level	Max $J_{nr3.2}$ (kPa^{-1})	Max J_{nrdiff} (%)
Standard Traffic "S" Grade	4.0	75
Heavy Traffic "H" Grade	2.0	75
Very Heavy Traffic "V" Grade	1.0	75
Extremely Heavy Traffic "E" Grade	0.5	75

Note: The specified test temperature is based on the average 7-day maximum pavement design temperature.

4.3 Dynamic Modulus Testing

Dynamic modulus testing was performed for each of the plant-produced mix types placed during the 2009 Test Track research cycle. Due to sampling limitations, if a particular mix design was placed in multiple lifts or sections, this mix was only sampled one time and tested as representative of that mix type.

The samples for this testing were prepared in accordance with AASHTO PP 60-09. For each mix, three samples were compacted to a height of 170 mm and a diameter of 150 mm and then cut and cored to 150 mm high and 100 mm in diameter. All the specimens were prepared to meet the tolerances allowed in AASHTO PP 60-09. The target air void level for the compacted samples is not specified in AASHTO PP 60-09. However, the samples were compacted to 7 ± 0.5% air voids, which were selected as a common target air void level for pavements compacted in the field.

Dynamic modulus testing was performed in an IPC Global® Asphalt Mixture Performance Tester (AMPT), shown in Figure 4.1. Dynamic modulus testing was performed to quantify the modulus behavior of the asphalt mixture over a wide range of testing temperatures and loading rates (or frequencies). The temperatures and frequencies used for the Test Track mixes were those recommended in AASHTO PP 61-09. The high test temperature was dependent on the high PG grade of the binder in the mixture. Table 4.5 shows the temperatures and frequencies used, while Table 4.6 shows the selection criteria for the high testing temperature. The two Kraton mix designs (surface and base layer) and the control section intermediate course were tested with a high test temperature of 45°C since they were graded as a PG 76-22 or higher. The control base course using a PG 64-22 binder was tested at 40°C high test temperature. Originally, the control surface course using a PG 76-22 binder was tested with a high test temperature of 45°C. However, due to issues with data quality (deformation drift into tension) the high test temperature was reduced to 40°C, as allowed in AASHTO PP 61-09. This vastly improved the quality of data collected while testing that particular mix.

Figure 4.1 IPC Global Asphalt Mixture Performance Tester

Table 4.5 Temperatures and Frequencies used for Dynamic Modulus Testing

Test Temperature (^{o}C)	Loading Frequencies (Hz)
4	10, 1, 0.1
20	10, 1, 0.1
40 (for PG 64-XX) and 45 (for PG 76-XX and higher)	10, 1, 0.1, 0.01

Table 4.6 High Test Temperature for Dynamic Modulus Testing

High PG Grade of Base Binder	High Test Temperature (^{o}C)
PG 58-XX and lower	35
PG 64-XX and PG 70-XX	40
PG 76-XX and higher	45

Dynamic modulus testing was performed in accordance with AASHTO TP 79-09. This testing was performed both confined and unconfined. The confined testing was conducted at 20 psi confining pressure, and each compacted specimen was tested at all temperatures and frequencies in the confined mode before proceeding with unconfined testing. Test data were screened for data quality in accordance with the limits set in AASHTO TP 79-09. Variability of dynamic modulus values at specific temperatures and frequencies were checked to have a coefficient of variation (COV) at or below 13%. All data were checked for reasonableness as well (reduction in moduli with increasing temperature, slower loading). Data with borderline data quality statistics were evaluated on a case by case basis.

The collected data were used to generate a master curve for each individual mix. The master curve uses the principle of time-temperature superposition to horizontally shift data at multiple temperatures and frequencies to a reference temperature so that the stiffness data can be viewed

without temperature as a variable. This method of analysis allows for visual relative comparisons to be made between multiple mixes. A reference temperature of 20◦C was used for this study.

Generation of the master curve also allows for creation of the dynamic modulus data over the entire range of temperatures and frequencies required for mechanistic-empirical pavement design using the MEPDG. By having an equation for the curve describing the stiffness behavior of the asphalt mix, both interpolated and extrapolated data points at various points along the curve can then be calculated. The temperatures and frequencies needed as an input for the MEPDG are listed in Section 10.6.1 of AASHTO PP 61-09. Also, it must be noted that only unconfined master curve data should be entered into the MEPDG since calibration of the design system was originally based on unconfined master curves.

Data analysis was conducted per the methodology in AASHTO PP 61-09. The general form of the master curve equation is shown as Equation 4.1. As mentioned above, the dynamic modulus data were shifted to a reference temperature. This was done by converting testing frequency to a reduced frequency using the Arrhenius equation (Equation 4.2). Substituting Equation 4.2 into 4.1 yields the final form of the master curve equation, shown as Equation 4.3. The shift factors required at each temperature are given in Equation 4.4 (the right-hand portion of Equation 4.2). The limiting maximum modulus in Equation 4.3 was calculated using the Hirsch Model, shown as Equation 4.5. The P_c term, Equation 4.6, is simply a variable required for Equation 4.5. A limiting binder modulus of 1 GPa was assumed for this equation. Data analysis was performed in the MasterSolver® program developed under the NCHRP 9-29 research project. This program uses non-linear regression to develop the coefficients for the master curve equation. Typically, these curves have an S_e/S_y term of less than 0.05 and an R^2 value of greater than 0.99. Definitions for the variables in Equations 4.1-4.6 are given in Table 4.7.

$$Log|E^*| = \partial + \frac{(Max-\partial)}{1+e^{\beta+\gamma log f_r}} \tag{4.1}$$

$$log f_r = log\ f + \frac{\Delta E_a}{19.14714}\left[\frac{1}{T} - \frac{1}{T_r}\right] \tag{4.2}$$

$$log|E^*| = \partial + \frac{(Max-\partial)}{1+e^{\beta+\gamma\left\{log f + \frac{\Delta E_a}{19.14714}\left[\frac{1}{T}-\frac{1}{T_r}\right]\right\}}} \tag{4.3}$$

$$\log[a(T)] = \frac{\Delta E_a}{19.14714}\left[\frac{1}{T} - \frac{1}{T_r}\right] \tag{4.4}$$

$$|E^*|_{max} = P_c\left[4{,}200{,}000\left(1 - \frac{VMA}{100}\right) + 435{,}000\left(\frac{VFA*VMA}{10{,}000}\right) + \frac{1-P_c}{\frac{\left(1-\frac{VMA}{100}\right)}{4{,}200{,}000} + \frac{VMA}{435{,}000(VFA)}}\right] \tag{4.5}$$

$$P_c = \frac{\left(20+\frac{435{,}000(VFA)}{VMA}\right)^{0.58}}{650+\left(\frac{435{,}000(VFA)}{VMA}\right)^{0.58}} \tag{4.6}$$

Table 4.7 Master Curve Equation Variable Descriptions

Variable	Definition
$\|E^*\|$	Dynamic Modulus, psi
δ,β, and γ	Fitting Parameters
Max	Limiting Maximum Modulus, psi
f_r	Reduced frequency at the reference temperature, Hz
f	The loading frequency at the test temperature, Hz
ΔE_a	Activation Energy (treated as a fitting parameter)
T	Test Temperature, ^oK
T_r	Reference Temperature, ^oK
a(T)	The shift factor at Temperature, T
$\|E^*\|_{max}$	The limiting maximum HMA dynamic modulus, psi
VMA	Voids in Mineral Aggregate, %
VFA	Voids filled with asphalt, %

The dynamic modulus results for both the Kraton and control sections at the Test Track are documented in the following paragraphs. Five plant-produced mix types were tested. It should be noted that the base and intermediate courses for section N7 were from the same 19 mm NMAS mix design. Therefore, for laboratory testing, the base-lift material was sampled and tested as representative of both materials. Appendix D contains the complete dynamic modulus data set that is required for conducting an MEPDG analysis with these mixes. Tables 4.8 and 4.9 show the regression coefficients and fitting statistics for the individual master curves for the unconfined and confined tests, respectively. The fitting statistics for each mix tested (in both a confined and unconfined state) indicate a very high quality of curve fit for both the Kraton and control mixtures. Hence it can be inferred that the high level of polymer modification does not negatively impact the dynamic modulus master curve fitting process.

Table 4.8 Master Curve Coefficients – Unconfined

Mix ID	$\|E^*\|_{max}$, ksi	δ, ksi	β	γ	ΔE_A	R^2	Se/Sy
Surface-Control	3057.15	6.20	-0.799	-0.484	198757.5	0.995	0.050
Surface - Kraton	3069.92	4.77	-1.336	-0.409	212777.7	0.997	0.038
Intermediate-Control	3189.49	8.86	-1.246	-0.472	198827.1	0.997	0.038
Base-Control	3177.54	6.52	-1.086	-0.522	178209.5	0.992	0.063
Intermediate/Base-Kraton	3171.23	8.86	-1.064	-0.504	199864.4	0.998	0.031

Table 4.9 Master Curve Coefficients – 20 psi Confinement

Mix ID	$\|E^*\|_{max}$, ksi	δ, ksi	β	γ	ΔE_A	R^2	Se/Sy
Surface-Control	3057.15	62.92	-0.118	-0.560	191188.3	0.994	0.053
Surface-Kraton	3069.92	61.82	-0.657	-0.467	211724.1	0.997	0.039
Intermediate-Control	3189.49	90.93	-0.491	-0.549	202747.7	0.997	0.039
Base-Control	3177.54	77.56	-0.321	-0.602	179802.0	0.994	0.056
Intermediate/Base-Kraton	3171.23	84.64	-0.311	-0.587	201921.7	0.996	0.043

Figures 4.2 and 4.3 compare the dynamic modulus master curves for the surface mixes (9.5 mm NMAS) for both the confined and unconfined data, respectively. Figures 4.4 and 4.5 compare

the dynamic modulus master curves for the intermediate and base course mixes (19 mm NMAS) for the confined and unconfined data, respectively. Visual comparisons between multiple master curves give a good representation of the relative stiffness of multiple mixes. To supplement this relative ranking, statistical testing was performed on the raw dynamic modulus data to determine if the separation in comparable master curves was or was not statistically significant.

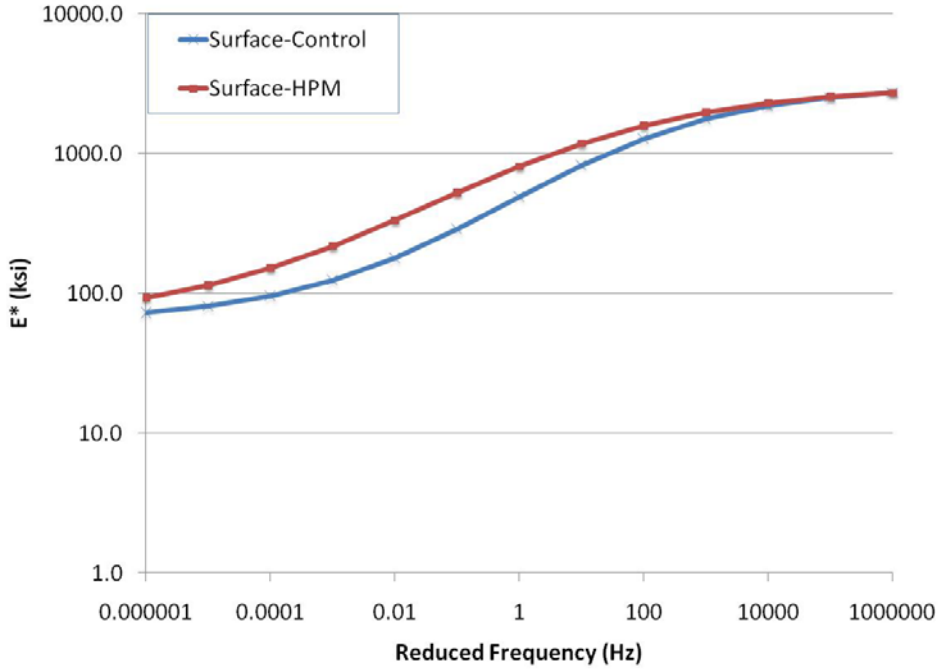

Figure 4.2 Confined Dynamic Modulus Testing Results – 9.5 mm NMAS Mixtures

Visual inspection of the dynamic modulus master curves (Figures 4.2 and 4.3) for the surface mixes shows the Kraton mix to be stiffer than the control surface mix for both the confined and unconfined testing. Visually, the separation in moduli between the two mixes increases from the low temperature and high frequency end of the curve (right side) to the high temperature and low frequency end of the curve (left side). This result was expected given the stiffening effect of the polymer modification in the Kraton mixes. Additionally, the addition of confinement did not have an impact on the relative stiffness ranking of the two mixes but in the magnitude of the dynamic modulus values at the low temperature and high frequency end of the master curve.

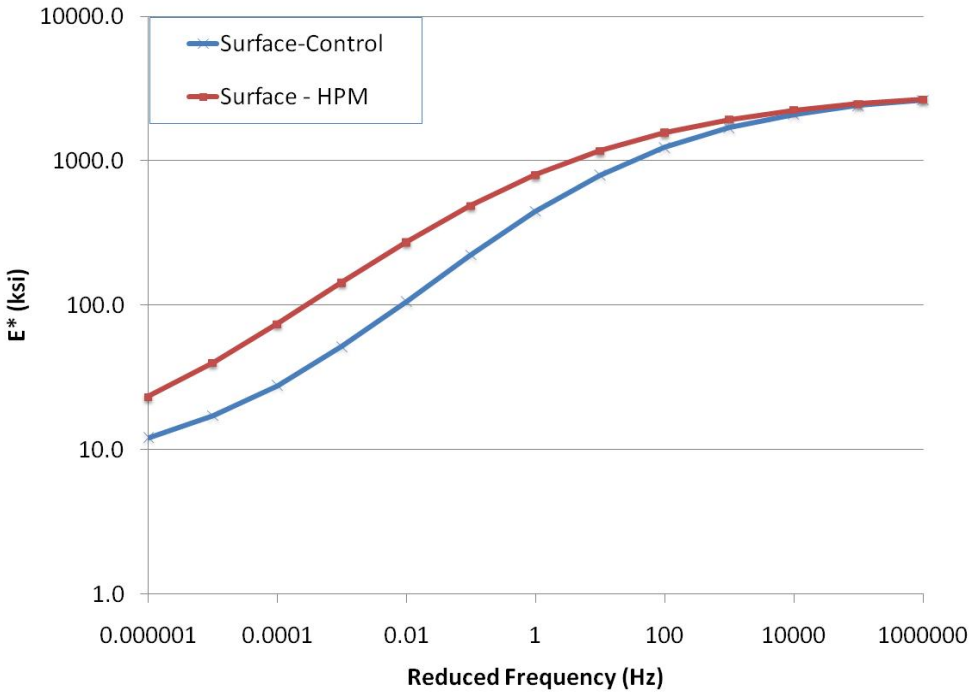

Figure 4.3 Unconfined Dynamic Modulus Testing Results – 9.5 mm NMAS Mixtures

To determine if the separation between the two curves was statistically significant, a two-sample t-test ($\alpha = 0.05$) was performed comparing the test data for the control and Kraton surface mixes. This statistical test compared the data for both the confined and unconfined mixes at the different testing temperatures and frequencies. A summary of the p-values from these t-tests is given in Table 4.10. Recall that the high temperatures selected for dynamic modulus testing were different for the control and Kraton mixtures. Therefore, the 4.0°C and 20.0°C temperatures were used to gage whether or not there was a statistical separation between the two curves. The p-values given in Table 4.10 show a strong evidence of a statistical difference in the dynamic modulus data for the control and Kraton mixes at the low and intermediate test temperatures. As such, this confirms the visual observations in Figures 4.3 and 4.4 that the stiffness of the Kraton surface mix is statistically higher than that of the control surface mix.

Table 4.10 Two-Sample t-test p-values ($\alpha = 0.05$) comparing Kraton Surface Mix to Control Surface Mix Dynamic Modulus – Raw Data

Test Temperature (°C)	Test Frequency (Hz)	p-value of Two Sample t-test	
		Confined (20 psi)	Unconfined (0 psi)
4	0.1	0.0003	0.0012
4	1	0.0005	0.0012
4	10	0.0033	0.0015
20	0.1	0.0023	0.0019
20	1	0.0014	0.0011
20	10	0.0009	0.0008

A similar examination methodology was used to determine if the Kraton intermediate and base course (recall that the same mix design was used in the lower two lifts of section N7, but only the base lift was sampled for testing purposes) provided a tangible stiffness benefit over the control intermediate and base courses. Visual inspection of the confined dynamic modulus testing results (Figure 4.4) appears to suggest that the intermediate control mix has a higher stiffness than the Kraton 19mm NMAS mix and control base mix at the high temperature and low loading frequency portion of the curve. A similar trend is witnessed in the unconfined data (Figure 4.5) in which the Kraton base mix appears to outperform the control base course at the high temperature and low loading frequency portion of the curve.

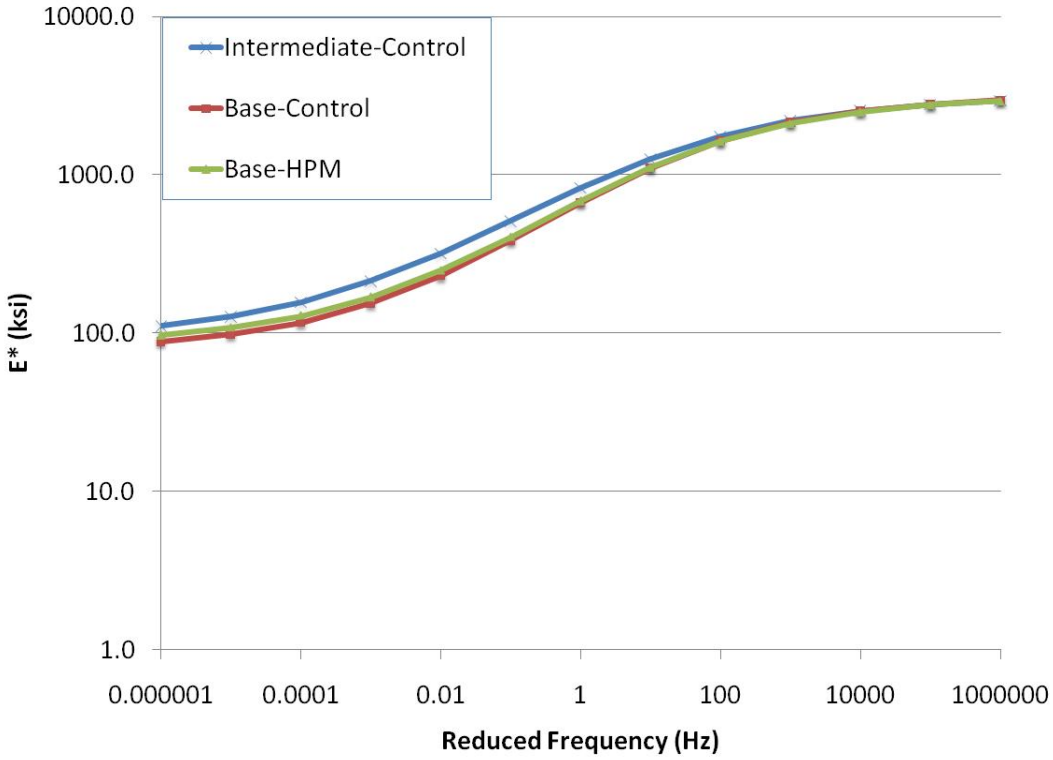

Figure 4.4 Confined Dynamic Modulus Testing Results – 19 mm NMAS Mixtures

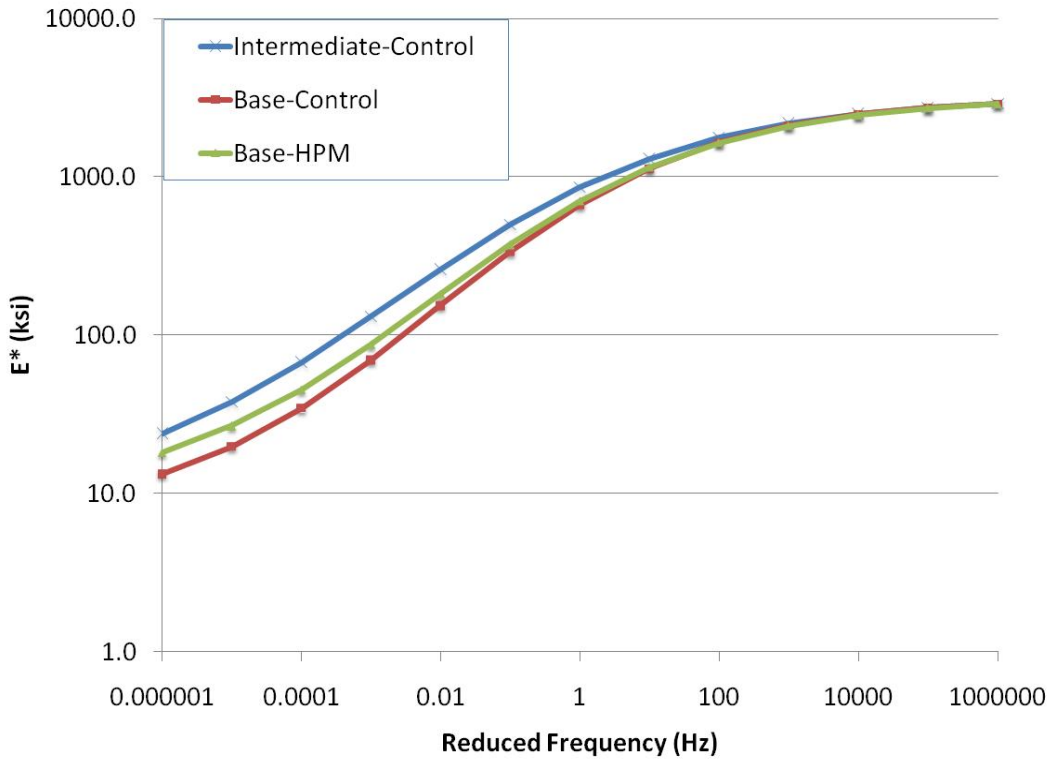

Figure 4.5 Unconfined Dynamic Modulus Testing Results – 19 mm NMAS Mixtures

Table 4.11 shows the results of two-sample t-tests ($\alpha = 0.05$) that compare the Kraton Intermediate/Base mix to both the control intermediate lift and the control base course. The data in Table 4.11 confirms that there is no evidence of a statistical difference between the stiffness of the control base and the Kraton-modified base at the 4.0°C and 20.0°C testing temperatures (again, no comparisons could be made at the high temperature due to testing protocol). The data in Table 4.11 also shows there is a statistical difference between the performance of the Kraton-modified intermediate layer and the control intermediate layer, with the exception of the data collected at 4.0°C and 10 Hz. Therefore, the results show the control intermediate layer had a statistically higher measured stiffness than the Kraton intermediate layer in the dynamic modulus test.

Table 4.11 Two-Sample t-test p-values (α = 0.05) comparing Kraton Intermediate/Base Mix to Control Intermediate/Base Mix Dynamic Modulus – Raw Data

Kraton Intermediate/Base versus Control Base		Two Sample t-test p-value	
Test Temperature (^oC)	Test Frequency (Hz)	Confined (20 psi)	Unconfined
4	0.1	0.161	0.477
4	1	0.166	0.695
4	10	0.099	0.875
20	0.1	0.266	0.079
20	1	0.453	0.106
20	10	0.498	0.141
Kraton Intermediate/Base versus Control Intermediate		Two Sample t-test p-value	
Test Temperature (^oC)	Test Frequency (Hz)	Confined (20 psi)	Unconfined
4	0.1	0.019	0.009
4	1	0.043	0.006
4	10	0.131	0.004
20	0.1	0.002	0.003
20	1	0.005	0.002
20	10	0.018	0.000
45	0.01	0.003	0.016
45	0.1	0.000	0.006
45	1	0.001	0.002
45	10	0.003	0.000

Overall, the collected data suggest that the polymer modification in the Kraton section had a much greater impact on the measured dynamic modulus for the surface courses (9.5mm NMAS) than that of the intermediate and base courses (19 mm). Little effect was seen on the modulus values at the low temperature and high loading frequency portion of the curve. The confinement had significant effects on the modulus magnitudes, particularly at the lower reduced frequencies (i.e., below 1 Hz). At the lowest reduced frequency, there was an approximate order of magnitude increase in the dynamic modulus for all mixtures.

4.4 Beam Fatigue Testing

Bending beam fatigue testing was performed in accordance with AASHTO T 321-07 to determine the fatigue limits of the base mixtures of the Kraton and control sections described in Section 4.1. Nine beam specimens were tested for each mix. Within each set of nine, three beams each were tested at 400 and 800 microstrain. The remaining three beams for the Kraton mixture were tested at 600 microstrain while the three control mixture beams were tested at 200 microstrain.

The specimens were originally compacted in a kneading beam compactor, shown in Figure 4.6, then trimmed to the dimensions of 380 ± 6 mm in length, 63 ± 2 mm in width, and 50 ± 2 mm in

height. The beams were compacted to a target air void level of 7 ± 1.0 percent. Additionally, the orientation in which the beams were compacted (top and bottom) was marked and maintained for the fatigue testing.

Figure 4.6 Kneading Beam Compactor

The beam fatigue apparatus, shown in Figure 4.7, applies haversine loading at a frequency of 10 Hz to maintain a constant level of strain at the bottom of the specimen. Testing was performed at 20 ± 0.5°C. At the beginning of each test, the initial beam stiffness was calculated at 50th cycle. According to AASHTO T 321-07, beam failure was defined as a 50% reduction in beam stiffness. Upon finding the cycles to failure at three different strain magnitudes, the fatigue endurance limit was calculated for each mixture.

Figure 4.7 IPC Global Beam Fatigue Testing Apparatus

Using a proposed procedure developed under NCHRP 9-38 (Prowell et al., 2010), the endurance limit for each mixture was estimated using Equation 4.7 based on a 95 percent lower prediction limit of a linear relationship between the log-log transformation of the strain levels and cycles to failure. All the calculations were conducted using a spreadsheet developed under NCHRP 9-38.

$$\text{Endurance Limit} = \hat{y}_0 - t_\alpha s\sqrt{1+\frac{1}{n}+\frac{(x_0-\bar{x})^2}{S_{xx}}} \quad (4.7)$$

where:

$\hat{y}_o$ = log of the predicted strain level (microstrain)

t_α = value of t distribution for n-2 degrees of freedom = 2.131847 for n = 6 with $\alpha = 0.05$

s = standard error from the regression analysis

n = number of samples = 9

S_{xx} = $\sum_{i=1}^{n}(x_i-\bar{x})^2$ (Note: log of fatigue lives)

x_o = log (50,000,000) = 7.69897

$\bar{x}$ = log of average of the fatigue life results

A summary of the bending beam fatigue test results for the plant-produced base layer mixes is presented in Table 4.12. Figure 4.8 compares the fatigue cracking resistance of the two mixtures determined based on AASHTO T 321-07 results. A power model transfer function ($\varepsilon = \alpha_1 N^{\alpha_2}$) was used to fit the results for each mixture. A summary of the model coefficients and R^2 values is given in Table 4.13. There was a significant difference between the magnitude of the intercept (α_1) and the slope (α_2) between the control mixture and the Kraton mixture. These differences were 48% and 44%, respectively. The R^2 values for each of the mixes were above 0.90, showing a good model fit for the dataset.

Table 4.12 Bending Beam Fatigue Results

Mix	Specimen	Microstrain Level	Number of Cycles to Failure
Control Base	1	800	7,890
	2		17,510
	3		4,260
	4	400	201,060
	5		141,250
	6		216,270
	7	200	6,953,800
	8		5,994,840
	9		2,165,480
Kraton Base	1	800	83,600
	2		20,520
	3		14,230
	4	600	287,290
	5		195,730
	6		186,920
	7	400	11,510,940
	8		1,685,250
	9		4,935,530

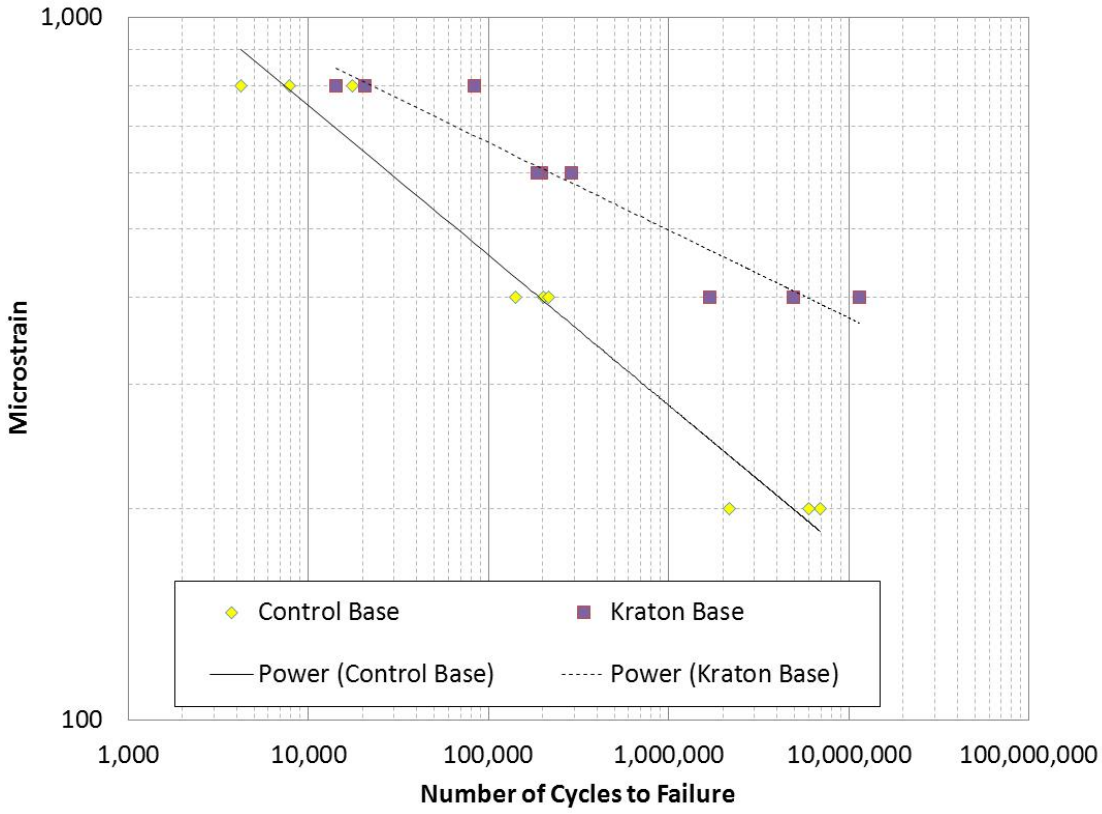

Figure 4.8 Comparison of Fatigue Resistance for Mixtures

Table 4.13 Fatigue Curve Fitting Coefficients (Power Model Form)

Mixture	AASHTO T321-07		
	α_1	α_2	R^2
Control Base	5374.2	-0.214	0.969
Kraton Base	2791.8	-0.125	0.913

The difference between the average fatigue life of the control mixture to that of the Kraton mixture at two strain levels was determined using the failure criteria (50% reduction in beam stiffness) defined by AASHTO 321-07. This information helps evaluate important aspects of the material behavior shown in Figure 4.8 as follows:

- At the highest strain magnitude, the HPM was able to withstand almost 4 times more loading cycles than the control mixture.
- At 400 με, the average fatigue life of the Kraton mixture was much better than the control mixture. The average cycles until failure for the control mixture was 186,193 while the Kraton mixture averaged 6,043,907 loading cycles.

Table 4.14 shows the 95 percent one-sided lower prediction of the endurance limit for each of the two mixes tested in this study based on the number of cycles to failure determined in accordance with AASHTO T 321-07. The procedure for estimating the endurance limit was developed under NCHRP 9-38 (Prowell et al., 2010). Based on the results shown in Table 4.15, the Kraton base mixture had a fatigue endurance limit three times larger than the control mixture.

Table 4.14 Predicted Endurance Limits

Mixture	Endurance Limit (Microstrain)
Control Base	77
Kraton Base	231

4.5 Asphalt Pavement Analyzer (APA) Testing

The rutting susceptibility of the Kraton and control base and surface mixtures were evaluated using the APA equipment shown in Figure 4.9. Often, only surface mixtures are evaluated using the APA. For this experiment, however, it was directed by the sponsor to test the surface mixture, in addition to each of the Kraton mixtures. For comparison purposes, the base control mixture was also evaluated. The intermediate control mix was not sampled in sufficient quantities to allow for APA testing since it was not part of the original APA testing plan.

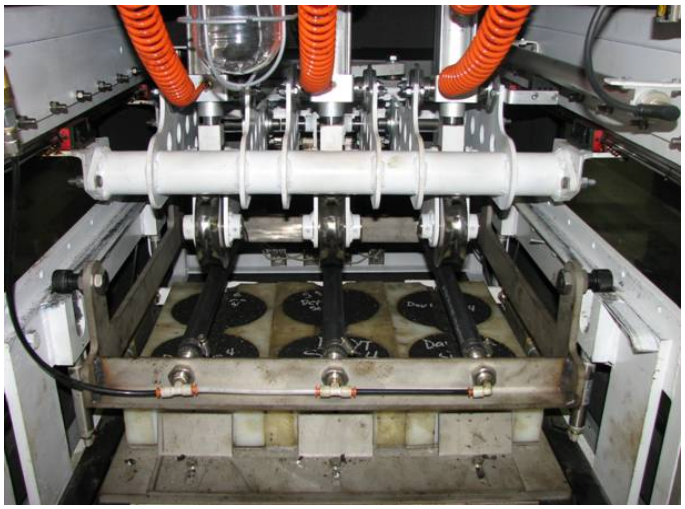

Figure 4.9 Asphalt Pavement Analyzer

Testing was performed in accordance with AASHTO TP 63-09. The samples were prepared to a height of 75 mm and an air void level of 7 ± 0.5 percent. Six replicates were tested for each mix. Typically, these samples are tested at the high binder PG grade. However, for the Test Track a constant testing temperature for all mixes was desired to facilitate relative comparisons between the mixes. Therefore, the samples were tested at a temperature of 64°C (the 98 percent reliability temperature for the high PG grade of the binder for the control base mix). The samples were loaded by a steel wheel (loaded to 100 lbs) resting atop a pneumatic hose pressurized to 100 psi for 8,000 cycles. Manual depth readings were taken at two locations on each sample after 25 loading cycles and at the conclusion of testing to determine the average rut depth (Table 4.15).

Table 4.15 APA Test Results

Mixture	Average Rut Depth, mm	StDev, mm	COV,%	Rate of Secondary Rutting, mm/cycle
Control-Surface	3.07	0.58	19	0.000140
Control-Base	4.15	1.33	32	0.000116
Kraton-Surface	0.62	0.32	52	0.0000267
Kraton-Base	0.86	0.20	23	0.0000280

The APA is typically used as a pass/fail type test to ensure mixtures susceptible to rutting are not placed on heavily trafficked highways. Past research at the Test Track has shown that if a mixture has an average APA rut depth less than 5.5 mm, it should be able to withstand at least 10 million equivalent single axle loads (ESALs) of traffic at the Test Track without accumulating more than 12.5 mm of field rutting. Considering this threshold, a one-sample *t*-test ($\alpha = 0.05$) showed all four mixtures had average rut depths less than the given threshold. Thus, the mixtures are not expected to fail in terms of rutting on the 2009 Test Track.

An ANOVA ($\alpha = 0.05$) was conducted on the data and showed statistical differences between rut depth measurements of the four mixtures. A Tukey-Kramer statistical comparison ($\alpha = 0.05$) was then used to statistically rank or group the mixtures in terms of rutting performance. The statistical analysis placed the four mixtures into two different groups. The best performing group contained both Kraton mixtures while the two control mixtures were more susceptible to rutting.

The APA test results are also appropriate for determining a rate of secondary rutting for each mixture. Rutting typically occurs in three stages: primary, secondary, and tertiary. Primary rutting develops during the early phases of pavement loading due to initial mixture consolidation (i.e., further compaction). Secondary rutting begins after initial consolidation with a gradual nearly linear increase in rut depth. Tertiary rutting represents a shear flow condition. The confined state provided by the molds prevents the mixture from truly ever achieving tertiary flow. Therefore, once the mixture has overcome the stresses induced during primary consolidation, it is possible to determine the rate at which secondary rutting occurs.

The secondary rutting rate was determined in the APA by fitting a power function to the rut depths measured automatically in the APA during testing (Figure 4.10). The primary consolidation of a sample can be seen as the initial steep line when comparing rut depth to the number of cycles; however, as the slope of the line decreases, the samples move into secondary consolidation. The rate of rutting was determined by finding the slope of the power function at the 8000th loading repetition. The results of this analysis are also given in Table 4.16.

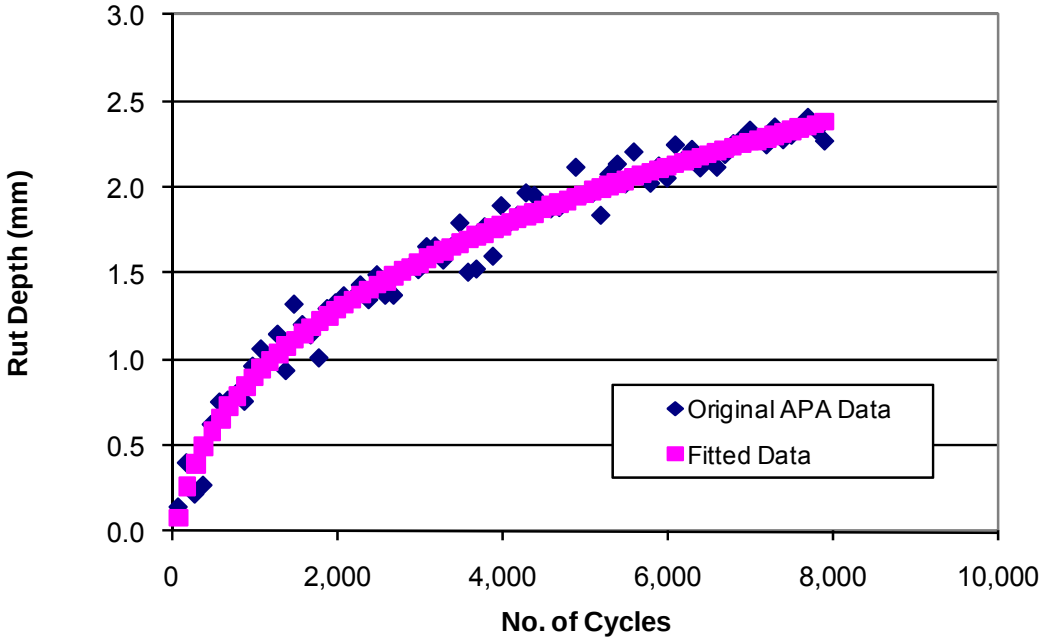

Figure 4.10 Rate of Rutting Plot

Of the four mixtures, the Kraton surface mixture had the best, or smallest, rate of rutting. This mixture also had the least amount of total rutting during the test. The second most resistant mixture in terms of total rutting and rutting rate was the Kraton base mixture. This suggests that using the Kraton modified asphalt binder will allow engineers to design both a flexible and rut resistant asphalt mixture.

4.6 Flow Number

The determination of the Flow Number (F_n) for the Kraton and control surface and base mixtures was performed using an Asphalt Mixture Performance Tester (AMPT). Flow number testing was conducted on new specimens which had not been tested for dynamic modulus. The

specimens were fabricated as described in section 4.3. F_n tests were performed at 59.5°C, which is the LTPPBind version 3.1 50% reliability temperature at the Test Track 20 mm below the surface of the pavement. Additionally, the specimens were tested using a deviator stress of 87 psi without the use of confinement. The tests were terminated when the samples reached 10% axial strain. The Francken model (Biligiri et al., 2007) shown in Equation 4.8 was used to determine tertiary flow. Non-linear regression analysis was used to fit the model to the test data.

$$\varepsilon_p(N) = aN^b + c(e^{dN} - 1) \quad (4.8)$$

where:
ε_p (N) = permanent strain at 'N' cycles
N = number of cycles
a, b, c, d = regression coefficients

Figure 4.11 compares the average flow number values for each of the four mixtures evaluated. One sample of the Kraton surface mixture never achieved tertiary flow; therefore, this test result was removed from the evaluation and considered an outlier. Even with this outlier removed, the Kraton surface mixture had the largest flow number. The second best performance mixture was the Kraton base mixture. With a flow number of 944, its flow number was approximately 5.76 times greater than the control base mixture.

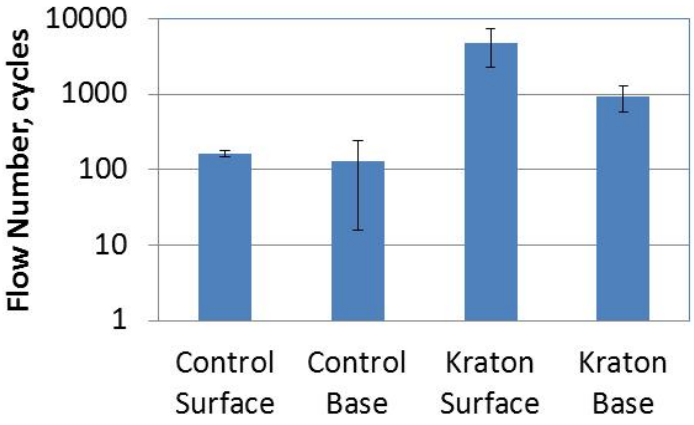

Figure 4.11 Flow Number Test Results

An ANOVA ($\alpha = 0.05$) conducted on the test results showed statistical differences ($p = 0.004$) between the performance of the four mixtures. A Tukey-Kramer analysis ($\alpha = 0.05$) was conducted to group the mixtures based on flow number performance. The Kraton surface mixture had a statistically larger flow number than the three other mixtures ($p = 0.0136$); however, the other three mixtures were grouped together in terms of flow number performance despite the differences in mixture performance. This is likely due to the high variability in the control base mixture flow number results. The COV for this mixture was higher than the recommended COV of 20% in AASHTO TP 79-09. However, inspection of the data set for the three samples yielded no significant outliers.

In summary, the Kraton surface mixture showed the highest resistance to deformation of the four mixtures. While numerical differences were noted between the Kraton base mixture and the two control mixtures, the differences were not statistically significant.

4.7 Indirect Tension (IDT) Creep Compliance and Strength

The critical cracking temperature where the estimated thermal stress exceeds the tested indirect tensile strength of a mixture can be used to characterize the low temperature cracking performance of asphalt mixtures. This type of analysis could be referred to as a "critical temperature analysis." A mixture that exhibited a lower critical cracking temperature than those of other mixtures would have better resistance to thermal cracking. Both surface and base mixtures were evaluated using a critical temperature analysis for this study.

To estimate the thermal stress and measure the tensile strength at failure, the indirect tensile creep compliance and strength tests were conducted for three replicates of each mixture as specified in AASHTO T322-07. A thermal coefficient of each mixture was estimated based on its volumetric properties and typical values for the thermal coefficient of asphalt and aggregate. This computation is explained in more detail below.

The IDT system was used to collect the necessary data for the critical cracking temperature analysis. The testing was conducted using a Material Testing System® (MTS) load frame equipped with an environmental chamber capable of maintaining the low temperature required for this test. Creep compliance at 0°, -10°C, and -20°C and tensile strength at -10°C in accordance with AASHTO T322-07 were measured. These temperatures are specified as a function of the low temperature PG grade of the binder in AASHTO T322-07. The creep test applies a constant load to the asphalt specimen for 100 seconds while the horizontal and vertical strains are measured on each face of the specimen using on-specimen instrumentation.

Four samples were prepared for each mixture. The first sample was used to find a suitable creep load for that particular mixture at each testing temperature. The remaining three samples were used to develop the data set. Samples used for the creep and strength tests were 38 to 50 mm thick and 150 mm in diameter. Samples were prepared to 7 ± 0.5% air voids. Table 4.16 shows the average measured tensile strengths of the tested mixtures.

Table 4.16 Average Measured IDT Strength Data

Indirect Tensile Strength at -10°C (MPa)	Control – Surface	Control – Base	Kraton – Surface	Kraton - Base
	4.71	4.16	4.55	5.27

An ANOVA test ($\alpha = 0.05$) showed statistical differences between the IDT strengths of the four mixtures. A Tukey-Kramer statistical analysis ($\alpha = 0.05$) only grouped two mixtures together in terms of performance: the Kraton and control surface mixtures. The Kraton base mixture had a statistically greater strength than the other three mixtures while the control base mixture was statistically lower than the rest.

Theoretical and experimental results indicate that for linear visco-elastic materials, the effect of time and temperature can be combined into a single parameter through the use of the time-

temperature superposition principle. A creep compliance master curve can be generated by shifting creep compliance data at different temperatures into a single curve at a reference temperature. The reference temperature is typically the lowest creep compliance temperature (-20◦C in this case). The relationship between real time, *t*, reduced time, ζ, and shift factor, a_T, are given in Equation 4.9.

$$\zeta = t/a_T \tag{4.9}$$

An automated procedure to generate the master curve was developed as part of the Strategic Highway Research Program (Buttlar et al., 1998). The system requires the measurement of creep compliance test data at three different test temperatures. The final products of the system are a generalized Maxwell model (or Prony series), which is several Maxwell elements connected in parallel, and temperature shifting factors. The generalized Maxwell model and shifting factors are used for predicting thermal stress development of the asphalt mixture due to changes in temperature.

In addition to thermo-mechanical properties, the thermal coefficient of the asphalt mixture must also be estimated. The linear thermal coefficient, α, was estimated for each mixture using the relationship in Equation 4.10 (Jones et al., 1968).

$$\alpha_{mix} = \frac{VMA * B_{AC} + V_{Agg} * B_{Agg}}{3 * V_{Total}} \tag{4.10}$$

where:
α_{mix} = linear coefficient of thermal contraction of the asphalt mixture (1/°C)
B_{AC} = volumetric coefficient of thermal contraction of the asphalt cement in the solid state (3.45×10^{-4}/°C)
B_{Agg} = volumetric coefficient of thermal contraction of the aggregate (1×10^{-6}/°C)
VMA = percent volume of voids in mineral aggregate
V_{Agg} = percent volume of aggregate in mixture
V_{Total} = 100 percent

Based on the above parameters, the change in thermal stress for each mixture was estimated at the cooling rate of 10°C per hour starting at 20°C. The finite difference solution developed by Soules et al (1987) was used to estimate the thermal stress development based on the Prony Series coefficients and was performed in a MATHCAD program.

A complete description of the thermal stress analysis procedure can be found in Hiltunen and Roque (1994) and Kim et al. (2008). Figure 4.12 shows the thermal stress development as a function of temperature reduction. Table 4.17 shows the critical temperature and time to failure determined at the point where thermal stress exceeds the tensile strength.

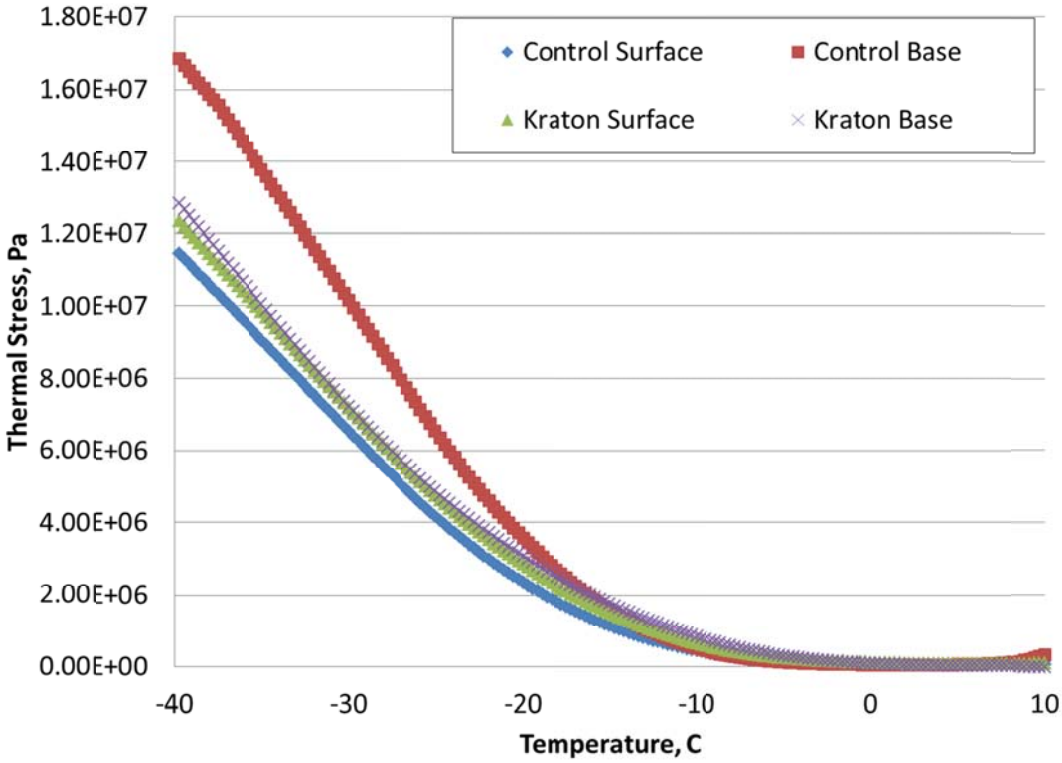

Figure 4.12 Indirect Tension Critical Temperature Analysis Data

Table 4.17 Failure Time and Critical Temperature

Data	Control – Surface	Control – Base	Kraton – Surface	Kraton - Base
Failure Time (hour)	4.64	4.14	4.47	4.61
Failure Temperature (°C)	-26.4	-21.4	-24.7	-26.1

Based on these results, the control base mixture seems to accumulate thermal stress at a faster rate than that of the Kraton base mixture. The opposite is seen in the surface mixtures. These trends are also seen in the critical temperature analysis. The Kraton base mixture has a lower critical temperature than the control base mixture by about 4.5°C. The Kraton control surface layer has a critical temperature 1.7°C higher than the control surface mixture. Only the control base mixture does not have a critical temperature below its low temperature binder performance grade.

In summary, the Kraton binder seemed to improve the low-temperature cracking resistance of the base mixture in tensile strength, critical temperature and failure time. Overall, the poorest performing mixture at low temperatures was the control base mixture. Both of the Kraton mixtures had critical temperatures lower than the required low temperature binder grade.

4.8 Energy Ratio (ER)

The energy ratio was developed to assess a mixture's resistance to top-down or surface cracking (Roque and Buttlar, 1992). To quantify this property, three 150 mm diameter specimens were cut from gyratory compacted samples with 7 ± 0.5% air voids. Resilient modulus, creep

compliance, and tensile strengths for each mixture were determined at 10°C. Equation 4.11 was used to evaluate the surface cracking performance of the control and surface mixtures.

$$ER = \frac{DSCE_f (7.294*10^{-5} * \sigma^{-3.1}(6.36 - S_t) + 2.46*10^{-8})}{m^{2.98} * D_1} \quad (4.11)$$

where:

ER = energy ratio
σ = tensile stress, 150 psi
D_1 and m = resilient modulus power function parameters
S_t = tensile strength, MPa
$DSCE_f$ = dissipated creep strain energy at failure

Table 4.18 summarizes the energy ratio data for the two surface mixtures evaluated. The energy ratio values were indicators of cracking performance of the sections due to the two different binders utilized. The energy ratio is calculated by analyzing multiple test samples to arrive at a singular value.

After analyzing these data, only slight differences between the ER of the Kraton and control mixtures were found. The higher ER for the control surface mixture suggests that it would perform slightly better in terms of surface cracking. However, statistical analyses could not be conducted on the data due to the final results being aggregated to form one value.

Table 4.18 Energy Ratio Test Results

Parameter	Control – Surface	Kraton - Surface
m-value	0.327	0.282
D_1	9.00×10^{-7}	7.08×10^{-7}
S_t (MPa)	2.51	2.51
Mr (GPa)	9.93	9.23
FE (kJ/m^3)	8.1	4.2
$DSCE_{HMA}$ (kJ/m^3)	7.78	3.86
Stress (psi)	150	150
a	4.61×10^{-8}	4.61×10^{-8}
$DSCE_{MIN}$ (kJ/m^3)	0.70	0.35
ER	11.10	10.97

Current recommendations suggest that a minimum ER of 1.95 is needed to resist surface cracking if trafficking is less than 1,000,000 ESALs per year (Roque et al. 2004). While Test Track trafficking is heavier than this level, one can see that these mixtures were more than 5 times greater than the required ER.

4.9 Moisture Susceptibility

The moisture susceptibility of the four mixtures was determined using AASHTO T 283-07. Six specimens of each mix were compacted to a height of 95 mm and an air void level of 7 ± 0.5%. Three conditioned specimens were vacuum saturated to the point at which 70 to 80 percent of the interval voids were filled with water. These samples underwent a freeze-thaw cycle as specified by AASHTO T 283-07.

The indirect tensile strength was determined using a Pine Instruments® Marshall Stability press which loads the samples at a rate of 2 in/min. The IDT strength was then calculated based on the failure loading and measured specimen dimensions. AASHTO M 323-07 recommends a tensile-strength ratio (TSR) value of 0.8 and above for moisture resistant mixtures.

Table 4.19 gives a summary of the results from the TSR testing of the four mixtures. The TSR values for each of the four mixes exceeded the suggested 0.80 lower limit. Table 4.19 also shows the average splitting tensile strengths for both the control and Kraton mixtures. The splitting tensile strengths of both the base and surface Kraton mixtures were greater than those of the control mixtures. There was a slight decrease in TSR values for the Kraton surface mixture when compared to the control surface mixture. The opposite was true for the Kraton base mixture.

Table 4.19 Summary of TSR Testing

Mixture	Treatment	Average Splitting Tensile Strength (psi)	TSR
Control – Surface	Conditioned	137.2	0.94
	Unconditioned	145.4	
Control – Base	Conditioned	116.2	0.86
	Unconditioned	134.6	
Kraton – Surface	Conditioned	197.1	0.89
	Unconditioned	222.1	
Kraton – Base	Conditioned	208.4	0.88
	Unconditioned	237.6	

Statistical analyses were conducted to compare the splitting tensile strengths of the mixtures in both their conditioned and unconditioned states. An ANOVA ($\alpha = 0.05$) showed that for both the conditioned and unconditioned tensile strengths, statistical differences ($p = 0.000$) were found between the mixtures. The Tukey-Kramer statistical analysis ($\alpha = 0.05$) grouped the control mixtures together in terms of splitting tensile strengths in both the conditioned ($p = 0.263$) and unconditioned ($p = 0.836$) states. The Kraton test results were also statistically equivalent for both the conditioned ($p = 0.721$) and unconditioned ($p = 0.646$) strengths. The Tukey-Kramer analyses showed that Kraton mixtures had statistically higher splitting tensile strengths than the control mixtures.

5. FALLING WEIGHT DEFLECTOMETER TESTING AND BACKCALCULATION

The 2009 Test Track was opened to traffic on August 28, 2009. Beginning at that time, the control section was subjected to falling weight deflectometer (FWD) testing three Mondays per month. The Kraton section was tested on corresponding alternating Mondays. This schedule was necessary because of time constraints and the need to test a total of sixteen sections within the structural experiment. The off-Monday within each month was used to perform relative calibration of the FWD equipment. The test data presented below were from August 28, 2009 through June 13, 2011.

The FWD was a Dynatest Model 8000 FWD (Figure 5.1). Nine sensors, as listed in Table 5.1, were used with a 5.91 in. radius split plate. Three replicates at four drop heights, listed in Table 5.2, were applied in each FWD test sequence.

Figure 5.1 Dynatest Model 8000 FWD

Table 5.1 FWD Sensor Spacing

Sensor	Offset, in.
1	0
2	8
3	12
4	18
5	24
6	36
7	48
8	60
9	72

Table 5.2 FWD Drop Heights and Approximate Weights

Drop Height	Approximate Weight, lb	Replicates
1	6,000	3
2	9,000	3
3	12,000	3
4	16,000	3

Testing on a particular date consisted of proceeding around the Test Track at a particular offset (inside wheelpath, between wheelpath or outside wheelpath) stopping at each random location within a section to apply three replicate drops at each of the four drop heights. An entire offset was tested around the track before progressing to the next offset. This process typically consumed six to eight hours on any given test date. The starting offset was randomized week-to-week to be sure that each offset was tested during different times of the day (morning, mid-day, afternoon) over the course of all the test dates. In-situ pavement temperatures were recorded for each section at each offset during testing.

Backcalculation of the deflection basins was conducted using EVERCALC 5.0. For both the Kraton and control sections, a three-layer pavement section (AC over aggregate base over subgrade) was simulated. Surveyed layer thicknesses at each offset and random location were used in the backcalculation process. The data presented below represent those deflection basins for which the root mean square error (RMSE) was below 3%.

Figures 5.2, 5.3 and 5.4 summarize the backcalculated results for the AC, granular base and subgrade, respectively. Data points within each plot represent the average backcalculated modulus across the entire test section at the 9,000-lb load level. The seasonal effects of temperature on AC modulus are clearly evident in Figure 5.2 while the unbound materials were largely unaffected by seasonal temperature changes (Figures 5.3 and 5.4). These results are consistent with previous findings at the Test Track (Timm and Priest, 2006; Taylor and Timm, 2009).

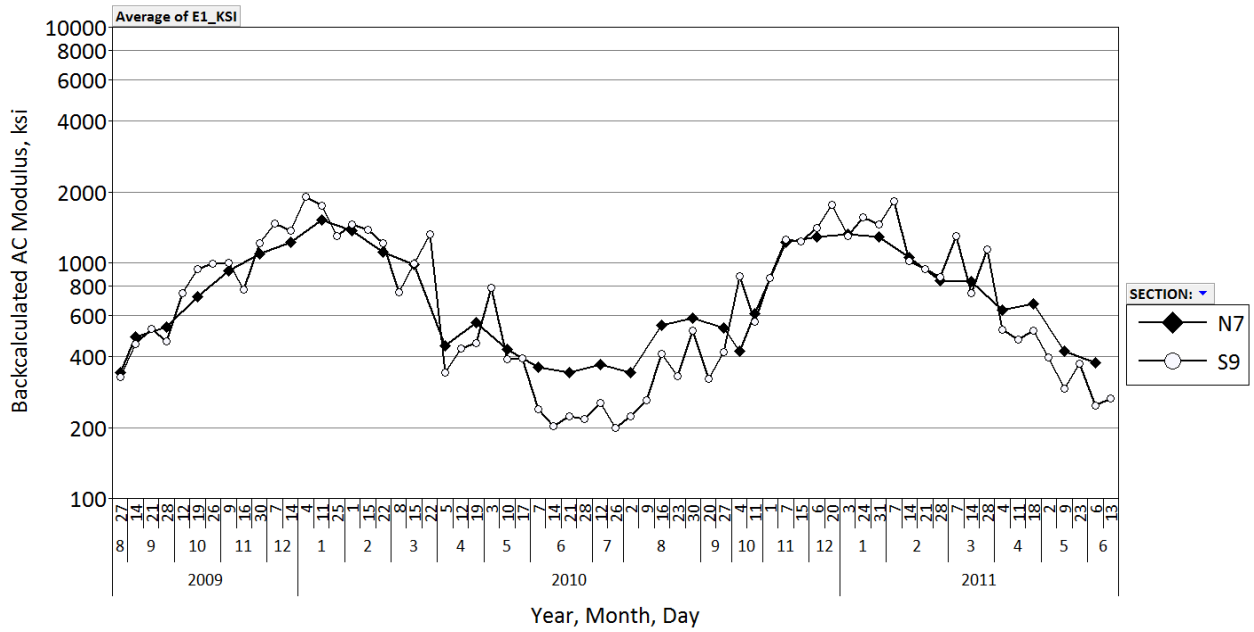

Figure 5.2 Backcalculated AC Modulus vs. Date (Section-Wide Average)

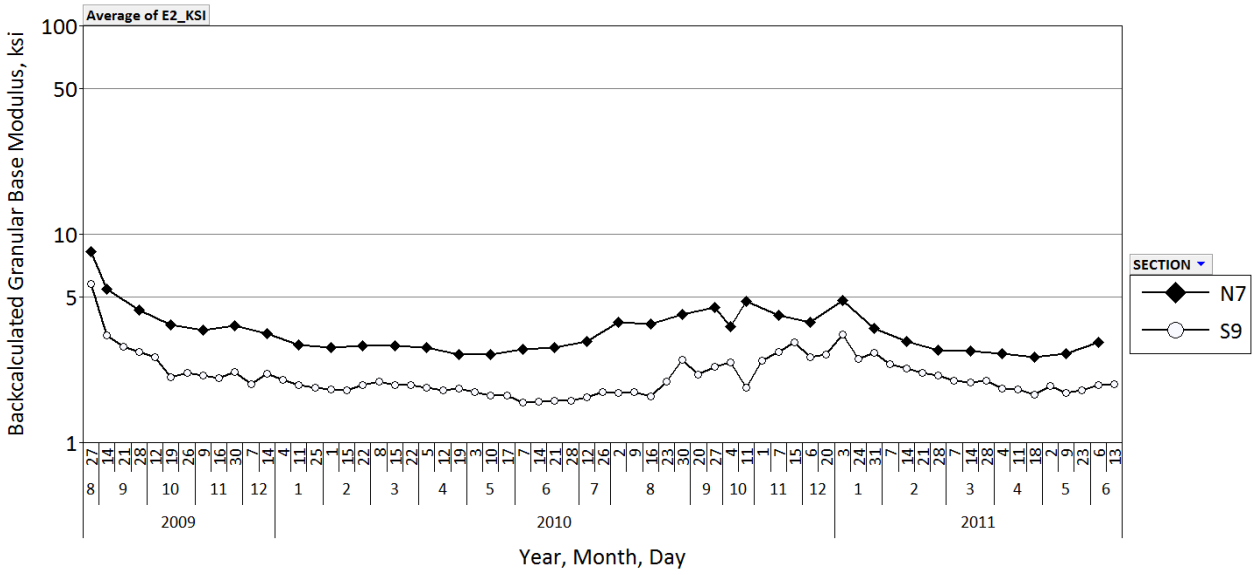

Figure 5.3 Backcalculated Granular Base Modulus vs. Date (Section-Wide Average)

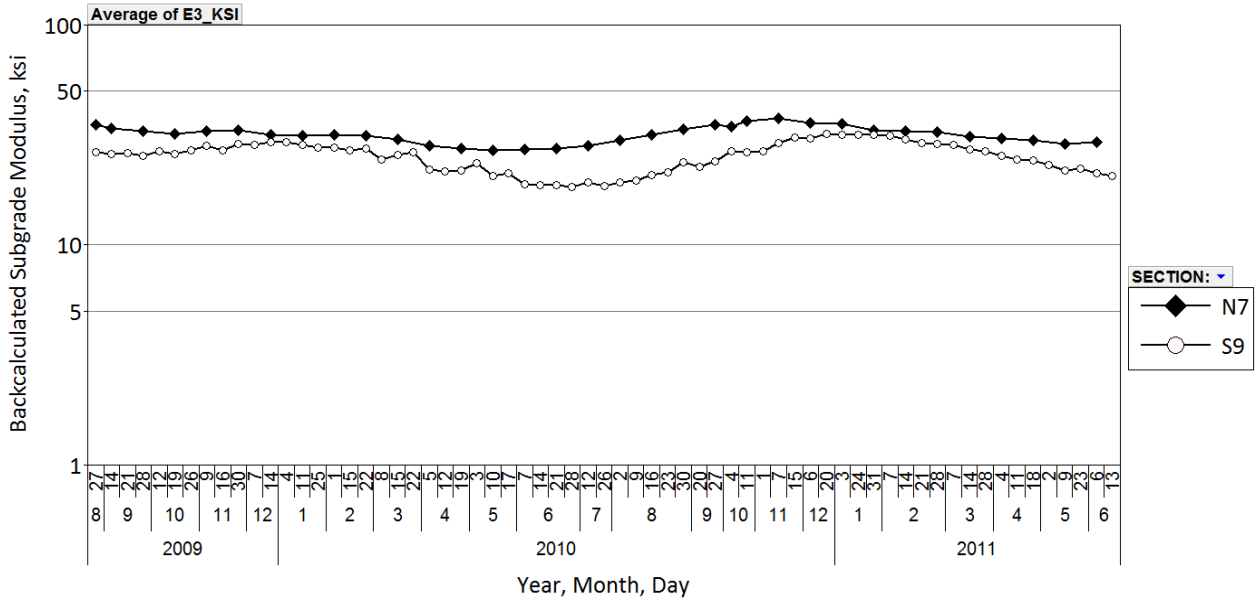

Figure 5.4 Backcalculated Subgrade Soil Modulus vs. Date (Section-Wide Average)

Figure 5.3 shows relatively low granular base moduli in each of the test sections. Though these values may seem artificially low, these are consistent with findings from previous laboratory triaxial resilient modulus testing and values obtained from FWD evaluation at the Test Track on this crushed granite material (Timm and Priest, 2006; Taylor and Timm, 2009). It is also important to note the general decline in aggregate base modulus during the first few months that occurred in both sections. The reason for this is not immediately clear and will be further investigated upon forensic evaluation at the conclusion of traffic. However, it could derive from a possible slip condition between layers. EVERCALC assumes full bond between layers during backcalculation. If there was in-fact slippage occurring between the layers, the result could be an artificially-low granular base modulus.

Figure 5.4 indicates the soil modulus under the Kraton section was somewhat greater than the soil under the control section. This difference likely resulted from the construction history of the respective sections. Section N7 was placed in a test cell used previously for structural evaluations with relatively thin cross-sections. Therefore, in preparation for paving, N7 only required milling through the previous AC and granular base leaving the subgrade largely intact. This subgrade had been quarried and placed in 2003 from the lower cut of the West curve at the Test Track. Section S9 was placed in a cell that required deep milling (26 inches) of the AC followed by placement and compaction of newly quarried material from the upper hill area of the West curve at the Test Track. Slight differences in materials and duration of consolidation could be responsible for the differences in the subgrade moduli. With respect to structural modeling, the fact that they are different is not as critical as accurately quantifying the difference.

At the time of each FWD test, the mid-depth temperatures were recorded by embedded temperature probes in each section. Figure 5.5 plots the backcalculated AC modulus versus mid-depth temperature for each section in addition to best-fit exponential functions. Each data point in Figure 5.5 represents the AC modulus determined from the backcalculation of three deflection basins at the 9,000 lb load level. Therefore, there is more scatter in the data than that shown previously in Figure 5.2. Despite the increased scatter, the change in AC modulus was well explained by change in mid-depth temperature ($R^2 > 0.87$). It is interesting to note that the two regression lines cross at approximately 77^{o}F. At cooler temperatures, the control section has higher modulus. At warmer temperatures, the Kraton section had higher modulus. The effect of temperature on modulus was also less on the Kraton material compared to the control section. Despite these differences, the fact that the materials could be modeled in a very similar fashion leads to the conclusion that the Kraton material can be modeled using conventional approaches (e.g., layered elastic analysis) up to 110^{o}F.

Another interesting observation from Figure 5.5 is that the Kraton data are cut off at 110^{o}F while the control section extends to 120^{o}F. This difference was due to the 3% RMSE restriction imposed on both data sets. The control section had data below 3% RMSE above 110^{o}F while the Kraton section did not. Figure 5.6 shows the Kraton data with and without the 3% RMSE restriction applied. Including data above 3% RMSE effectively increased average backcalculated AC moduli at warmer temperatures. The coefficient of determination, R^2, for the best-fit exponential regression equation also improved slightly when including data above 3% RMSE. The fact that the Kraton section did not have acceptably-low RMSE above 110^{o}F implies it may not follow strict linear-elastic assumptions at very high temperatures.

At cooler temperatures, the control section appeared to have higher backcalculated moduli, while at warmer temperatures the Kraton section had higher backcalculated moduli. Attempting to correlate these results to laboratory-measured E* proves especially challenging. Recall from Figures 4.3 through 4.6 that there were complex relationships between the control and Kraton master curves. The surface control mixture had the lowest laboratory-determined E* in all conditions. However, depending on the portion of the master curve inspected, the sorting of mixtures according to E* magnitude changed. Therefore, a direct comparison between backcalculated moduli and master curves is not practical. It is important to keep in mind that some significant differences exist between laboratory E* testing and backcalculation of dynamic modulus. First, backcalculation considers the entire depth of AC that includes all the AC lifts in

each section while E* testing considers each lift separately. Second, E* tests are conducted at uniform temperatures throughout the specimen while there are thermal gradients throughout the depth of AC in the field. Third, E* tests are conducted at fixed frequencies throughout the specimen. FWD tests in the field are actually tested under a frequency gradient that is derived from a mixture's proximity to the surface. Given these significant testing differences, one could expect to see differences between laboratory and field data.

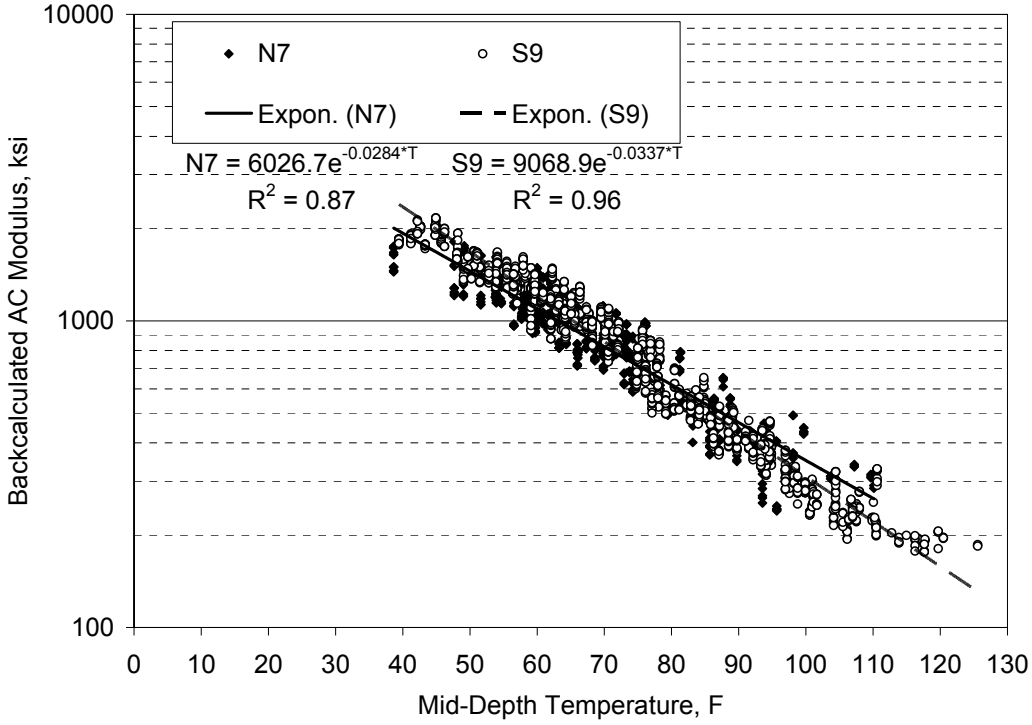

Figure 5.5 Backcalculated AC Modulus vs. Mid-Depth Temperature (RMSE<3%)

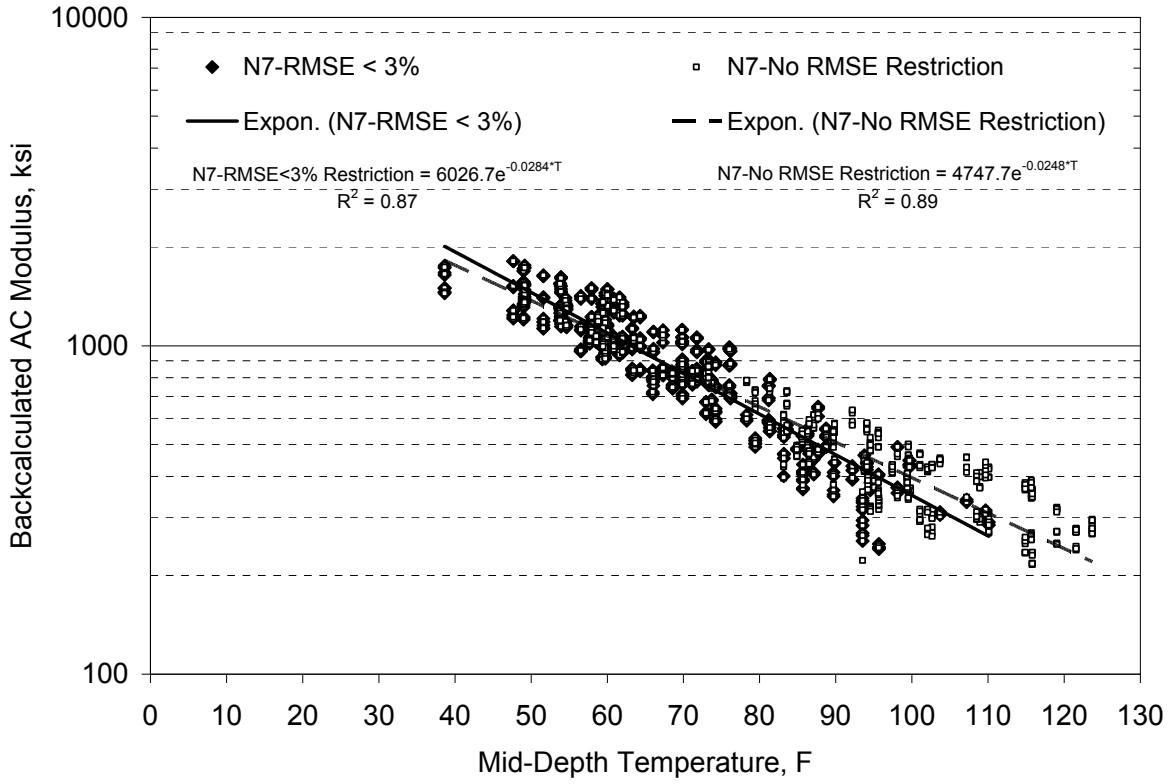

Figure 5.6 N7 Backcalculated AC Modulus vs. Mid-Depth Temperature RMSE Comparison

To examine the differences between sections in backcalculated AC moduli over a range of temperatures, the moduli were temperature-corrected using the coefficients from Figure 5.5. Three reference temperatures were selected (50, 68 and 110°F) that represented the range of FWD test temperatures. As noted in Figure 5.5, each data set was fitted by an exponential function:

$$E = \alpha_1 e^{\alpha_2 T} \tag{5.1}$$

where:
E = backcalculated AC modulus, ksi
T = mid-depth pavement temperature, °F
α_1, α_2 = best-fit regression constants

Equation 5.1 has been used in previous Test Track research cycles to characterize the modulus-temperature relationship for both laboratory and field-determined moduli (Timm and Priest, 2006; Taylor and Timm, 2009). A temperature-corrected AC modulus (E_{Tref}) was determined from Equation 5.1 at a given reference temperature (T_{ref}) by dividing Equation 5.1 at T_{ref} by the same equation at the measured temperature (T_{meas}). After canceling terms and solving for E_{Tref}, the following equation was determined:

$$E_{T_{ref}} = E_{T_{meas}} e^{\alpha_2 \left(T_{ref} - T_{meas}\right)} \tag{5.2}$$

Equation 5.2 illustrates that the key variable in performing the temperature correction is the exponential regression coefficient, α_2. The results of temperature-correction are summarized in Figure 5.7.

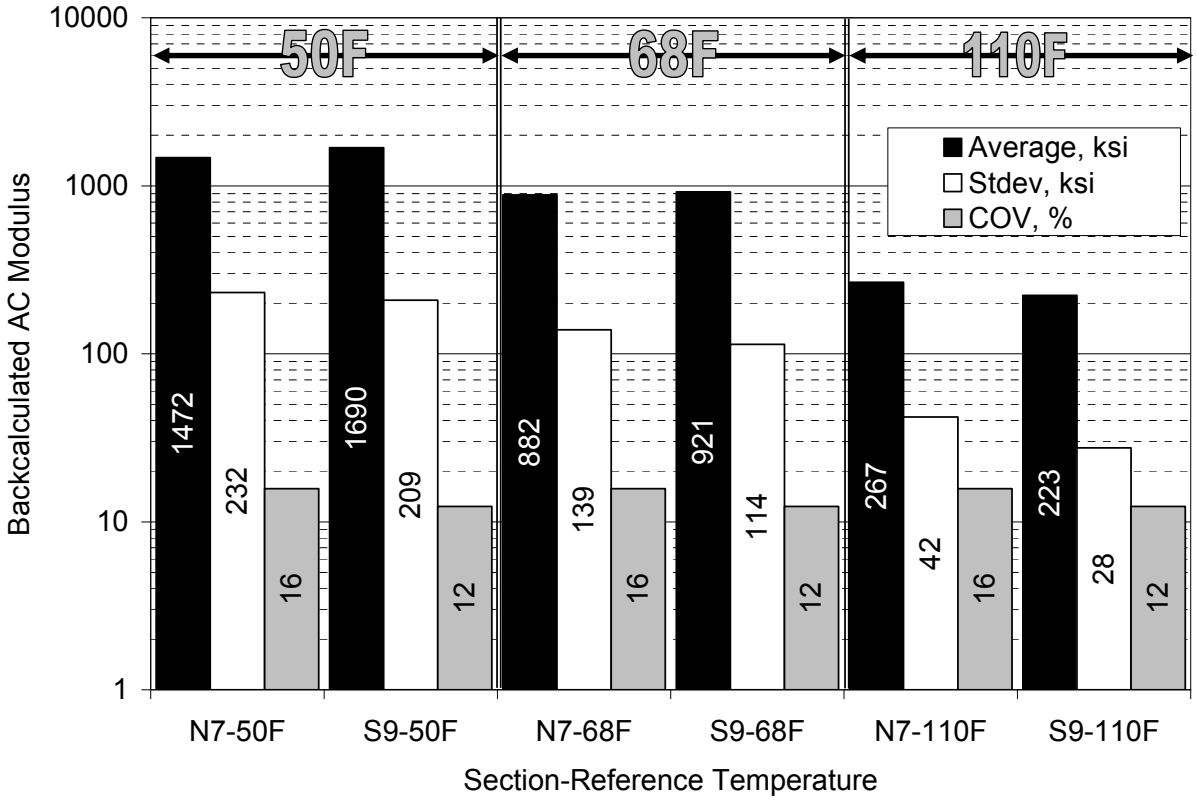

Figure 5.7 Backcalculated AC Modulus Corrected to Reference Temperatures

Figure 5.7 shows the average, standard deviation and coefficient of variation (COV) of each section's AC modulus at each reference temperature. In each case, the COV was less than 30%, which is a common benchmark for backcalculated AC modulus variability (Allen and Graves, 1994; Noureldin, 1994; Timm et al., 1999). Therefore, the AC moduli appear remarkably consistent within each section.

Statistical testing was conducted using a two-tailed Students' t-test ($\alpha = 0.05$) assuming unequal variance with the null-hypothesis that the mean values were equivalent between sections at each reference temperature. At each reference temperature in Figure 5.7, the mean backcalculated moduli were found to be statistically different. At 50 and 68^{o}F, the control section had statistically higher modulus. At 110^{o}F, the reverse was true.

A final step in this analysis was to plot backcalculated AC modulus at 68^{o}F versus date to look for dramatic changes in AC modulus that would indicate possible pavement distress. Figure 5.8 shows relatively little change in modulus over time through the first 21 months of testing. It is interesting to note the large gap in N7 data from May – August, 2010. These missing data correspond to backcalculated moduli whose RMSE exceeded 3%. Figure 5.9 includes all the

data for N7 which fills in this gap. The figure also includes the RMSE plotted on the right y-axis with the critical level (3%) indicated. A definite seasonal trend is noted indicating that at warmer temperatures, the Kraton material is less well-modeled by layered elastic analysis. It is important to further note that using the 3% cutoff essentially eliminates higher moduli. Therefore, the data presented with a 3% cutoff could be considered a conservative lower estimate of in situ moduli.

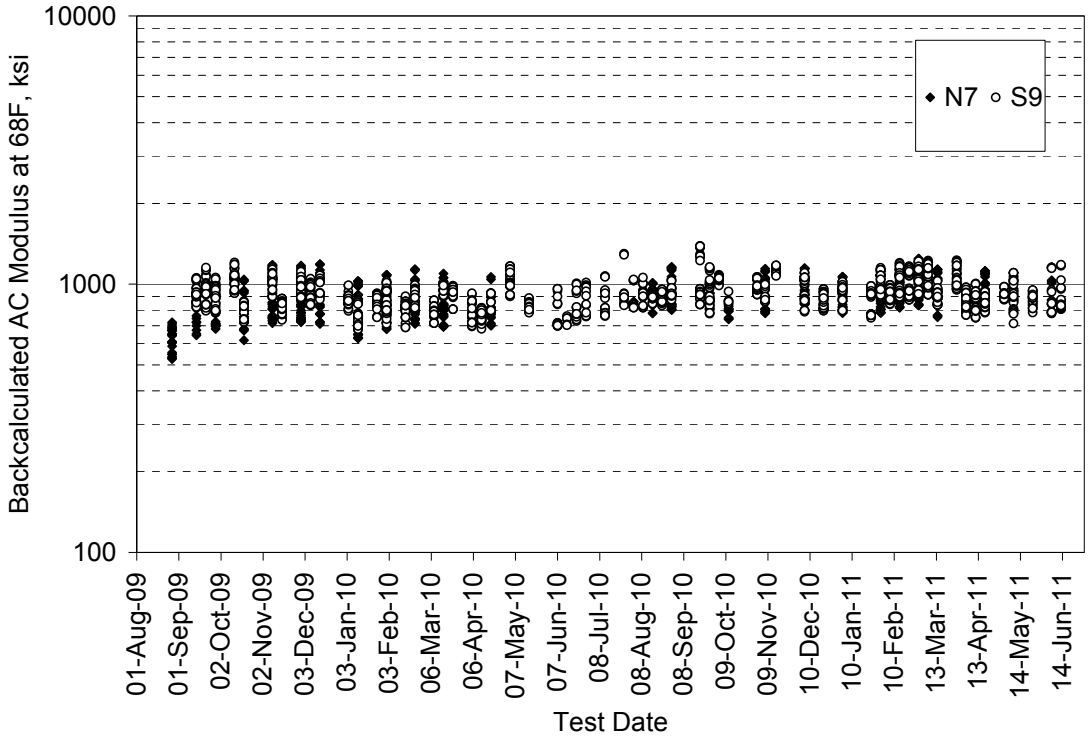

Figure 5.8 Backcalculated AC Modulus vs. Date at 68°F (RMSE < 3%)

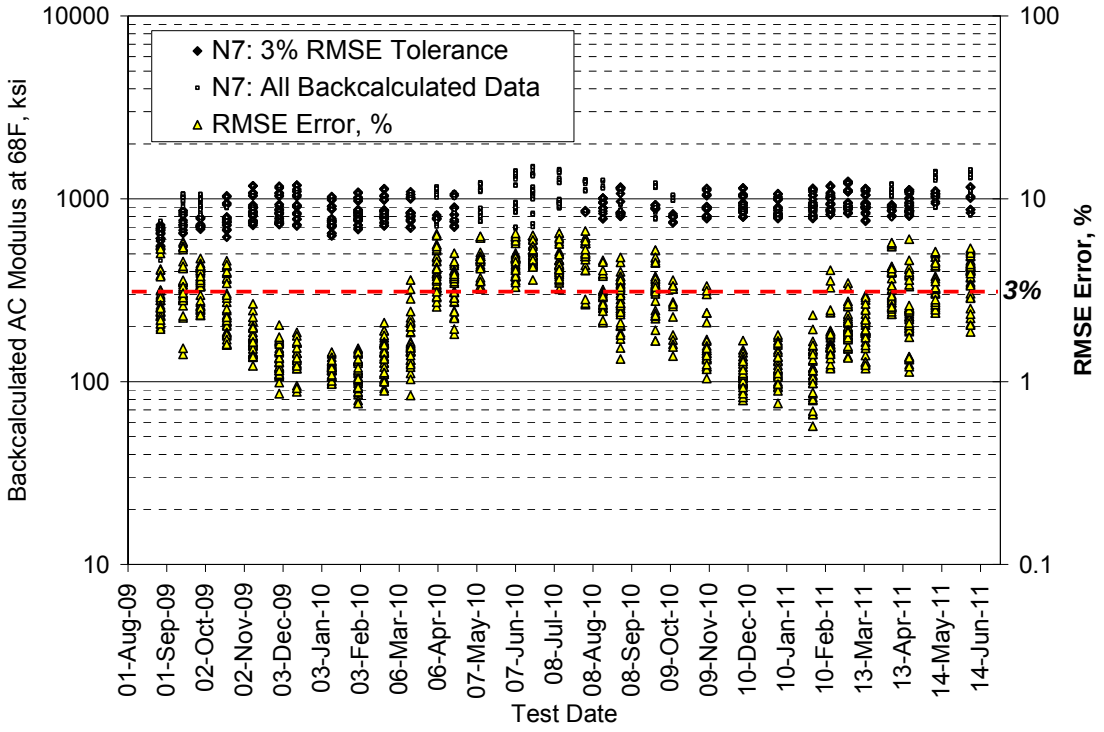

Figure 5.9 Backcalculated AC Modulus (N7) vs. Date at 68°F (No RMSE Restriction)

6. PAVEMENT RESPONSE MEASUREMENTS

As noted previously, traffic began on August 28, 2009. At that time, weekly pavement response measurements using the embedded asphalt strain gauges and earth pressure cells in the granular base and subgrade soil commenced. Weekly data collection consisted of collecting approximately fifteen truck passes (three passes of five trucks) in each section. The frequency of testing and number of trucks collected were consistent with previous data collection efforts at the Test Track which were shown to be sufficient to capture daily variability, seasonal variability and wheel wander effects (Timm and Priest, 2005; Priest and Timm, 2006). The response data in this report were gathered between August 28, 2009 and June 9, 2011.

Strain and pressure readings were acquired using a DATAQ DI-785 data acquisition system at a frequency of 1,000 samples/second/gauge. Raw signals were recorded in voltage versus time and customized processing templates developed in DaDISP were developed to clean the signals using a frequency filter, determine the peak responses for a given truck pass and convert the voltage output into engineering units of stress or strain, as appropriate. Figure 6.1 shows a sample truck pass over the aggregate base and subgrade soil earth pressure cells. The signals are in voltage versus time with peaks noted for each axle in the tractor-trailer combination. The processing scheme tabulates the peak responses, relative to the baseline, for each axle pass.

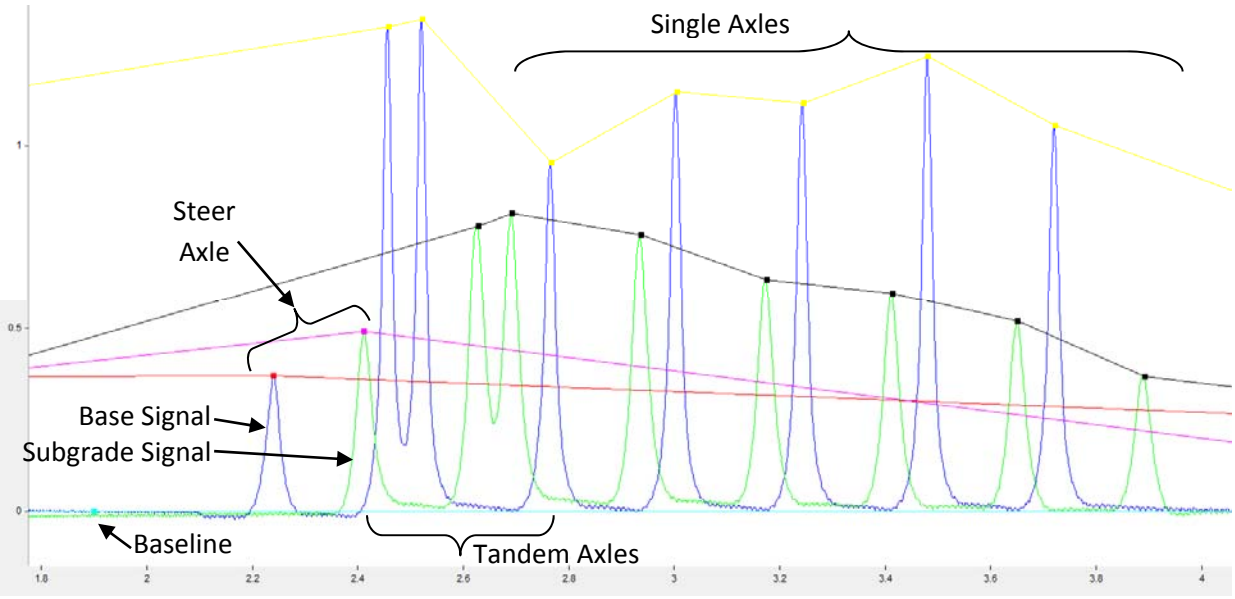

Figure 6.1 DaDISP Screen Capture of Pressure Measurements for Truck Pass

Figures 6.2 and 6.3 show typical strain response measurements in the longitudinal and transverse directions, respectively. The longitudinal measurements (Figure 6.2) usually have compressive strain as the axle approaches the gauge followed by peak tensile response when the axle is directly over the gauge. Finally, the pavement again goes into compression as the axle departs. This cyclic effect is seen throughout each of the axle passes in Figure 6.2.

Transverse strain responses (Figure 6.3) were distinctly different than the longitudinal strain measurements. The processing scheme was the same as that described above, but the signals typically were unilaterally compressive or tensile without the strain reversal seen in the longitudinal measurements. Full explanation of this behavior has been documented previously (Timm and Priest, 2008).

For each truck pass on each gauge, maximum (tensile) and minimum (compressive) responses, in addition to the amplitude (maximum-minimum) for each axle were recorded relative to the baseline. An Access database system was used to archive the data from which the "best-hit" response on a given day was determined on an axle-type basis. The "best-hit" represents the 95th percentile reading on a particular test day from all the readings made under a particular axle type. For example, on a typical day there could be 450 longitudinal strain readings made under single axles in a particular section (6 longitudinal gauges∗5 trucks∗3 passes/truck∗5 single axles/truck = 450 strain readings). The 95th percentile of these 450 readings represented the "best-hit" response for longitudinal strain The 95th percentile was used in previous research cycles at the Test Track (Willis and Timm, 2009) and was found to reasonably represent the true best-hit but guard against erroneously-high readings. This same approach was used for all axle types and the other measurements (base pressure, subgrade pressure and transverse strain).

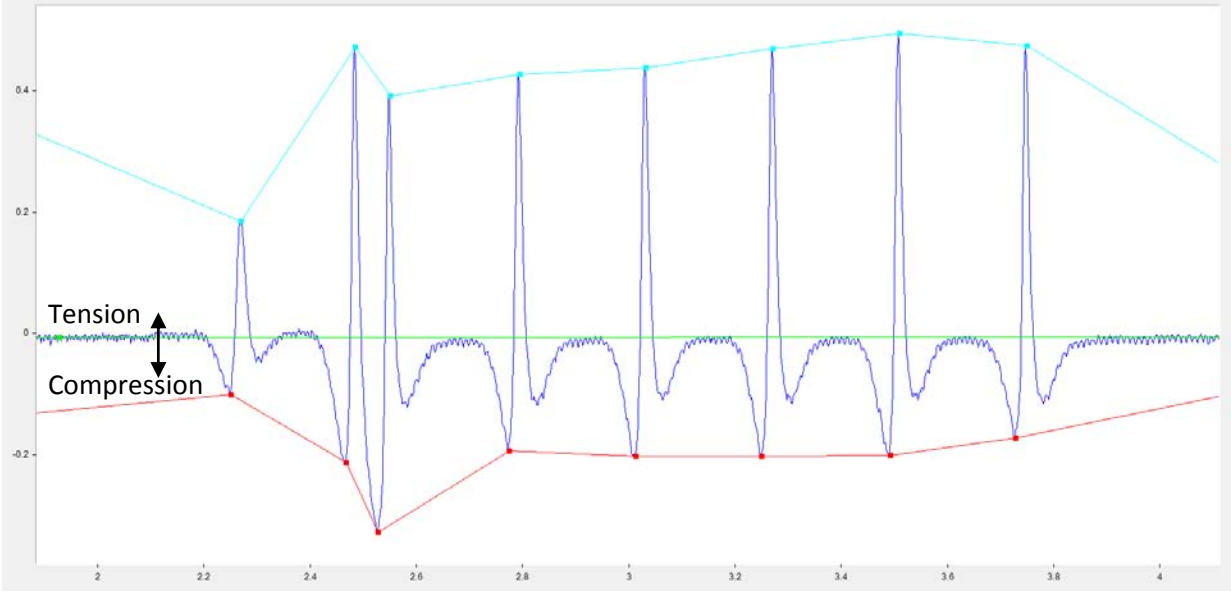

Figure 6.2 DaDISP Screen Capture of Longitudinal Strain Measurements

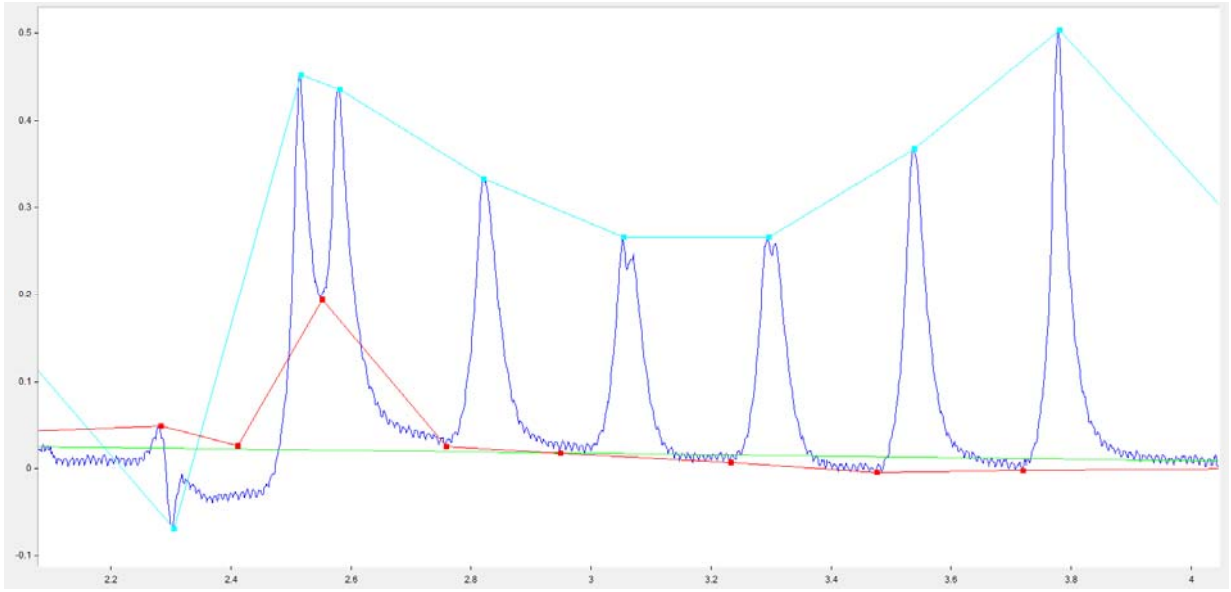

Figure 6.3 DaDISP Screen Capture of Transverse Strain Measurements

After collecting, processing and archiving the data, there were a number of analyses conducted. The following subsections examine seasonal trends in pavement response, temperature effects on pavement response, responses normalized to particular reference temperatures, responses over time at a normalized temperature and distributions of pavement response.

6.1 Seasonal Trends in Pavement Response

As discussed above, there are four primary measured pavement responses: longitudinal strain in the AC, transverse strain in the AC, vertical pressure in the aggregate base and vertical pressure in the subgrade soil. Figures 6.4 through 6.7 plot these responses versus test date for the single axle loadings only, though similar trends were observed with the other axle types. Each data

point in each plot represents the "best-hit" on that particular test date. The seemingly large fluctuation between consecutive test dates is a product of alternating collection times between morning and afternoon on a week-to-week basis. This ensures that a fuller range of temperatures are sampled during a particular season.

In each plot, the seasonal trends are clearly evident with lower responses during the cooler months and increased responses during warmer months. It is interesting to note that the longitudinal strain responses in Figure 6.4 were generally higher in N7 compared to S9 through February 2010. After February 2010, the N7 responses appeared erratic – sometimes higher, sometimes lower, compared to those of S9. This trend was also evident in the transverse strain (Figure 6.5) but did not appear in the pressure response data (Figures 6.6 and 6.7). Possible reasons for this behavior could be cracking in the AC, slippage between layers or gauge malfunction. This will be more fully explored below.

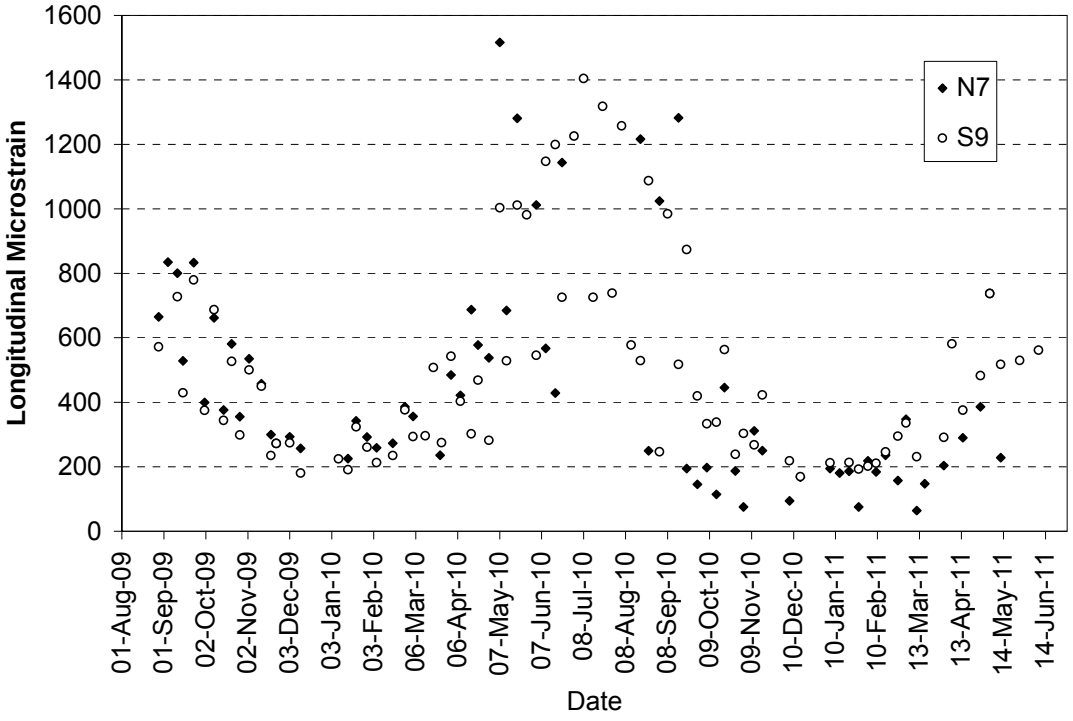

Figure 6.4 Longitudinal Microstrain Under Single Axles

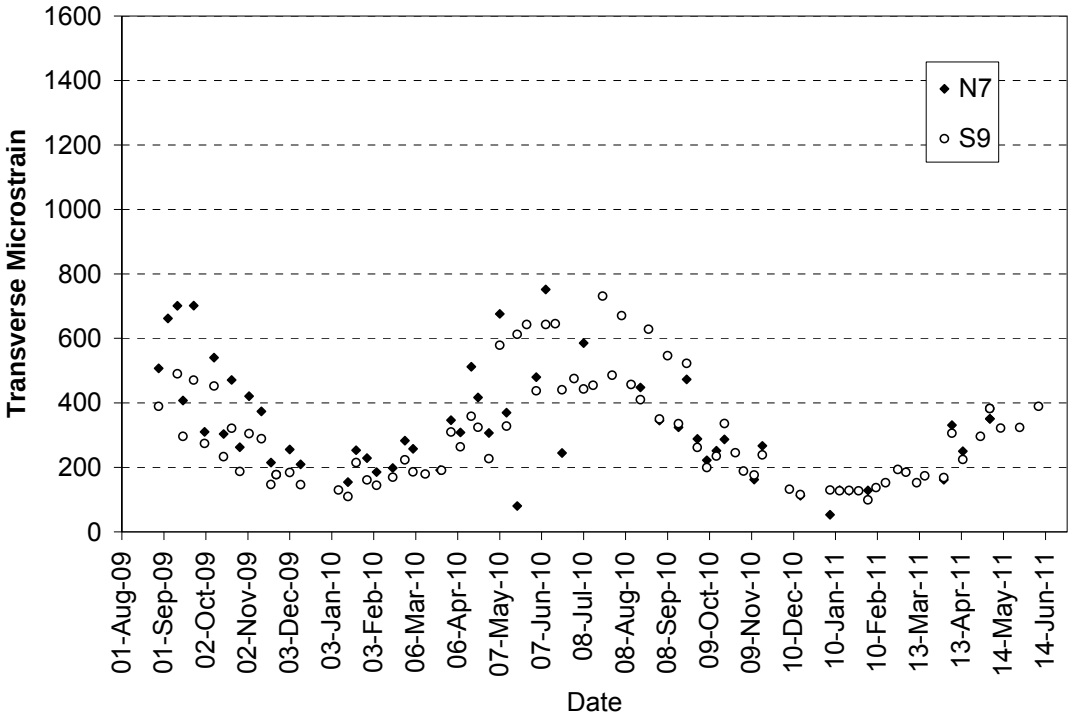

Figure 6.5 Transverse Microstrain Under Single Axles

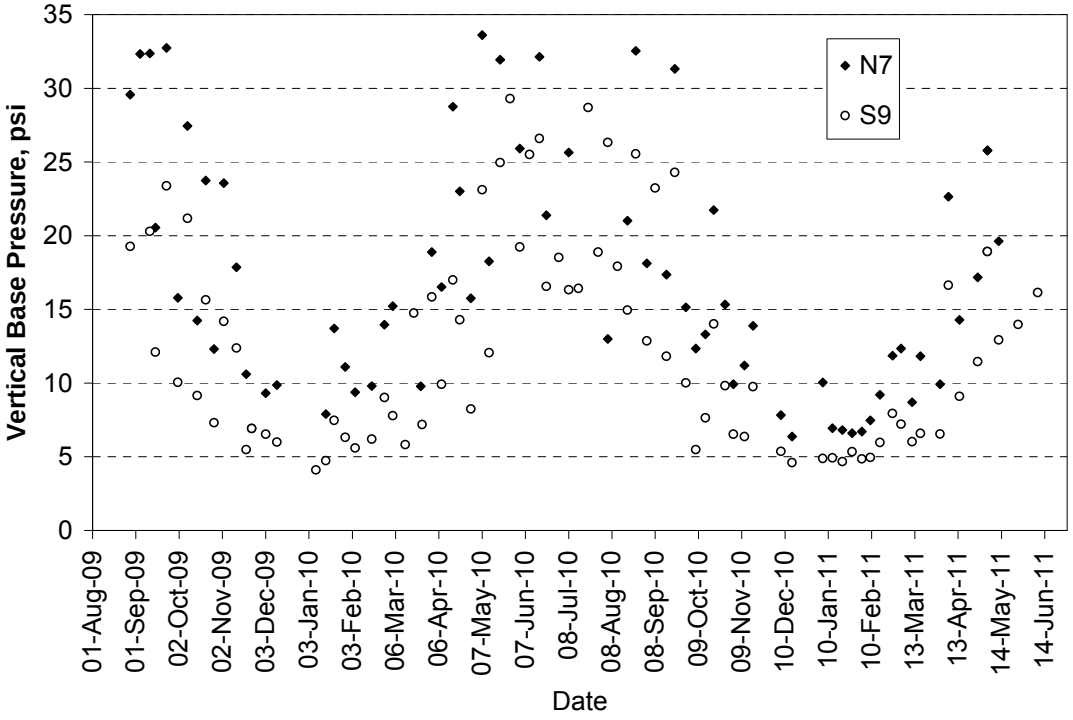

Figure 6.6 Aggregate Base Pressure Under Single Axles

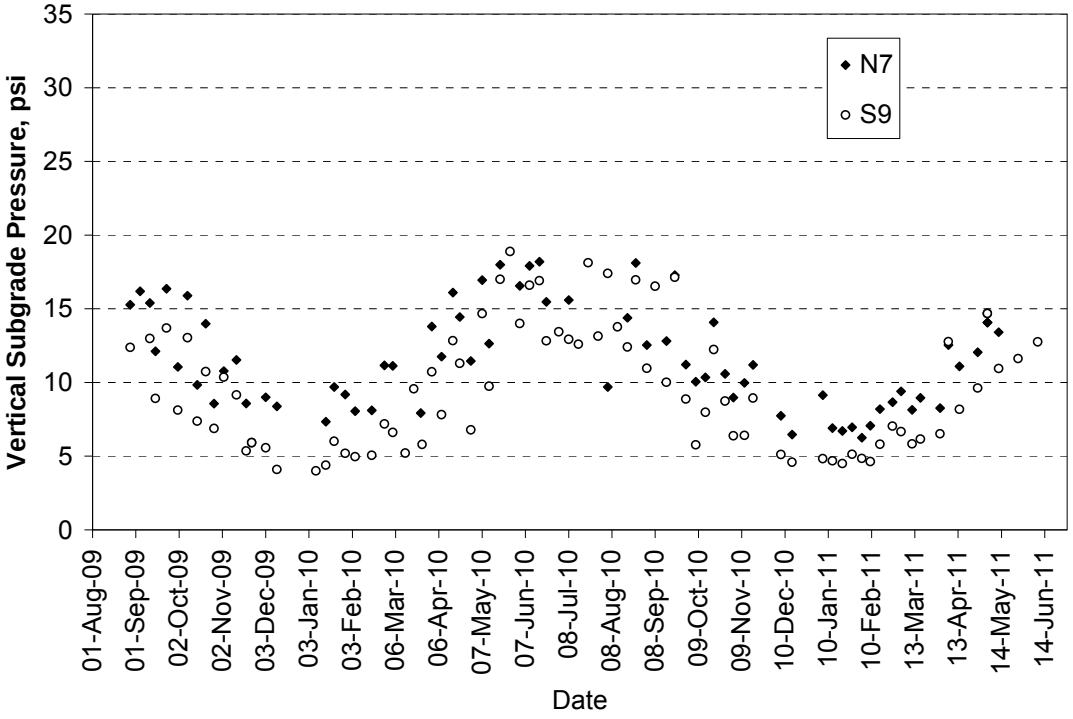

Figure 6.7 Subgrade Pressure Under Single Axles

6.2 Pavement Response vs. Temperature

The data presented in Figures 6.4 through 6.7 were the best-hit pavement responses on a particular test date. These data were re-plotted in Figures 6.8 through 6.11 against their corresponding mid-depth pavement temperature. Exponential regression equations, much like those determined for the backcalculated AC moduli, were best-fit to each data set in Figures 6.8 through 6.11, representing single axles. Additional equations were developed for each of the axle types, the results of which are presented in Table 6.1. In total, 24 sets of regression parameters were determined (2 sections x 4 responses x 3 axle types = 24). For the control section, all R^2 values were above 70%. In contrast, within strain measurements for N7, five of six regression equations had R^2 below 70% indicating a generally poor fit to the exponential equation. Within pressure measurements, only the steer axles R^2 values were below 70%. Clearly, the data were more scattered within the Kraton section, with particularly high scatter seen within the strain measurements. As noted above, more erratic data were observed for N7 after mid-February, 2010 which prompted further investigation.

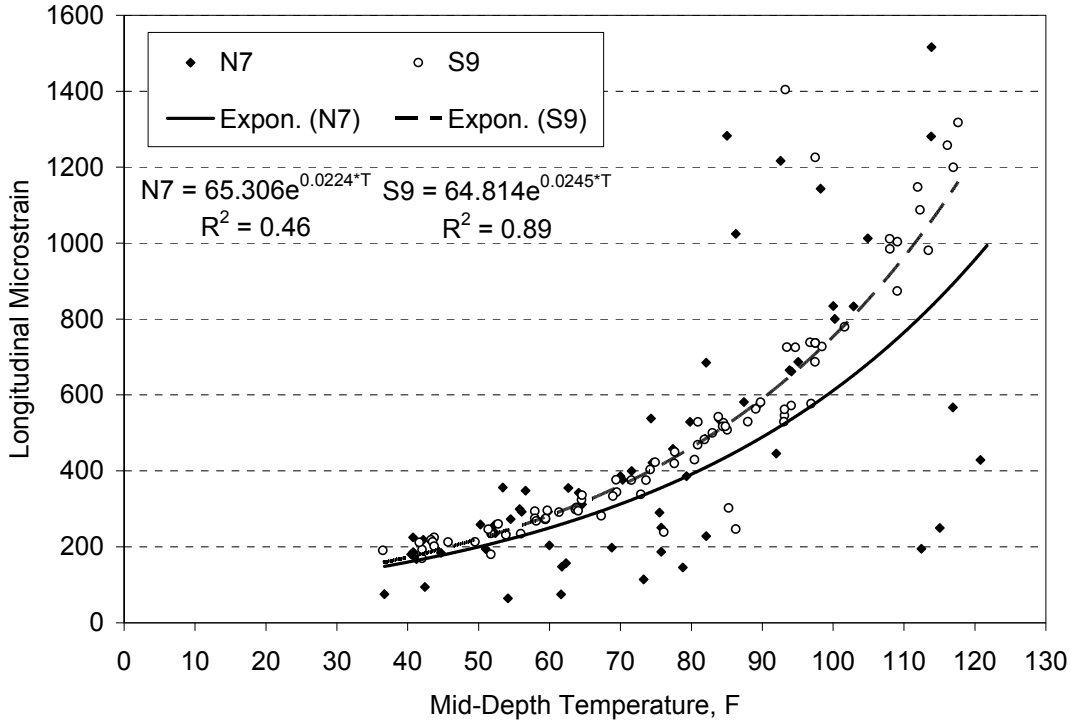

Figure 6.8 Longitudinal Strain vs. Mid-Depth Temperature Under Single Axles

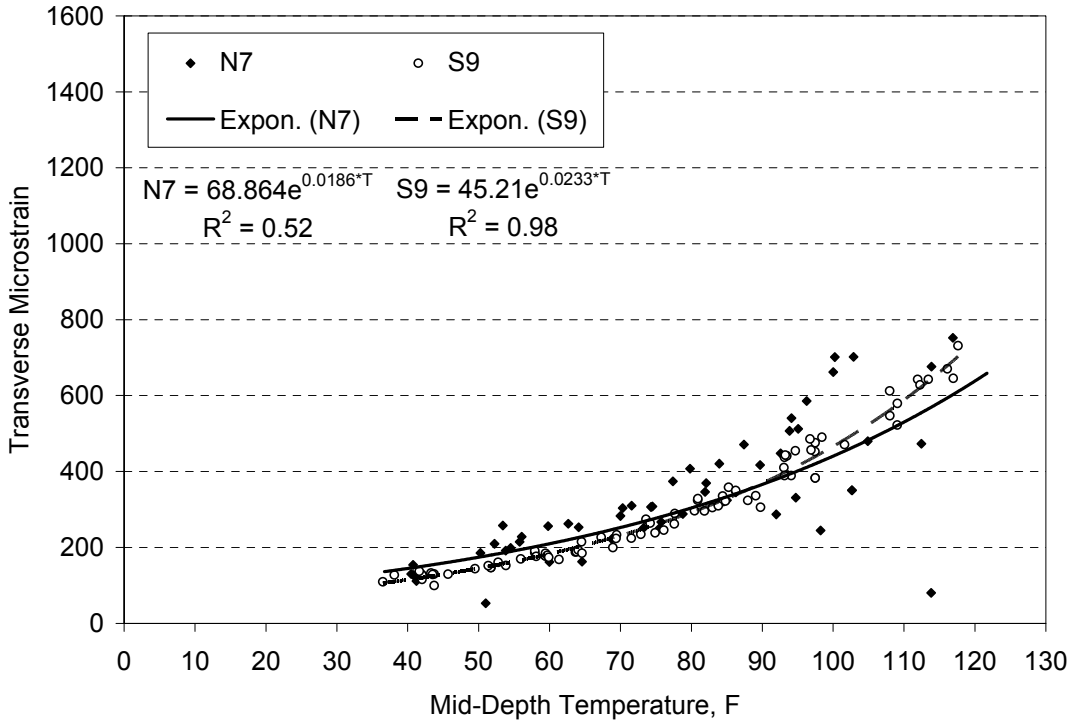

Figure 6.9 Transverse Strain vs. Mid-Depth Temperature Under Single Axles

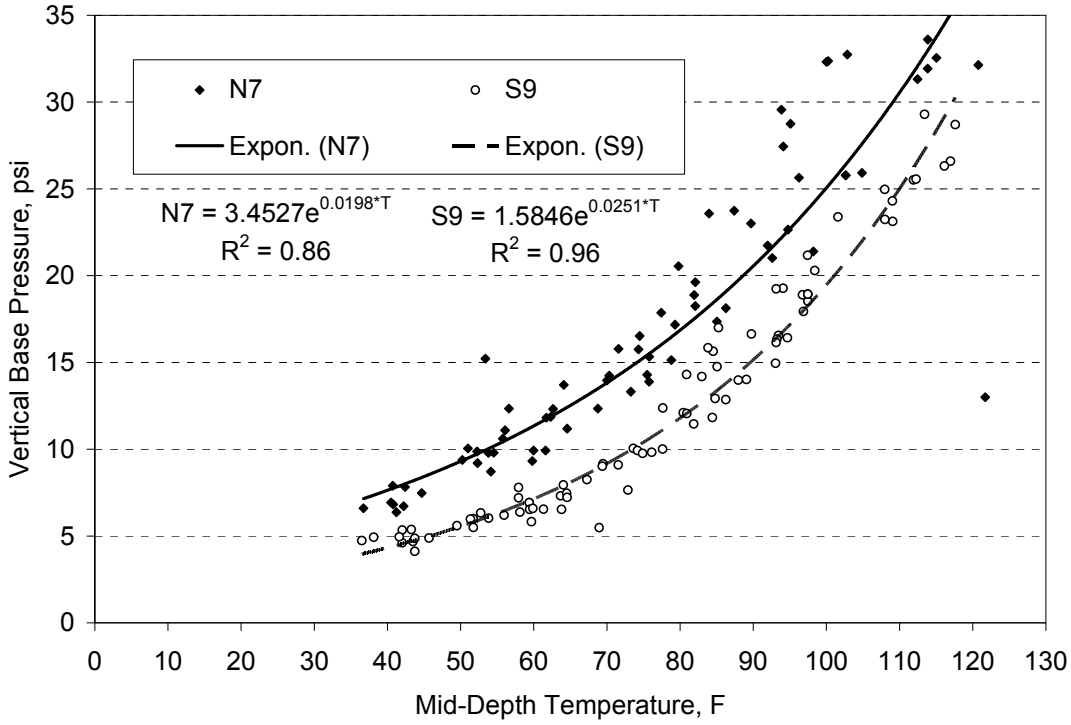

Figure 6.10 Base Pressure vs. Mid-Depth Temperature Under Single Axles

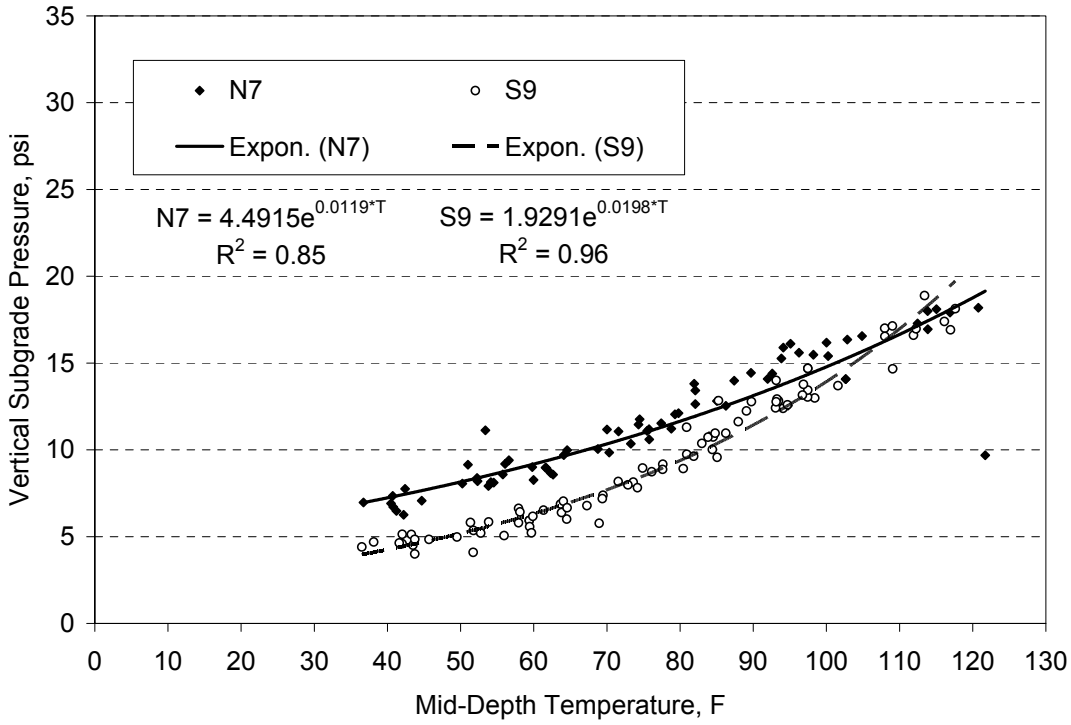

Figure 6.11 Subgrade Pressure vs. Mid-Depth Temperature Under Single Axles

Table 6.1 Pavement Response vs. Temperature Regression Terms

		Longitudinal Strain			Transverse Strain			Base Pressure			Subgrade Pressure		
Section	Axle	k_1	k_2	R^2	k_1	k_2	R^2	k_1	k_2	R^2	k_1	k_2	R^2
N7 (Kraton)	Steer	22.076	0.028	0.47	51.935	0.016	0.11	1.845	0.020	0.38	2.191	0.013	0.45
	Single	65.306	0.022	0.46	68.864	0.019	0.52	3.453	0.020	0.86	4.492	0.012	0.85
	Tandem	79.289	0.023	0.78	120.775	0.012	0.16	4.311	0.017	0.70	4.832	0.010	0.74
S9 (Control)	Steer	26.856	0.029	0.87	24.597	0.031	0.95	0.817	0.023	0.73	0.895	0.020	0.82
	Single	64.814	0.025	0.89	45.210	0.023	0.98	1.585	0.025	0.96	1.929	0.020	0.96
	Tandem	46.970	0.028	0.91	43.669	0.023	0.98	1.964	0.023	0.95	2.491	0.017	0.94

Gray shading = $R^2 < 0.70$

As noted previously, the increased scatter appeared to begin in February 2010. To further explore the time effect within each data set, a cut-off date of February 17, 2010 was established. N7 data were plotted before and after this date with exponential trendlines attached to each data set. Figures 6.12 through 6.15 contain the data sets for longitudinal strain, transverse strain, base pressure and subgrade pressure, respectively. In the strain plots, a dramatic difference, approximately 50% for the R^2 values of before versus after, is seen relative to this cut-off date. The differences were less pronounced within the pressure data sets. Clearly, something changed in the pavement around mid-February 2010 that severely affected measured strain response. Lacking any surface cracking observations, corresponding trends in the backcalculated moduli data, or any known gauge malfunctions, it is difficult to pinpoint the exact cause at this time. Further monitoring and forensic investigation will be needed to fully identify the origin of the change.

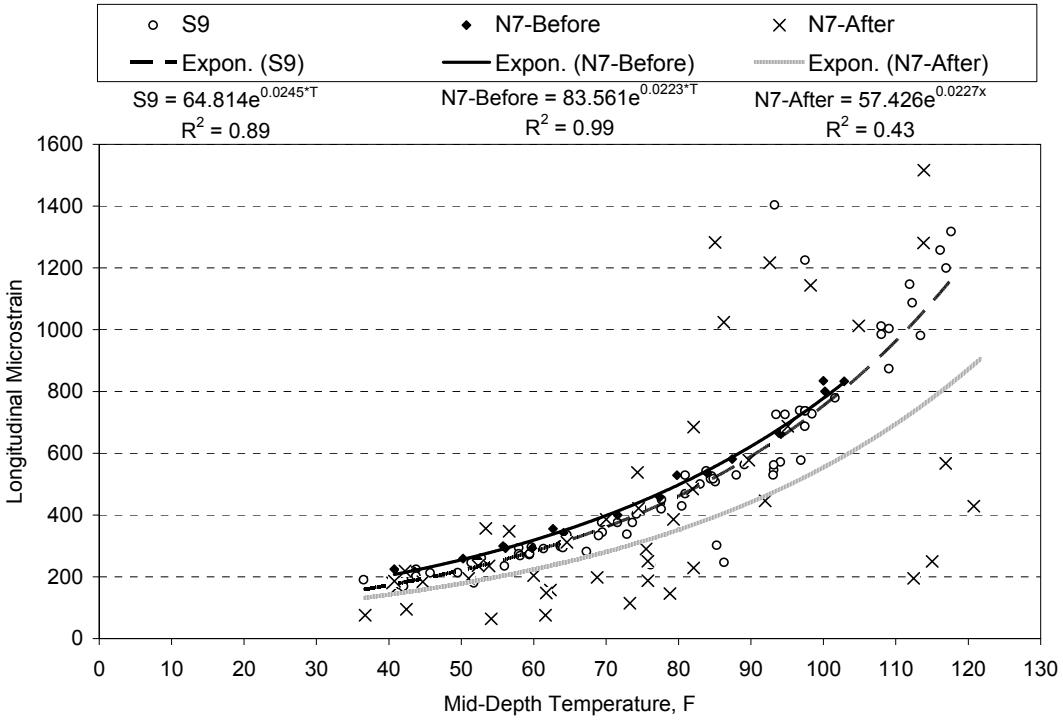

Figure 6.12 Longitudinal Strain vs. Mid-Depth Temperature Under Single Axles (N7 – 2/17/2010 Cutoff)

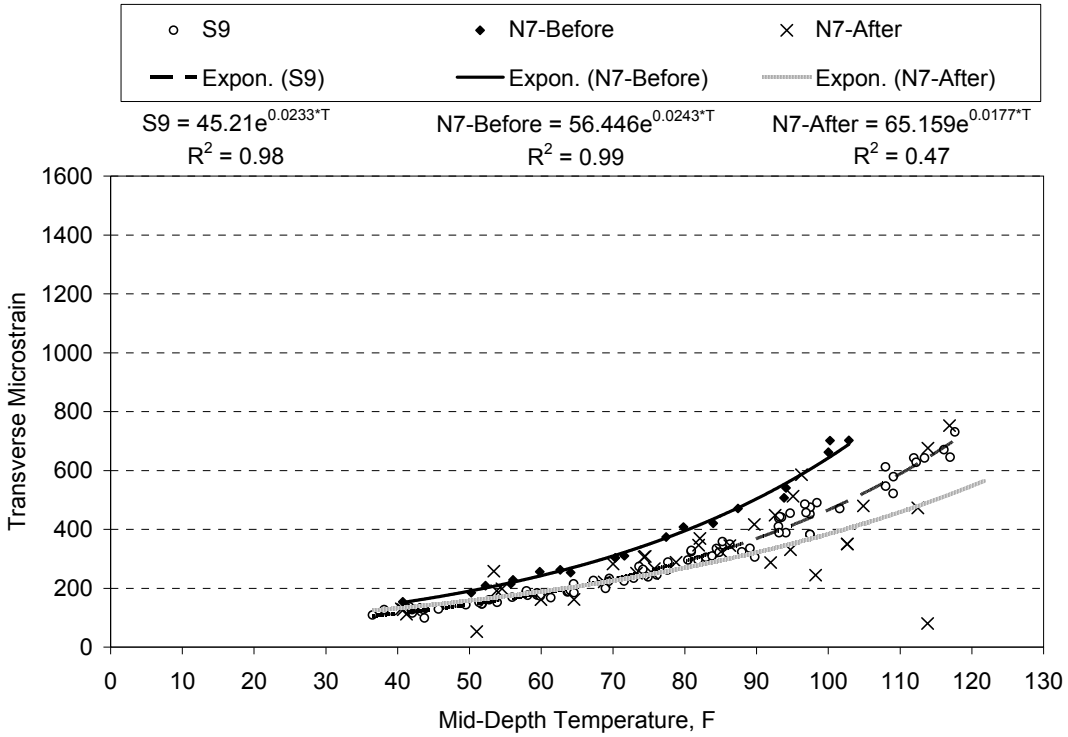

Figure 6.13 Transverse Strain vs. Mid-Depth Temperature Under Single Axles (N7 – 2/17/2010 Cutoff)

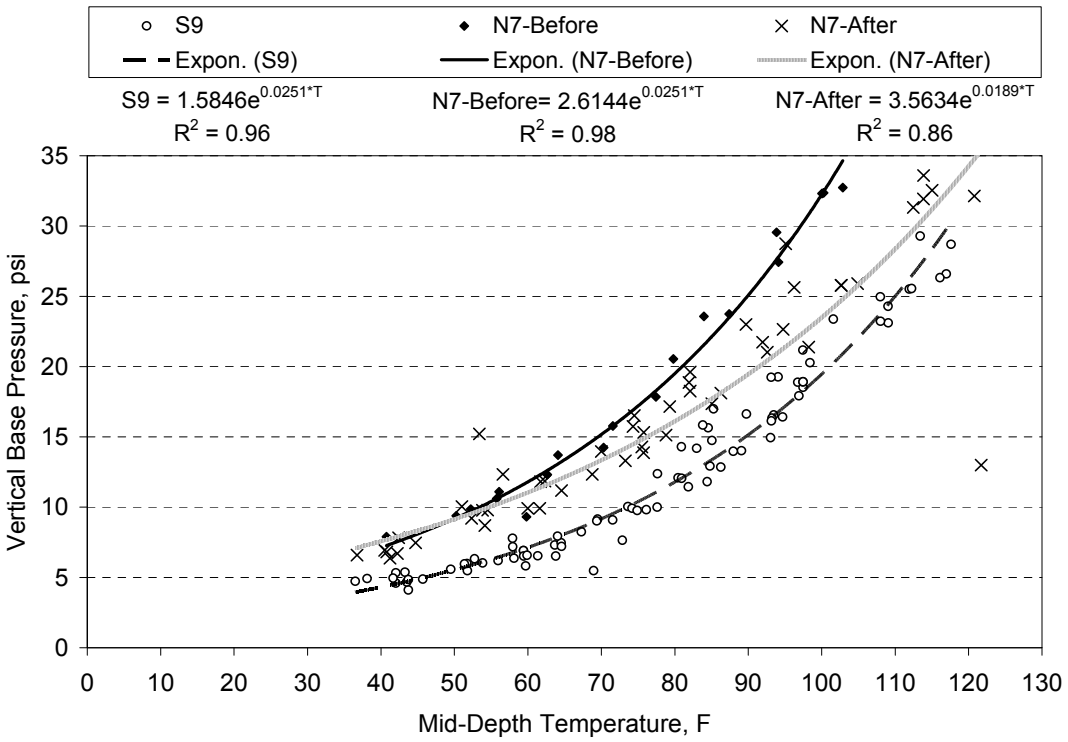

Figure 6.14 Aggregate Base Pressure vs. Mid-Depth Temperature Under Single Axles (N7 – 2/17/2010 Cutoff)

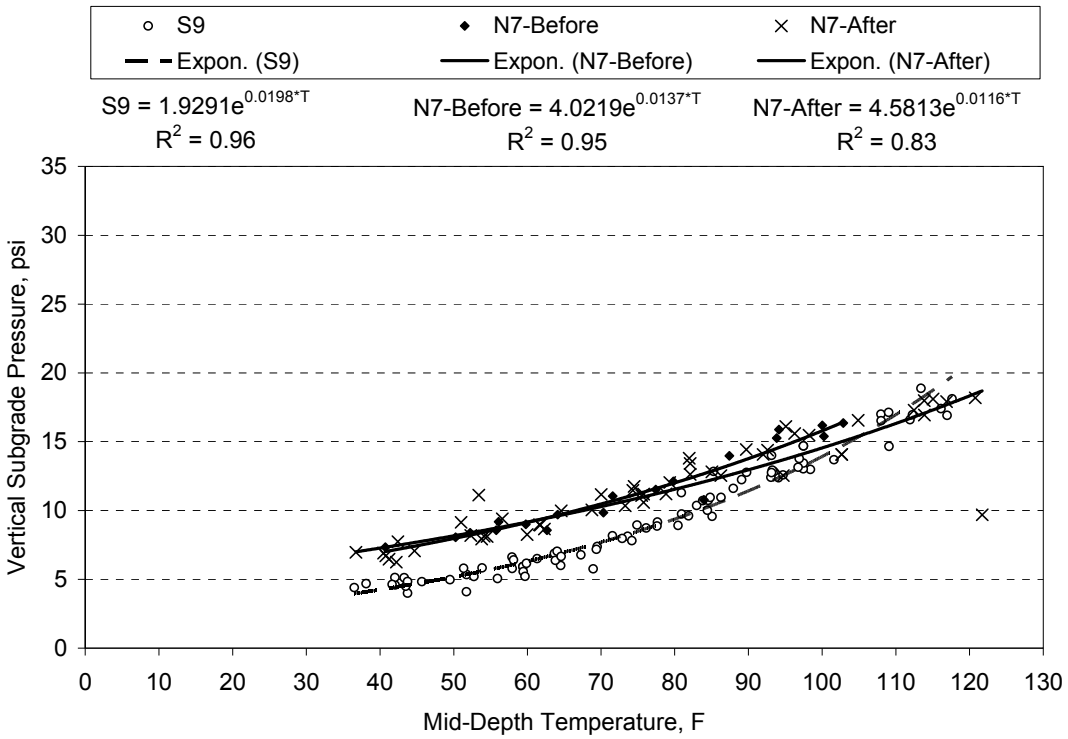

Figure 6.15 Subgrade Pressure vs. Mid-Depth Temperature Under Single Axles (N7 – 2/17/2010 Cutoff)

6.3 Pavement Responses Normalized to Reference Temperatures

To characterize statistical differences in pavement response between sections, temperature corrections were applied to each data set (longitudinal strain, transverse strain, base pressure, subgrade pressure) at 50, 68 and 110°F. The regression terms presented in Table 6.1 were used for this part of the analysis. Though one could argue for using the February 17, 2010 cutoff date for section N7, it was decided to use the entire data set to provide a complete comparison between the two sections. This analysis may be revised in the future based on forensic analysis. For both sections, temperature-corrected responses were determined according to:

$$response_{T_{ref}} = response_{T_{meas}} e^{k_2\left(T_{ref} - T_{meas}\right)} \quad (6.1)$$

where:

$response_{Tref}$ = response at T_{ref}

$response_{Tmeas}$ = response at T_{meas}

T_{ref} = mid-depth reference temperature (50, 68, 110°F)

T_{meas} = mid-depth measured temperature, F

k_2 = section, axle and response-specific regression constant from Table 6.1

The average, standard deviation and coefficient of variation were determined at each reference temperature. Two-tailed t-tests (α=0.05) were conducted at each reference temperature to establish statistical significance between average measured responses. Only results for the single axles are presented here, though similar trends were noted amongst the other axles.

6.3.1 Longitudinal Strain Responses

Figure 6.16 summarizes the average, standard deviation and coefficient of variation (COV) at each reference temperature. The variability, as measured by the COV was more than double for N7 relative to S9. At the two lower temperatures, the differences between measured responses were not significantly different. This was likely due to the high degree of variability in the N7 data set (i.e., differences are hard to detect when data are highly variable). However, at 110°F, N7 was statistically lower than S9. This observation is important for two reasons. First, a difference was detected which shows that despite a high-degree of variability in the N7 data, the average response was low enough that it was distinguishable from S9. Second, the total N7 AC thickness was approximately 1.25 inches less than S9 which implies that the increase in the N7 AC modulus at the highest temperature, from the higher polymer content, was enough to overcome the thickness advantage held by S9. Recall from the discussion of the temperature-normalized AC moduli in Figure 5.7 that N7 had a statistically-higher modulus at 110°F. The increased modulus, as demonstrated in Figure 6.16, resulted in statistically-lower strain response.

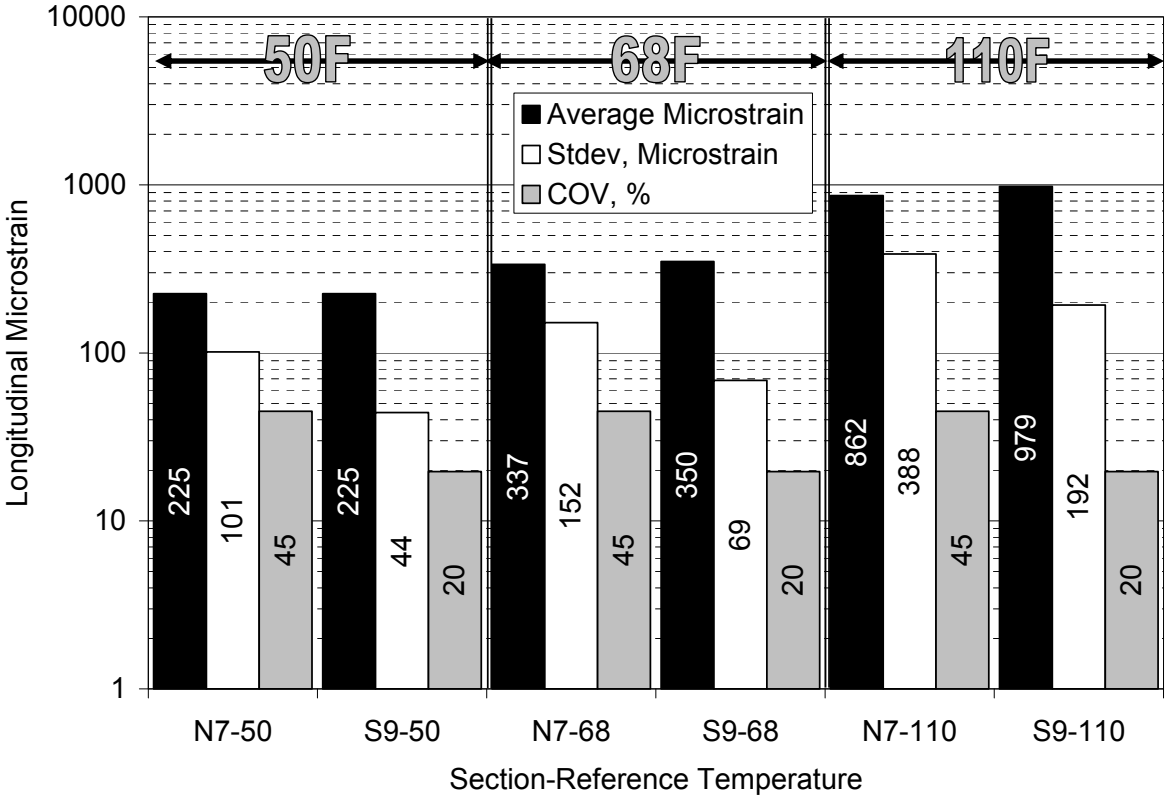

Figure 6.16 Longitudinal Strain Under Single Axles at Three Reference Temperatures

After one year of testing, there has been no fatigue cracking evident. However, preliminary fatigue estimates can be made for comparison purposes to evaluate relative performance estimates using the strain data in Figure 6.16 with the fatigue transfer functions developed previously in the laboratory. Table 6.2 lists the measured average strain at 68°F and the corresponding predicted fatigue life using the transfer functions presented in Table 4.13. It is important to note that despite N7 and S9 having statistically equivalent strain levels at 68°F,

along with N7 having a total thickness 1.25 inches less than S9, the improved fatigue characteristics of the Kraton base mixture yields an improvement of approximately 45 times in the predicted fatigue life over the control section.

Table 6.2 Predicted Fatigue Life at 68F

Section	Average Measured Microstrain at 68F	Predicted Fatigue Life – Cycles to Failure at 68F Using Laboratory-Determined Transfer Function
N7 (Kraton)	337	15,680,982
S9 (Control)	350	348,432

6.3.2 Transverse Strain Responses

Figure 6.17 summarizes the transverse strains under single axle loadings. As found in previous studies (Timm and Priest, 2008), the transverse strains were generally lower than their longitudinal counterparts. Also, the transverse strains were somewhat more consistent than longitudinal with COV's. The greater data consistency resulted in more easily detected differences between sections. At the two lower temperatures, differences in average values were statistically different when using a two-sample t-test assuming unequal variance ($\alpha = 0.05$). The fact that the control section was lower than the Kraton section can be attributed to its increased thickness and modulus at these temperatures. At 110°F, the differences were not statistically-distinguishable. As noted in the longitudinal strain discussion above, it is apparent that the increased modulus in the Kraton material, resulting from increased polymer contents, at high temperatures can overcome the 1.25 inch thickness advantage held by the control section.

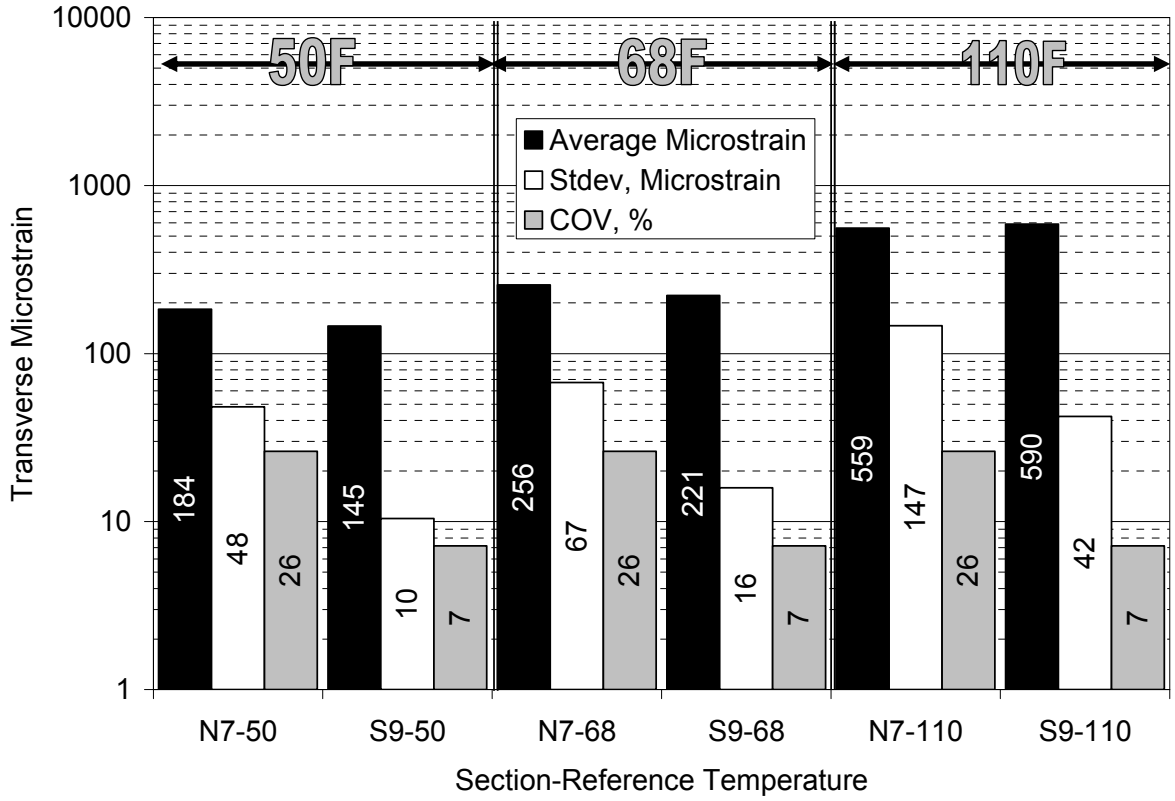

Figure 6.17 Transverse Strain Under Single Axles at Three Reference Temperatures

6.3.3 Aggregate Base Vertical Pressure Responses

Figure 6.18 summarizes the vertical pressures in the aggregate base under single axle loads. The consistency within the data sets certainly contributes to the statistically-significant mean values detected through two-tailed t-tests assuming unequal variance ($\alpha = 0.05$). At each temperature, the control section had lower vertical stress in the base layer than the Kraton section. The primary reason for these differences, as expected, was the increased thickness in the control section. In this case, the increased modulus of the Kraton material at high temperature was not enough to overcome the thickness disadvantage.

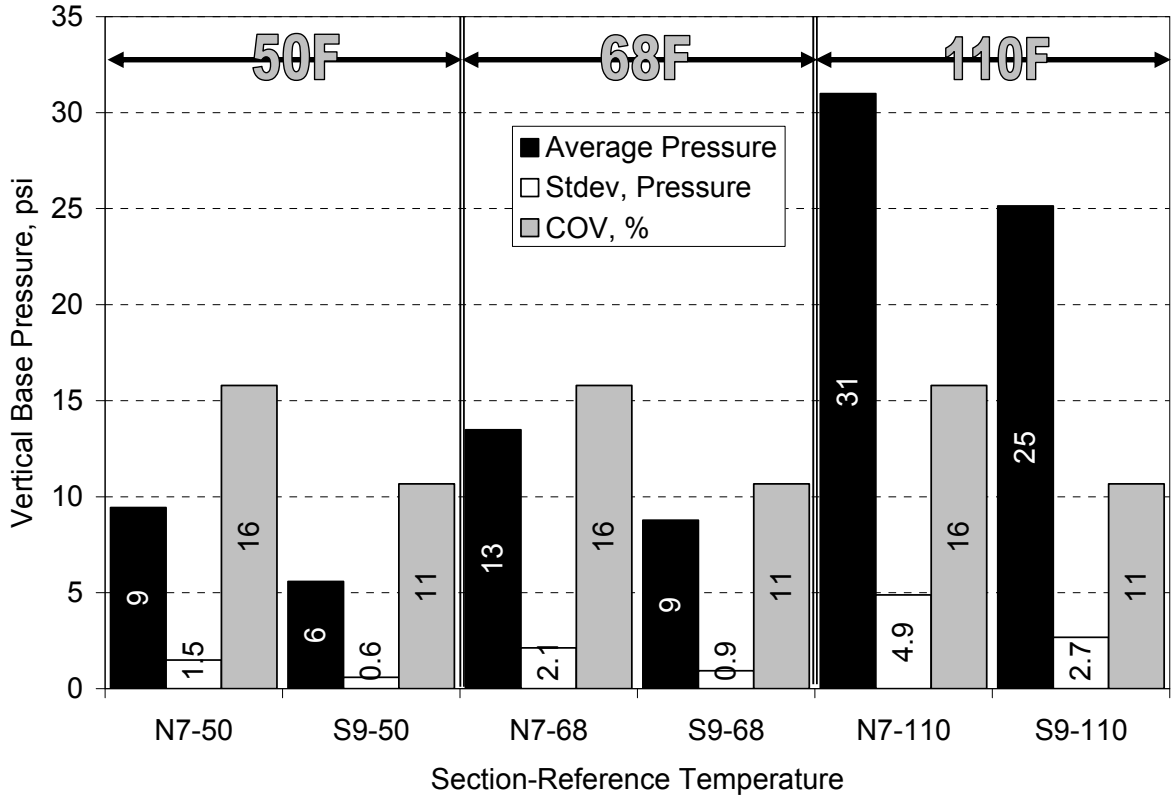

Figure 6.18 Base Pressure Under Single Axles at Three Reference Temperatures

*6.3.4 Subgrade Vertical Pressure Response***s**

The temperature-corrected vertical pressures in the subgrade are plotted in Figure 6.19. Statistically, the mean values at 50 and 68°F in Figure 6.19 are statistically significantly different (two-tailed t-test assuming unequal variance ($\alpha = 0.05$)). Again, the thickness difference between the two sections, at higher modulus of the control section at the two lower temperatures, explains these results. Interestingly, at 110°F, the mean values are the same. In this case, the increased modulus of the Kraton material at 110°F was sufficient to equalize pressures at this depth despite having a thinner pavement structure.

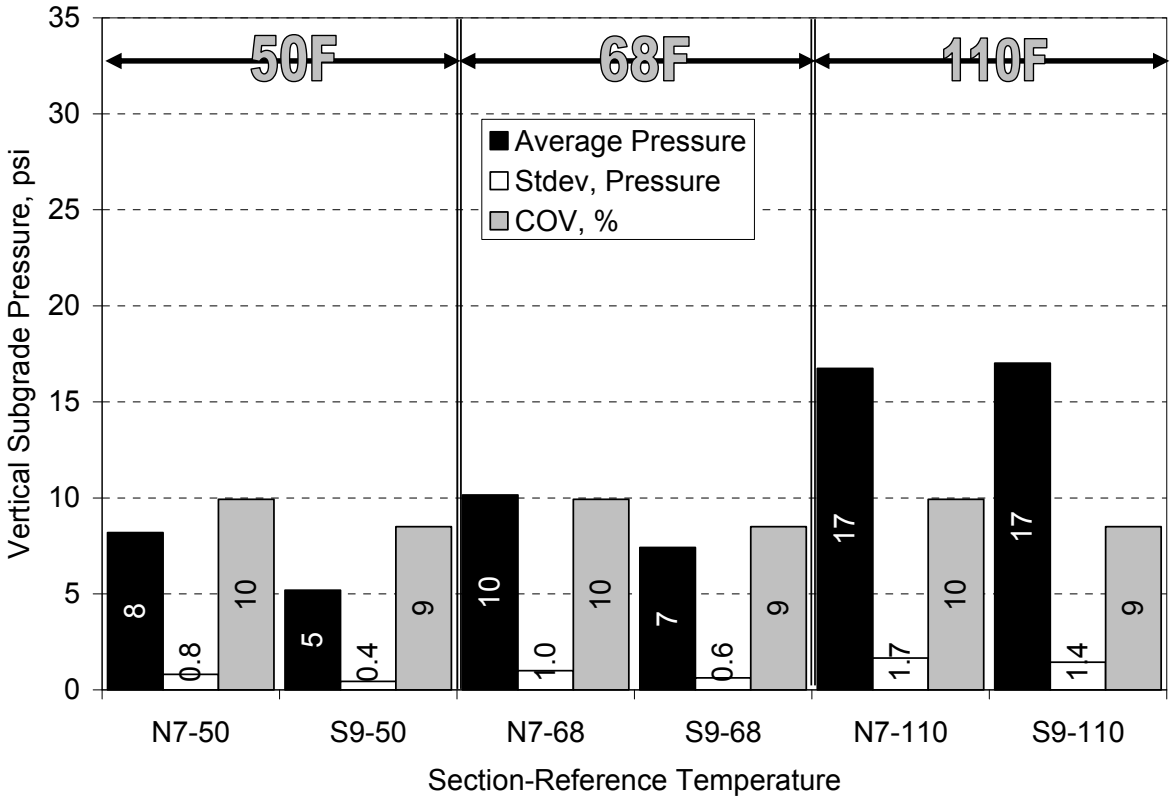

Figure 6.19 Subgrade Pressure Under Single Axles at Three Reference Temperatures

6.4 Pavement Response Over Time at 68°F

Pavement responses normalized to 68°F were plotted against test date, as done with the backcalculated AC moduli data, to look for signs of distress in the response measurements under single axles. It should again be noted that the regression coefficients from Table 6.1 were used for temperature normalization. In each graph, linear trendlines were determined for each data set so that the influence of pavement age could be evaluated.

Figure 6.20 clearly shows relatively consistent data for N7 through mid-February 2010 after which time the longitudinal strain measurements became very erratic. This phenomenon has already been discussed above, but is important to again recognize that the pavement reached a critical point at this time. The downward trend in N7, though in stark contrast to S9, is largely meaningless because of the high degree of scatter and relatively low R^2. Strain levels in S9 were unaffected by pavement age as indicated by the trendline's flat slope and R^2 equal to 0.00.

Interestingly, Figure 6.21 shows a general downward trend in N7's transverse strain response over time with nearly 50% of the variability explained by pavement age. It was previously hypothesized that there could be slippage between pavement layers within the Kraton section, as indicated by the highly erratic longitudinal strain. A general decline in measured strain could result from layer slippage where strains are not fully transferred at layer interfaces to the bottom of the pavement where the measurements were made.

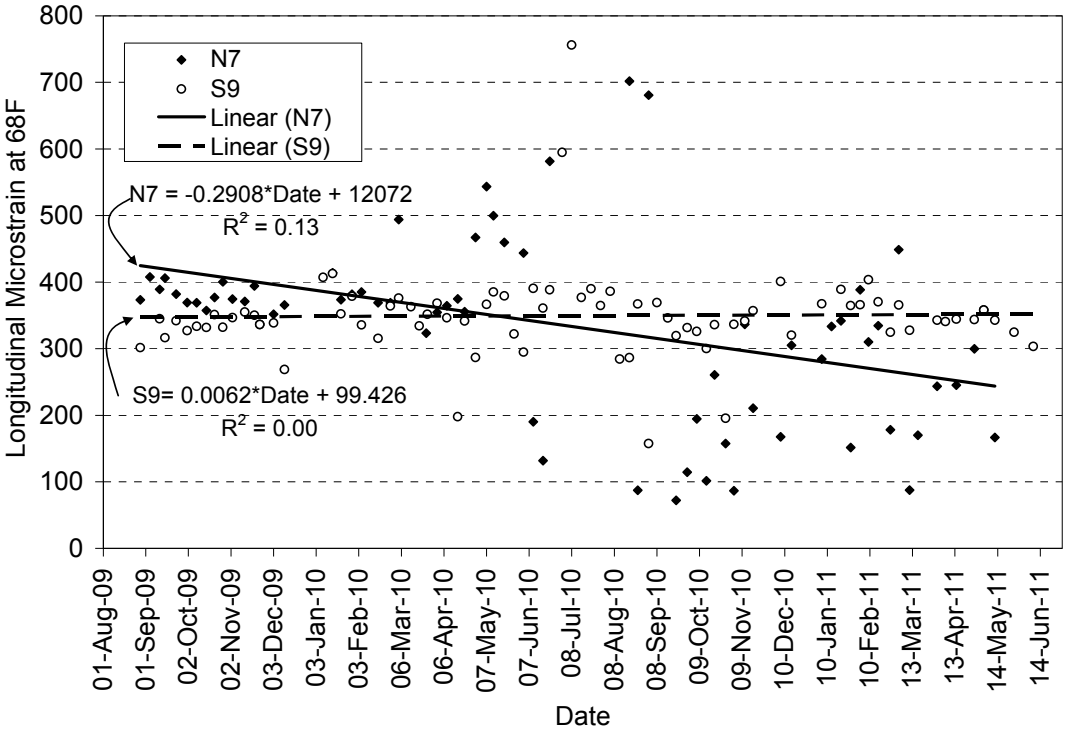

Figure 6.20 Longitudinal Microstrain Under Single Axles vs. Date at 68F

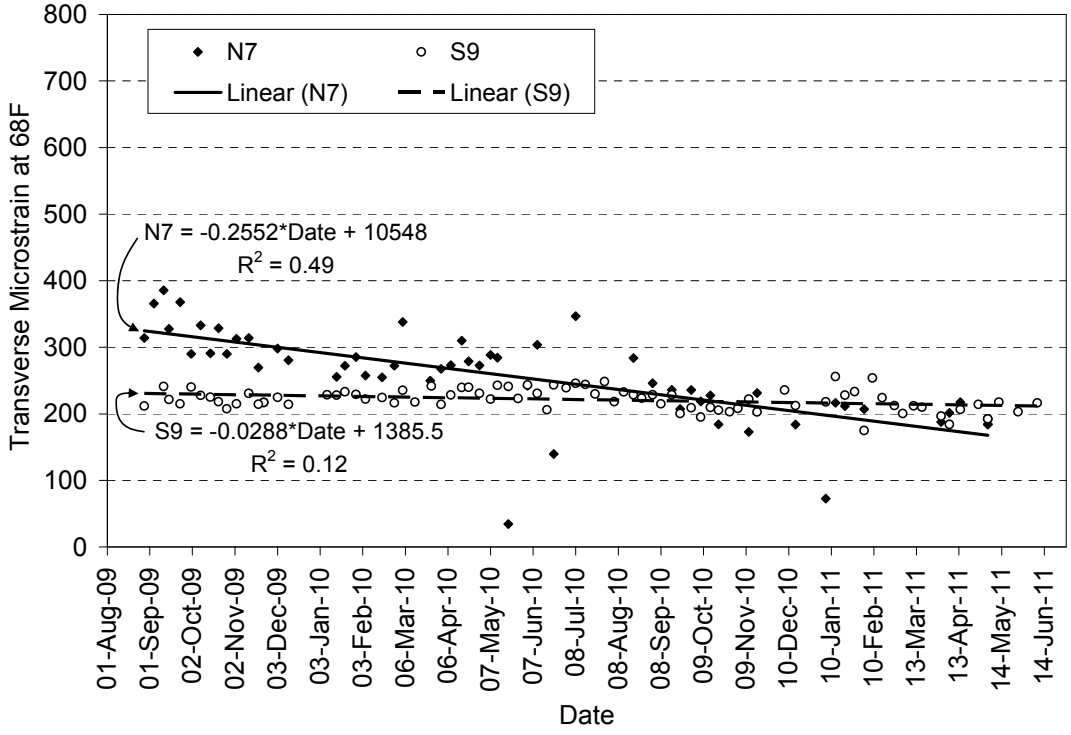

Figure 6.21 Transverse Microstrain Under Single Axles vs. Date at 68F

Figures 6.22 and 6.23 show relatively stable pressure measurements in the base and subgrade layers, respectively. The generally low R^2 values (< 25%) combined with small slopes (< .006 psi per day reduction) lead to the reasonable conclusion that these measurements are affected, at this point, by what may be occurring in the AC layers.

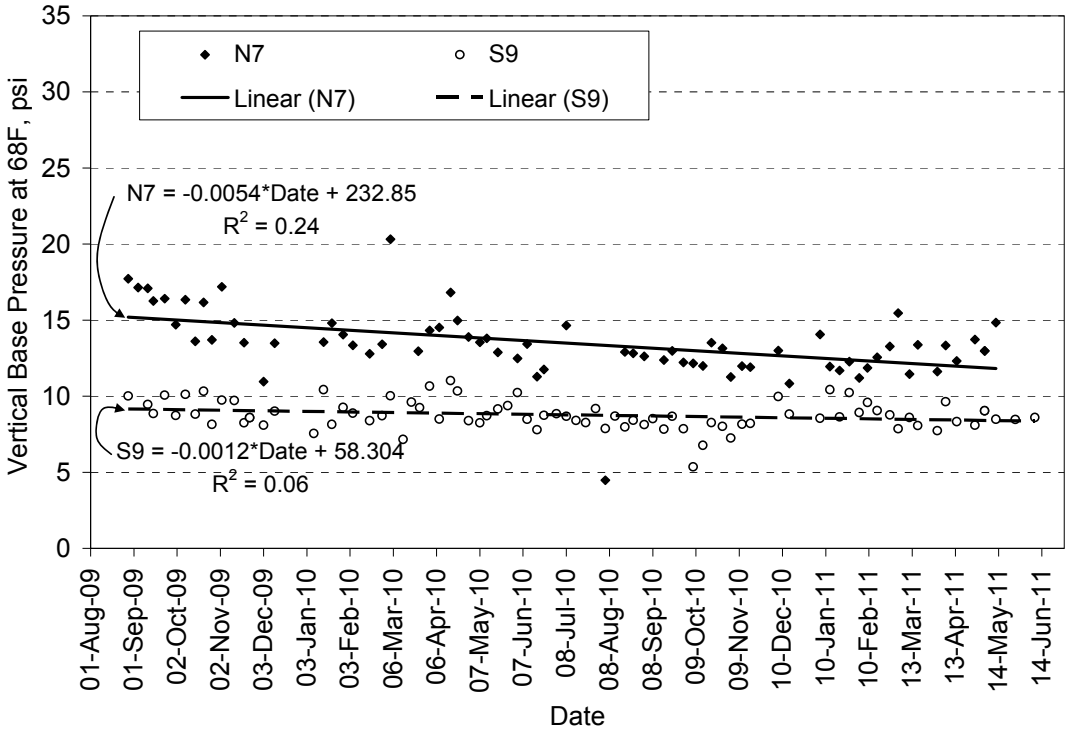

Figure 6.22 Base Pressure Under Single Axles vs. Date at 68F

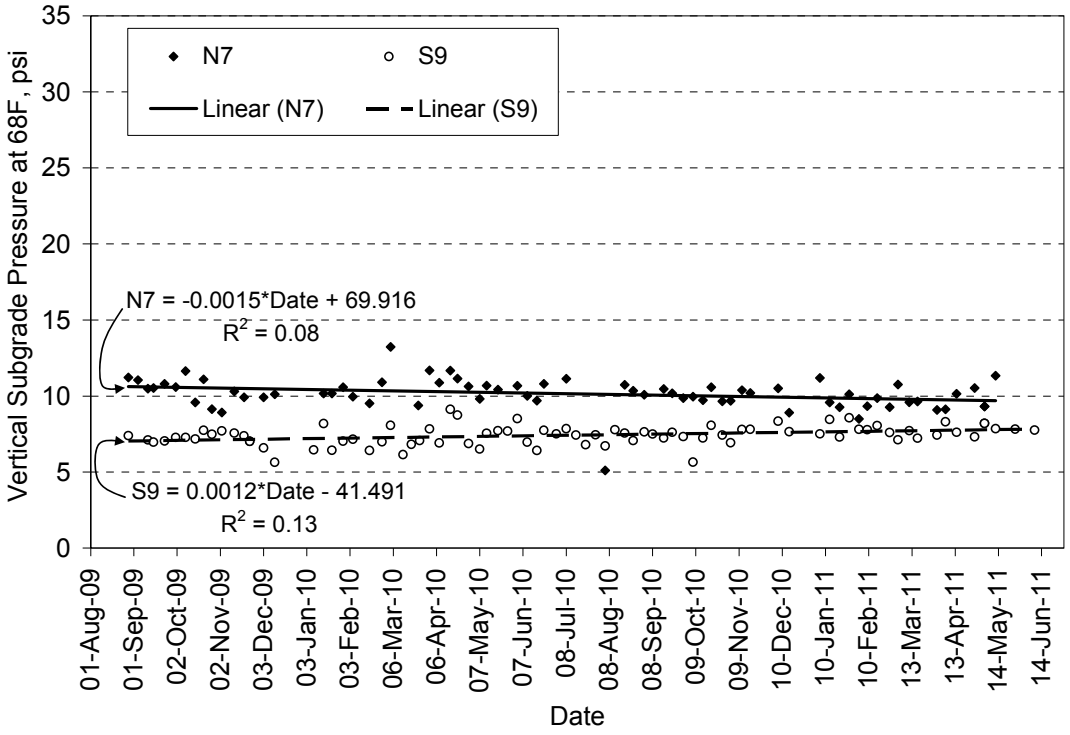

Figure 6.23 Subgrade Pressure Under Single Axles vs. Date at 68F

7. PAVEMENT PERFORMANCE

As of June 27, 2011 approximately 8.9 million ESALs had been applied to the test sections. At that time, there was no cracking evident on either of the sections. Weekly measurements of rut depths are plotted in Figure 7.1. Though the control section had greater rut depths than the Kraton section, both appear to be performing well in terms of rutting at less than 7 mm (1/4") after 8.9 million ESAL. Weekly-measured pavement roughness is plotted in Figure 7.2. Though the Kraton section was significantly rougher than the control section, this was attributed to as-built roughness over the first two subsections of N7. Figure 7.3 shows roughness versus distance in N7 at the start and end of the experiment subdivided into 25 ft subsections. Clearly, the high IRI of N7 is driven by the first two segements, which have gotten smoother over time.

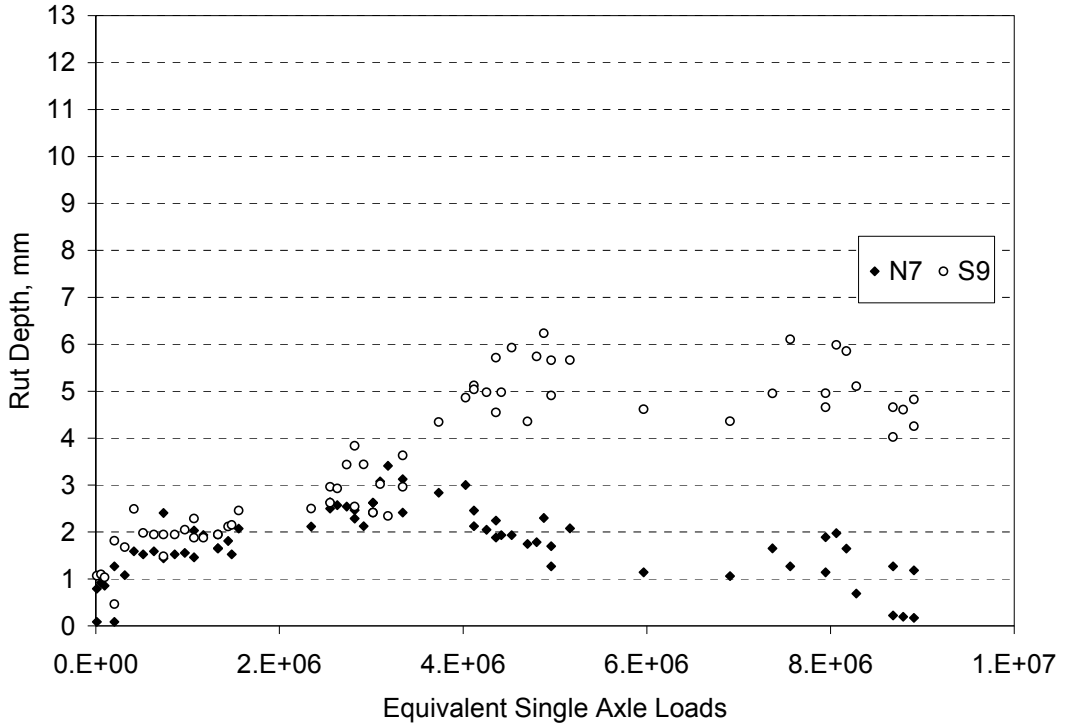

Figure 7.1 Measured Rut Depths

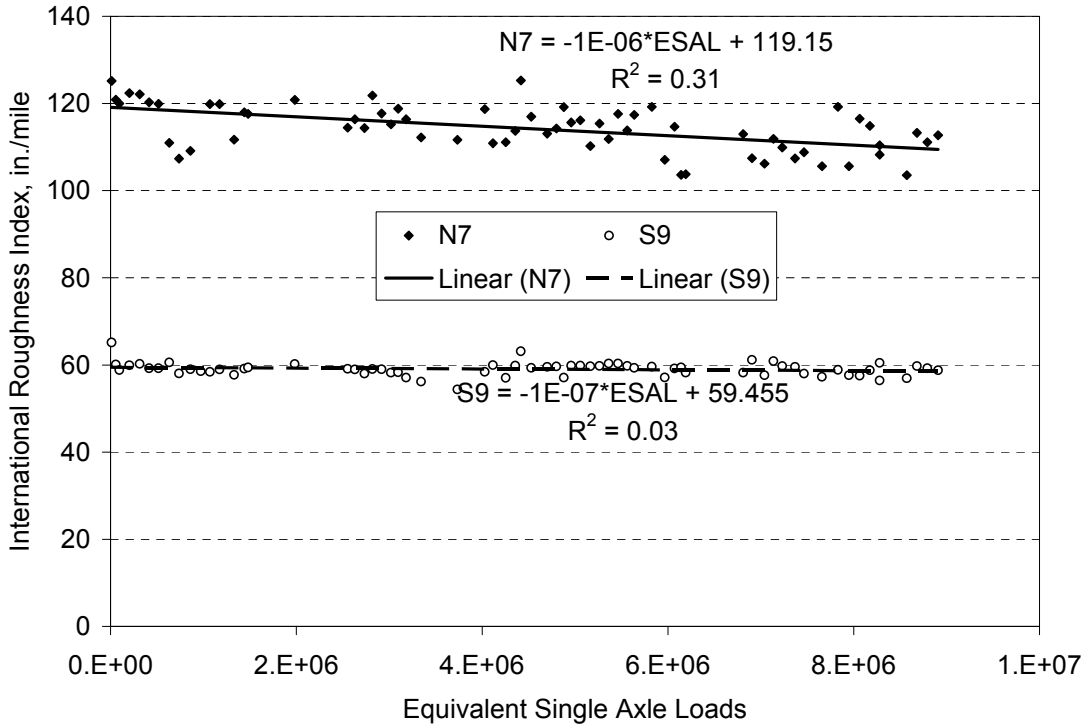

Figure 7.2 Measured IRI

Figure 7.3 Roughness vs. Distance in Kraton Section

8. KEY FINDINGS, CONCLUSIONS AND RECOMMENDATIONS

This report was intended to document the construction and testing conducted on the Kraton and control test sections during the first 22 months of testing at the NCAT Test Track. Based on the data presented herein the following key findings, conclusions and recommendations can be made:

1. The cooling of the AC layers during construction of the Kraton lifts, in addition to the control, was well-modeled by the MultiCool program. This finding will allow contractors to use MultiCool as a compaction planning/monitoring tool when using the Kraton high polymer mixture in the future.
2. Dynamic modulus testing of plant-produced laboratory-compacted specimens ranked the mixtures according to decreasing stiffness as follows: For the 9.5-mm NMAS surface mixes, the Kraton mix was significantly stiffer than the control surface mix. For the 19-mm NMAS mixes, the control intermediate layer was stiffer than the Kraton intermediate/base mixture and the control base mixture. As such, it appears that the additional polymer modification of the Kraton mixes were more impactful on dynamic modulus for the 9.5-mm NMAS mixtures.
3. Significant increases in AC dynamic modulus were achieved when switching from unconfined to confined test conditions. This was the case for the control and Kraton mixtures. This raises some question as to which mode of testing should be used for further structural modeling studies.
4. In bending beam fatigue testing the Kraton mixture lasted a greater number of cycles until failure than the control mixture at both 400 and 800 microstrain. Additionally, the Kraton base mixture had a fatigue endurance limit three times greater than the control base mixture.
5. Fatigue transfer functions developed from laboratory beam fatigue testing were combined with measured AC strain data from each test section to compare estimated fatigue performance between sections. An estimated 45 times improvement in fatigue performance was found when comparing N7 (Kraton) against S9 (control). This improvement was attributed to each section having approximately the same strain level while the Kraton base mixture had much improved fatigue performance over the control base mixture.
6. The results of APA testing on the control surface, control base, Kraton surface and Kraton base mixtures were all less than 5.5 mm of rutting after 8,000 cycles. It is expected that all mixtures will withstand the 10 million ESALs to be applied over the two year traffic cycle without developing 12.5 mm of rutting. Additionally, the Kraton mixtures had statistically lower rut depths than the control mixtures.
7. The Kraton surface mixture was least susceptible to rutting in the flow number test. While the Kraton base mixture had a higher flow number than the control mixtures, the results were not statistically significant.
8. The Kraton base mixture was least susceptible to low temperature cracking. The two Kraton mixtures and the control surface mixture each had critical low temperatures greater than the critical low temperature grade of the binder.
9. The control surface mixture had an energy ratio (ER) slightly higher than the Kraton surface mixture; however, both mixtures had ER 3.5 times higher than the required ER for trafficking of 1,000,000 ESALs per year.

10. All four mixtures (Kraton surface and base, and control surface and base) had TSR values greater than 0.80. The Kraton mixtures also had statistically higher splitting tensile strengths in both the conditioned and unconditioned states than the control mixtures.
11. Strong correlations between backcalculated composite AC moduli and mid-depth pavement temperature were determined for each test section. When applying a 3% RMSE limit on data from both sections, it was found that below 77°F, the control section trended toward higher modulus while above 77°F, the Kraton section was higher. Above 110°F, the Kraton material did not appear to be well-modeled by linear layered elasticity since no deflection basins were backcalculated above this temperature with RMSE below 3%. Future simulations should consider using more advanced modeling that accurately characterizes the material above 110°F.
12. Differences in backcalculated layer moduli at three reference temperatures (50, 68 and 110°F) were found to be statistically significant. At the two lower temperatures, as noted above, the control section had higher modulus while at 110°F, the Kraton section was higher. The increased modulus at high temperatures likely contributed to the improved rutting performance over the control section.
13. An examination of backcalculated composite AC modulus data versus test date through June 2011 did not indicate the initial stages of bottom-up fatigue cracking in either of the test sections. However, as noted below, signs of slippage and/or cracking may have been observed in the measured pavement response data.
14. Strong correlations between mid-depth pavement temperature and pavement response (AC strain, base pressure and subgrade pressure) were found for the control section. These strong correlations translated into relatively stable response measurements, normalized to 68°F, over time. This observation, combined with the normalized backcalculated AC modulus versus time, leads to the conclusion that the control section has not yet experienced cracking and/or slipping between layer interfaces.
15. The correlations between mid-depth pavement temperature and pavement response for the Kraton section were less strong that those observed in the control section. It appeared that mid-February, 2010 could be used as a cut-off date between “stable” and “erratic” data. Further forensic investigation is warranted at the end of the experiment to fully explore what occurred in the Kraton section at that time. These investigations may include trenching and coring to determine the extent and severity of cracking if present at the pavement surface.
16. Longitudinal strain measurements normalized to 50 and 68°F were found statistically equivalent between the two sections. At 110°F, the Kraton section had lower strain than the control. This is important since the Kraton section was 1.25 inches thinner than the control, yet had strain levels less than or equal to the control, depending upon temperature.
17. As of June, 2011, there was no cracking evident in either section. The control section had greater rutting than the Kraton section, but both were performing well at less than 7 mm after 8.9 million ESAL. The roughness of the Kraton section was higher than the control, but was attributed to an as-built rough spot in this section that has not increased since the start of traffic. Overall, both sections have not appreciably changed in roughness since August 2009. Monitoring will continue through the end of traffic in September 2011.
18. It is recommended to continue monitoring these sections to fully evaluate the initial pavement performance and trends developed herein. Further laboratory testing should be linked to final performance evaluations made at the conclusion of trafficking.

REFERENCES

1. Allen, D.L. and R.C. Graves. Variability in Measurement of In-Situ Material Properties. *Proceedings, Fourth International Conference on the Bearing Capacity of Roads and Airfields*, Vol. 2, 1994, pp. 989-1005.
2. Anderson, R. M. *Asphalt Modification and Additives*. The Asphalt Handbook MS-4, 7th ed., Asphalt Institute, Lexington, 2007, pp. 86-89.
3. Biligiri, K.P., K.E. Kaloush, M.W. Mamlouk, and M.W. Witczak, Rational Modeling of Tertiary Flow of Asphalt Mixtures, Transportation Research Record: Journal of the Transportation Research Board, No. 2001, 2007, pp. 63-72.
4. Buttlar, W.G., R. Roque, and B. Reid, "Automated Procedure for Generation of Creep Compliance Master Curve for Asphalt Mixtures," Transportation Research Record, 1630: 28-36, 1998.
5. Chadbourn, B. A., D. E. Newcomb, V. R. Voller, R. A. De Sombre, J. A. Luoma and D. H. Timm. *An Asphalt Paving Tool for Adverse Conditions*. Report MN/RC-1998-18, Minnesota Department of Transportation, 1998.
6. Erkens, S. M. J. G. *Asphalt Concrete Response (ACRe), Determination, Modelling and Prediction*. Ph.D. Dissertation, Delft University of Technology, The Netherlands, 2002.
7. Halper, W. M, and G. Holden. Styrenic Thermoplastic Elastomers in Handbook of Thermoplastic Elastomers. 2nd ed., B. M. Walker and C. P. Rader, Eds., Van Nostrand Reinhold, New York, 1988.
8. Hiltunen, D.R. and R. Roque. A Mechanics-Based Prediction Model for Thermal Cracking of Asphaltic Concrete Pavements, *Journal of the Association of Asphalt Paving Technologists*, Vol. 63, 1994, pp. 81-117.
9. Jones, G.M., M. I. Darter, and G. Littlefield. "Thermal Expansion-Contraction of Asphaltic Concrete," Journal of the Association of Asphalt Paving Technologists, 37, 1968: 56-97.
10. Kim, J., R. Roque, and B. Birgisson, "Integration of Thermal Fracture in the HMA Fracture Model," Journal of the Association of Asphalt Paving Technologists, 77, 2008: 631-662.
11. Kluttz, R. Q., A. A. A. Molenaar, M. F. C.van de Ven, M.R. Poot, X. Liu, A. Scarpas and E.J. Scholten. Modified Base Courses for Reduced Pavement Thickness and Improved Longevity. *Proceedings of the International Conference on Perpetual Pavement*, October, 2009, Columbus, OH.
12. Molenaar, A.A.A., M.F.C. van de Ven, X. Liu, A. Scarpas, T.O. Medani and E.J. Scholten. Advanced Mechanical Testing of Polymer Modified Base Course Mixes. *Proceedings, Asphalt – Road for Life,* Copenhagen, May 2008, pp. 842-853.
13. Morgan, P. and A. Mulder. The Shell Bitumen Industrial Handbook. Shell Bitumen, Surrey, 1995, pp. 161-196.
14. Noureldin, A.S. Influence of Stress Levels and Seasonal Variations on In Situ Pavement Layer Properties. *Transportation Research Record No. 1448*, Washington, D.C., 1994, pp. 16-24.
15. Priest, A.L. and D.H. Timm. *Methodology and Calibration of Fatigue Transfer Functions for Mechanistic-Empirical Flexible Pavement Design*. Report No. 06-03, National Center for Asphalt Technology, Auburn University, 2006.
16. Prowell, B.D., E.R. Brown, R.M. Anderson, J. Sias-Daniel, H. Von Quintus, S. Shen, S.H. Carpenter, S. Bhattacharjee and S. Maghsoodloo. *Validating the Fatigue Endurance Limit for Hot Mix Asphalt*. NCHRP Report 646, Transportation Research Board, Washington, D.C., 2010.

17. Roque, R. and W.G. Buttlar. The Development of a Measurement and Analysis System to Accurately Determine Asphalt Concrete Properties Using the Indirect Tensile Mode. *Journal of the Association of Asphalt Paving Technologists*, Vol. 61, 1992, pp. 304-332.
18. Roque, R., B. Birgisson, C. Drakos, and B. Dietrich. Development and Field Evaluation of Energy-Based Criteria for Top-down Cracking Performance of Hot Mix Asphalt, *Journal of the Association of Asphalt Paving Technologists*, Vol. 73, 2004, pp. 229-260.
19. Scarpas, A. and J. Blaauwendraad. Experimental Calibration of a Constitutive Model for Asphaltic Concrete. *Proceedings of Euro-C Conference on the Computational Modelling of Concrete Structures*, Badgastein, Austria, April 1998.
20. Scientific Electronic Library Online. http://www.scielo.br/img/fbpe/mr/v4n3/a13fig5a.gif, accessed July 27, 2010.
21. Soules, T.F., R. F. Busbey, S. M. Rekhson, A. Markovsky, and M. A. Burke. "Finite-Element Calculation of Stresses in Glass Parts Undergoing Viscous Relaxation," Journal of the American Ceramic Society, 70 (2), 1987: 90-95.
22. Taylor, A.J. and D.H. Timm. *Mechanistic Characterization of Resilient Moduli for Unbound Pavement Layer Materials*. Report No. 09-06, National Center for Asphalt Technology, Auburn University, 2009.
23. Timm, D.H. *Design, Construction, and Instrumentation of the 2006 Test Track Structural Study*. Report No. 09-01, National Center for Asphalt Technology, Auburn University, 2009.
24. Timm, D.H. and A.L. Priest, "Wheel Wander at the NCAT Test Track," Report No. 05-02, National Center for Asphalt Technology, Auburn University, 2005.
25. Timm, D.H. and A.L. Priest, "Material Properties of the 2003 NCAT Test Track Structural Study," Report No. 06-01, National Center for Asphalt Technology, Auburn University, 2006.
26. Timm, D.H. and A.L. Priest. Flexible Pavement Fatigue Cracking and Measured Strain Response at the NCAT Test Track. *Proceedings of the 87th Annual Transportation Research Board*, Washington, D.C., 2008.
27. Timm, D.H., D.E. Newcomb and B. Birgisson. *Mechanistic-Empirical Flexible Pavement Thickness Design: The Minnesota Method*. Staff Paper, MN/RC-P99-10, Minnesota Department of Transportation, St. Paul, MN, 1999.
28. Timm, D. H., V. R. Voller, E. Lee and J. Harvey. Calcool: A multi-layer Asphalt Pavement Cooling Tool for Temperature Prediction During Construction. *The International Journal of Pavement Engineering*, Vol. 2, 2001, pp. 169-185.
29. Timm, D.H., A.L. Priest and T.V. McEwen. *Design and Instrumentation of the Structural Pavement Experiment at the NCAT Test Track*. Report No. 04-01, National Center for Asphalt Technology, Auburn University, 2004.
30. Timm, D.H., M. M. Robbins and R.Q. Kluttz, "Full-Scale Structural Characterization of a Highly Polymer-Modified Asphalt Pavement," Proceedings of the 90th Annual Transportation Research Board, Washington, D.C., 2011.
31. van de Ven, M.F.C., M.R. Poot and T.O. Medani. *Advanced Mechanical Testing of Polymer Modified Asphalt Mixtures.* Report 7-06-135-3, Road and Rail Engineering, Delft University of Technology, the Netherlands, April 2007.
32. Vargas-Nordcbeck, A. and D.H. Timm. Validation of Cooling Curves Prediction Model for Non-Conventional Asphalt Concrete Mixtures. *Transportation Research Record*, Journal of the Transportation Research Board, Washington, D.C., accepted for publication, 2011.

33. von Quintus, H. *Quantification of the Effects of Polymer-Modified Asphalt*. Engineering Report ER 215, Asphalt Institute, 2005, pp. 1-8.
34. Willis, J.R. and D.H. Timm. *Field-Based Strain Thresholds for Flexible Perpetual Pavement Design*. Report No. 09-09, National Center for Asphalt Technology, Auburn University, 2009.

APPENDIX A – MIX DESIGN AND AS BUILT AC PROPERTIES

10/5/2009

Quadrant: N
Section: 7 *Mix Type = Surface - Kraton*
Sublot: 1

Laboratory Diary

General Descoription of Mix and Materials

Design Method:	Super
Compactive Effort:	80 gyrations
Binder Performance Grade:	94-xx
Modifier Type:	7.5% SBS
Aggregate Type:	Grn/Sand/Lms
Design Gradation Type:	Fine

Avg. Lab Properties of Plant Produced Mix

Sieve Size	Design	QC
25 mm (1"):	100	100
19 mm (3/4"):	100	100
12.5 mm (1/2"):	100	100
9.5 mm (3/8"):	100	100
4.75 mm (#4):	77	82
2.36 mm (#8):	60	63
1.18 mm (#16):	45	48
0.60 mm (#30):	31	32
0.30 mm (#50):	16	17
0.15 mm (#100):	9	10
0.075 mm (#200):	5.7	6.6
Binder Content (Pb):	5.9	6.3
Eff. Binder Content (Pbe):	5.3	5.7
Dust-to-Binder Ratio:	1.1	1.2
Rice Gravity (Gmm):	2.474	2.468
Avg. Bulk Gravity (Gmb):	2.375	2.367
Avg Air Voids (Va):	4.0	4.1
Agg. Bulk Gravity (Gsb):	2.667	2.678
Avg VMA:	16.2	17.2
Avg. VFA:	75	76

Construction Diary

Relevant Conditions for Construction

Completion Date:	July 22, 2009
24 Hour High Temperature (F):	88
24 Hour Low Temperature (F):	60
24 Hour Rainfall (in):	0.00
Planned Subot Lift Thickness (in):	1.3
Paving Machine:	Roadtec

Plant Configuration and Placement Details

Component	% Setting
Asphalt Content (Plant Setting)	6.2
89 Columbus Granite	36.0
8910 Opelika Limestone Screenings	23.0
M10 Columbus Granite	13.0
Shorter Coarse Sand	28.0

As-Built Sublot Lift Thickness (in):	1.1
Total Thickness of All 2009 Sublots (in):	5.8
Approx. Underlying HMA Thickness (in):	0.0
Type of Tack Coat Utilized:	NTSS-1HM
Target Tack Application Rate (gal/sy):	0.07
Approx. Avg. Temperature at Plant (F):	345
Avg. Measured Mat Compaction:	93.7%

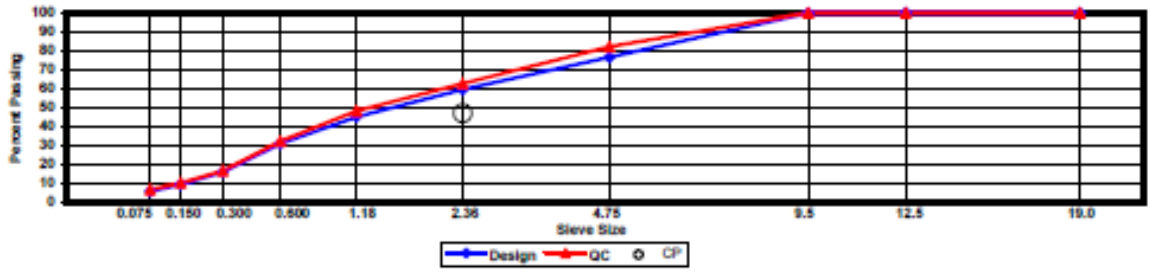

General Notes:
1) Mixes are referenced by quadrant (E=East, N=North, W=West, and S=South), section # (sequential) and sublot (top=1);
3) The total HMA thickness of all structural study sections (N1-N11 and S8-S12) ranges from 5-3/4 to 14 inches by design;
3) All non-structural sections are supprted by a uniform perpetual foundation in order to study surface mix performance;
4) SMA and OGFC refer to stone matrix asphalt and open-graded friction course, respectively; and
5) All liquid asphalt purchased for use in Track reconstruction contained LOF 6500 antistrip additive at a rate of 0.5 percent

10/5/2009

Quadrant: N
Section: 7 *Mix Type = Intermediate - Kraton*
Sublot: 2

Laboratory Diary

General Description of Mix and Materials

Design Method:	Kraton
Compactive Effort:	80 gyrations
Binder Performance Grade:	94-xx
Modifier Type:	7.5% SBS
Aggregate Type:	Lms/Sand/Gm
Design Gradation Type:	Fine

Avg. Lab Properties of Plant Produced Mix

Sieve Size	Design	QC
25 mm (1"):	100	98
19 mm (3/4"):	93	92
12.5 mm (1/2"):	82	82
9.5 mm (3/8"):	71	73
4.75 mm (#4):	52	56
2.36 mm (#8):	45	46
1.18 mm (#16):	35	37
0.60 mm (#30):	24	25
0.30 mm (#50):	12	13
0.15 mm (#100):	7	8
0.075 mm (#200):	3.9	5.2
Binder Content (Pb):	4.6	4.6
Eff. Binder Content (Pbe):	4.2	4.2
Dust-to-Binder Ratio:	0.9	1.2
Rice Gravity (Gmm):	2.570	2.549
Avg. Bulk Gravity (Gmb):	2.467	2.423
Avg Air Voids (Va):	4.0	4.9
Agg. Bulk Gravity (Gsb):	2.737	2.712
Avg VMA:	14.0	14.8
Avg. VFA:	72	67

Construction Diary

Relevant Conditions for Construction

Completion Date:	July 21, 2009
24 Hour High Temperature (F):	88
24 Hour Low Temperature (F):	60
24 Hour Rainfall (in):	0.00
Planned Subot Lift Thickness (in):	2.3
Paving Machine:	Roadtec

Plant Configuration and Placement Details

Component	% Setting
Asphalt Content (Plant Setting)	4.8
78 Opelika Limestone	30.0
57 Opelika Limestone	18.0
M10 Columbus Granite	25.0
Shorter Coarse Sand	27.0

As-Built Sublot Lift Thickness (in):	2.1
Total Thickness of All 2009 Sublots (in):	5.8
Approx. Underlying HMA Thickness (in):	0.0
Type of Tack Coat Utilized:	NTSS-1HM
Target Tack Application Rate (gal/sy):	0.07
Approx. Avg. Temperature at Plant (F):	345
Avg. Measured Mat Compaction:	92.7%

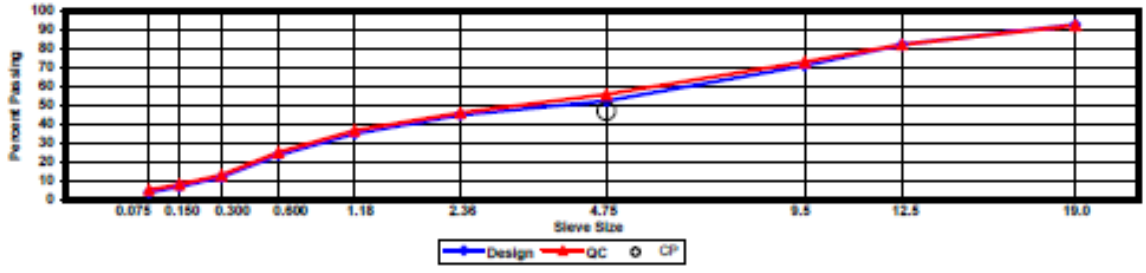

General Notes:

1) Mixes are referenced by quadrant (E=East, N=North, W=West, and S=South), section # (sequential) and sublot (top=1);
3) The total HMA thickness of all structural study sections (N1-N11 and S8-S12) ranges from 5-3/4 to 14 inches by design;
3) All non-structural sections are supprted by a uniform perpetual foundation in order to study surface mix performance;
4) SMA and OGFC refer to stone matrix asphalt and open-graded friction course, respectively; and
5) All liquid asphalt purchased for use in Track reconstruction contained LOF 6500 antistrip additive at a rate of 0.5 percent

10/5/2009

Quadrant: N
Section: 7 *Mix Type = Base - Kraton*
Sublot: 3

Laboratory Diary

General Descrription of Mix and Materials

Design Method:	Kraton
Compactive Effort:	80 gyrations
Binder Performance Grade:	94-xx
Modifier Type:	7.5% SBS
Aggregate Type:	Lms/Sand/Gm
Design Gradation Type:	Fine

Avg. Lab Properties of Plant Produced Mix

Sieve Size	Design	QC
25 mm (1"):	100	98
19 mm (3/4"):	93	91
12.5 mm (1/2"):	82	81
9.5 mm (3/8"):	71	72
4.75 mm (#4):	52	55
2.36 mm (#8):	45	45
1.18 mm (#16):	35	36
0.60 mm (#30):	24	25
0.30 mm (#50):	12	12
0.15 mm (#100):	7	7
0.075 mm (#200):	3.9	4.6
Binder Content (Pb):	4.6	4.6
Eff. Binder Content (Pbe):	4.2	4.2
Dust-to-Binder Ratio:	0.9	1.1
Rice Gravity (Gmm):	2.570	2.545
Avg. Bulk Gravity (Gmb):	2.467	2.427
Avg Air Voids (Va):	4.0	4.6
Agg. Bulk Gravity (Gsb):	2.737	2.707
Avg VMA:	14.0	14.5
Avg. VFA:	72	68

Construction Diary

Relevant Conditions for Construction

Completion Date:	July 20, 2009
24 Hour High Temperature (F):	85
24 Hour Low Temperature (F):	60
24 Hour Rainfall (in):	0.00
Planned Subot Lift Thickness (in):	2.3
Paving Machine:	Roadtec

Plant Configuration and Placement Details

Component	% Setting
Asphalt Content (Plant Setting)	4.8
78 Opelika Limestone	30.0
57 Opelika Limestone	18.0
M10 Columbus Granite	25.0
Shorter Coarse Sand	27.0

As-Built Sublot Lift Thickness (in):	2.5
Total Thickness of All 2009 Sublots (in):	5.8
Approx. Underlying HMA Thickness (in):	0.0
Type of Tack Coat Utilized:	NA
Target Tack Application Rate (gal/sy):	NA
Approx. Avg. Temperature at Plant (F):	340
Avg. Measured Mat Compaction:	92.8%

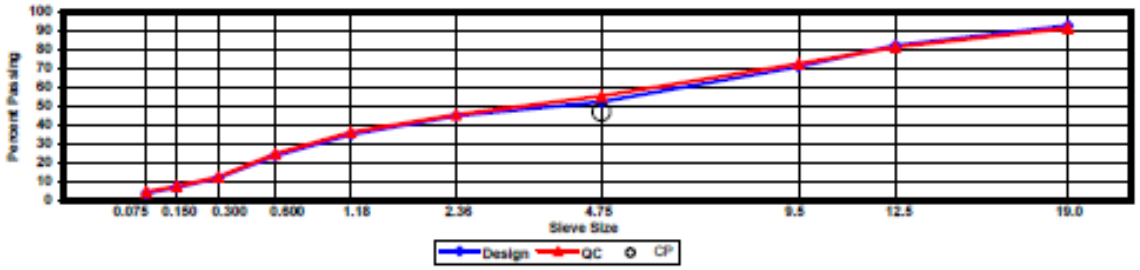

General Notes:

1) Mixes are referenced by quadrant (E=East, N=North, W=West, and S=South), section # (sequential) and sublot (top=1);
3) The total HMA thickness of all structural study sections (N1-N11 and S8-S12) ranges from 5-3/4 to 14 inches by design;
3) All non-structural sections are supprted by a uniform perpetual foundation in order to study surface mix performance;
4) SMA and OGFC refer to stone matrix asphalt and open-graded friction course, respectively; and
5) All liquid asphalt purchased for use in Track reconstruction contained LOF 6500 antistrip additive at a rate of 0.5 percent

10/5/2009

Quadrant: S
Section: 9 *Mix Type = Surface - Control*
Sublot: 1

Laboratory Diary

General Descciption of Mix and Materials

Design Method:	Super
Compactive Effort:	80 gyrations
Binder Performance Grade:	76-22
Modifier Type:	SBS
Aggregate Type:	Grn/Sand/Lms
Design Gradation Type:	Fine

Avg. Lab Properties of Plant Produced Mix

Sieve Size	Design	QC
25 mm (1"):	100	100
19 mm (3/4"):	100	100
12.5 mm (1/2"):	100	100
9.5 mm (3/8"):	100	100
4.75 mm (#4):	78	81
2.36 mm (#8):	60	59
1.18 mm (#16):	46	46
0.60 mm (#30):	31	31
0.30 mm (#50):	16	16
0.15 mm (#100):	10	9
0.075 mm (#200):	5.8	6.0
Binder Content (Pb):	5.8	6.1
Eff. Binder Content (Pbe):	5.1	5.4
Dust-to-Binder Ratio:	1.1	1.1
Rice Gravity (Gmm):	2.483	2.472
Avg. Bulk Gravity (Gmb):	2.384	2.374
Avg Air Voids (Va):	4.0	4.0
Agg. Bulk Gravity (Gsb):	2.667	2.670
Avg VMA:	15.8	16.5
Avg. VFA:	75	76

Construction Diary

Relevant Conditions for Construction

Completion Date:	July 16, 2009
24 Hour High Temperature (F):	92
24 Hour Low Temperature (F):	74
24 Hour Rainfall (in):	0.00
Planned Subot Lift Thickness (in):	1.3
Paving Machine:	Roadtec

Plant Configuration and Placement Details

Component	% Setting
Asphalt Content (Plant Setting)	6.5
89 Columbus Granite	36.0
8910 Opelika Limestone Screenings	23.0
M10 Columbus Granite	13.0
Shorter Coarse Sand	28.0

As-Built Sublot Lift Thickness (in):	1.2
Total Thickness of All 2009 Sublots (in):	7.0
Approx. Underlying HMA Thickness (in):	0.0
Type of Tack Coat Utilized:	NTSS-1HM
Target Tack Application Rate (gal/sy):	0.04
Approx. Avg. Temperature at Plant (F):	335
Avg. Measured Mat Compaction:	93.1%

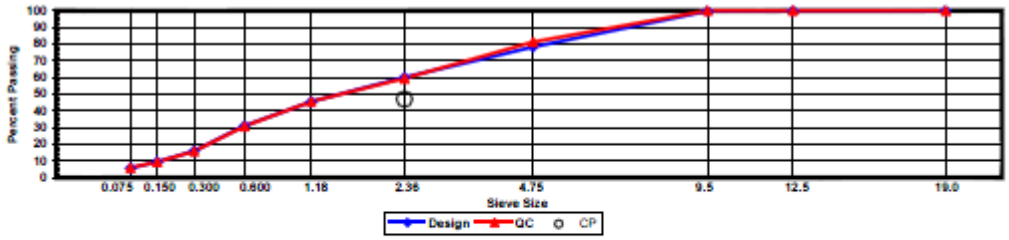

General Notes:

1) Mixes are referenced by quadrant (E=East, N=North, W=West, and S=South), section # (sequential) and sublot (top=1);
3) The total HMA thickness of all structural study sections (N1-N11 and S8-S12) ranges from 5-3/4 to 14 inches by design;
3) All non-structural sections are supprted by a uniform perpetual foundation in order to study surface mix performance;
4) SMA and OGFC refer to stone matrix asphalt and open-graded friction course, respectively; and
5) All liquid asphalt purchased for use in Track reconstruction contained LOF 6500 antistrip additive at a rate of 0.5 percent

10/5/2009

Quadrant: S
Section: 9 *Mix Type = Intermediate - Control*
Sublot: 2

Laboratory Diary

General Desccription of Mix and Materials

Design Method:	Super
Compactive Effort:	80 gyrations
Binder Performance Grade:	76-22
Modifier Type:	SBS
Aggregate Type:	Lms/Sand/Grn
Design Gradation Type:	Fine

Avg. Lab Properties of Plant Produced Mix

Sieve Size	Design	QC
25 mm (1"):	100	99
19 mm (3/4"):	93	92
12.5 mm (1/2"):	82	84
9.5 mm (3/8"):	71	76
4.75 mm (#4):	52	57
2.36 mm (#8):	45	47
1.18 mm (#16):	35	38
0.60 mm (#30):	24	26
0.30 mm (#50):	12	15
0.15 mm (#100):	7	9
0.075 mm (#200):	3.9	5.3
Binder Content (Pb):	4.7	4.4
Eff. Binder Content (Pbe):	4.1	3.9
Dust-to-Binder Ratio:	0.9	1.4
Rice Gravity (Gmm):	2.575	2.551
Avg. Bulk Gravity (Gmb):	2.472	2.439
Avg Air Voids (Va):	4.0	4.4
Agg. Bulk Gravity (Gsb):	2.737	2.695
Avg VMA:	13.9	13.5
Avg. VFA:	71	68

Construction Diary

Relevant Conditions for Construction

Completion Date:	July 14, 2009
24 Hour High Temperature (F):	93
24 Hour Low Temperature (F):	72
24 Hour Rainfall (in):	0.00
Planned Subot Lift Thickness (in):	2.8
Paving Machine:	Roadtec

Plant Configuration and Placement Details

Component	% Setting
Asphalt Content (Plant Setting)	4.7
78 Opelika Limestone	30.0
57 Opelika Limestone	18.0
M10 Columbus Granite	25.0
Shorter Coarse Sand	27.0

As-Built Sublot Lift Thickness (in):	2.8
Total Thickness of All 2009 Sublots (in):	7.0
Approx. Underlying HMA Thickness (in):	0.0
Type of Tack Coat Utilized:	NTSS-1HM
Target Tack Application Rate (gal/sy):	0.07
Approx. Avg. Temperature at Plant (F):	335
Avg. Measured Mat Compaction:	92.8%

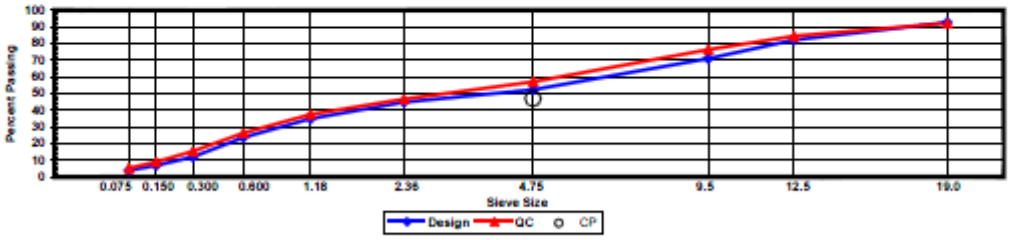

General Notes:

1) Mixes are referenced by quadrant (E=East, N=North, W=West, and S=South), section # (sequential) and sublot (top=1);
3) The total HMA thickness of all structural study sections (N1-N11 and S8-S12) ranges from 5-3/4 to 14 inches by design;
3) All non-structural sections are supprted by a uniform perpetual foundation in order to study surface mix performance;
4) SMA and OGFC refer to stone matrix asphalt and open-graded friction course, respectively; and
5) All liquid asphalt purchased for use in Track reconstruction contained LOF 6500 antistrip additive at a rate of 0.5 percent

10/5/2009

Quadrant: S
Section: 9
Sublot: 3

Mix Type = Base - Control

Laboratory Diary

General Descciption of Mix and Materials

Design Method:	Super
Compactive Effort:	80 gyrations
Binder Performance Grade:	67-22
Modifier Type:	NA
Aggregate Type:	Lms/Sand/Grn
Design Gradation Type:	Fine

Avg. Lab Properties of Plant Produced Mix

Sieve Size	Design	QC
25 mm (1"):	100	99
19 mm (3/4"):	93	95
12.5 mm (1/2"):	84	87
9.5 mm (3/8"):	73	77
4.75 mm (#4):	55	56
2.36 mm (#8):	47	46
1.18 mm (#16):	36	37
0.60 mm (#30):	25	26
0.30 mm (#50):	14	15
0.15 mm (#100):	8	9
0.075 mm (#200):	4.6	5.1
Binder Content (Pb):	4.6	4.7
Eff. Binder Content (Pbe):	4.1	4.2
Dust-to-Binder Ratio:	1.1	1.2
Rice Gravity (Gmm):	2.574	2.540
Avg. Bulk Gravity (Gmb):	2.471	2.439
Avg Air Voids (Va):	4.0	4.0
Agg. Bulk Gravity (Gsb):	2.738	2.699
Avg VMA:	13.9	13.9
Avg. VFA:	71	71

Construction Diary

Relevant Conditions for Construction

Completion Date:	July 3, 2009
24 Hour High Temperature (F):	92
24 Hour Low Temperature (F):	69
24 Hour Rainfall (in):	0.00
Planned Subot Lift Thickness (in):	3.0
Paving Machine:	Roadtec

Plant Configuration and Placement Details

Component	% Setting
Asphalt Content (Plant Setting)	4.9
78 Opelika Limestone	30.0
57 Opelika Limestone	18.0
M10 Columbus Granite	25.0
Shorter Coarse Sand	27.0

As-Built Sublot Lift Thickness (in):	3.0
Total Thickness of All 2009 Sublots (in):	7.0
Approx. Underlying HMA Thickness (in):	0.0
Type of Tack Coat Utilized:	NA
Target Tack Application Rate (gal/sy):	NA
Approx. Avg. Temperature at Plant (F):	325
Avg. Measured Mat Compaction:	92.6%

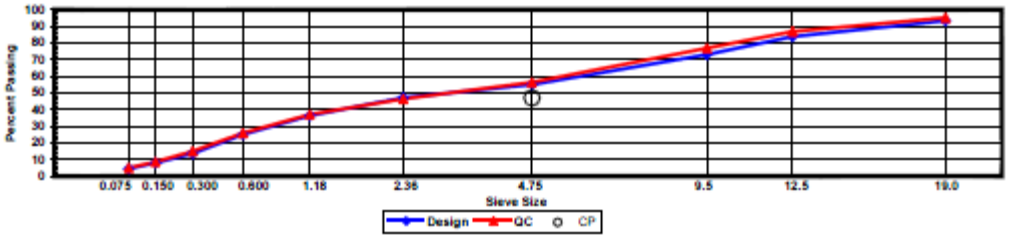

General Notes:

1) Mixes are referenced by quadrant (E=East, N=North, W=West, and S=South), section # (sequential) and sublot (top=1);
3) The total HMA thickness of all structural study sections (N1-N11 and S8-S12) ranges from 5-3/4 to 14 inches by design;
3) All non-structural sections are supprted by a uniform perpetual foundation in order to study surface mix performance;
4) SMA and OGFC refer to stone matrix asphalt and open-graded friction course, respectively; and
5) All liquid asphalt purchased for use in Track reconstruction contained LOF 6500 antistrip additive at a rate of 0.5 percent

APPENDIX B – SURVEYED PAVEMENT DEPTHS

TABLE B1. Surveyed Pavement Depths

				Layer Thickness, in.				
Section-Location	Section	RL	Offset	Lift 1	Lift 2	Lift 3	Total AC	Aggregate Base
N7-1	N7	1	I	1.236	2.064	2.604	5.904	4.524
N7-2	N7	1	B	0.996	2.280	2.616	5.892	4.92
N7-3	N7	1	O	1.140	2.220	2.616	5.976	5.016
N7-4	N7	2	I	1.164	1.956	2.568	5.688	4.932
N7-5	N7	2	B	1.200	2.208	2.544	5.952	4.836
N7-6	N7	2	O	1.044	2.292	2.820	6.156	4.416
N7-7	N7	3	I	0.936	2.316	2.388	5.640	6.432
N7-8	N7	3	B	0.840	2.220	2.268	5.328	6.672
N7-9	N7	3	O	0.948	2.052	2.292	5.292	6.816
N7-10	N7	4	I	1.068	1.740	2.784	5.592	5.928
N7-11	N7	4	B	0.792	1.872	2.592	5.256	6.348
N7-12	N7	4	O	0.756	1.836	2.448	5.040	5.376
S9-1	S9	1	I	1.524	2.784	2.952	7.260	5.868
S9-2	S9	1	B	1.272	2.916	2.988	7.176	5.628
S9-3	S9	1	O	1.224	2.772	3.048	7.044	5.808
S9-4	S9	2	I	1.212	2.868	2.988	7.068	5.856
S9-5	S9	2	B	1.188	2.892	2.856	6.936	6.036
S9-6	S9	2	O	1.104	2.916	2.832	6.852	6.12
S9-7	S9	3	I	1.140	2.796	2.880	6.816	5.208
S9-8	S9	3	B	1.164	2.640	3.060	6.864	5.46
S9-9	S9	3	O	1.164	2.712	3.072	6.948	5.832
S9-10	S9	4	I	1.320	2.628	3.324	7.272	5.628
S9-11	S9	4	B	1.152	2.700	3.132	6.984	5.88
S9-12	S9	4	O	1.128	2.724	2.976	6.828	6.216

RL = Random Location
Offset: B = Betwee Wheelpath, I = Inside Wheelpath, O = Outside Wheelpath

APPENDIX C – BINDER GRADING

Table C.1 PG Grading of Highly Modified Binder Used in All Lifts of Sections N7

Test Method			Test Results	Specification
Original Binder				
Rotational Viscosity @ 135°C, AASHTO T 316, PaS			3.575	≤ 3 PaS
Dynamic Shear Rheometer, AASHTO T 315				
Test Temperature, °C	G*, kPa	Phase Angle, δ°	G* / sinδ, kPa	
100	0.8	48.9	1.06	≥ 1.00 kPa
106	0.55	55.7	0.67	
Rolling Thin Film (RTFO) Aged Binder, AASHTO T 240				
Mass Change, %			-0.163	≤ 1.00%
Dynamic Shear Rheometer, AASHTO T 315				
Test Temperature, °C	G*, kPa	Phase Angle, δ°	G* / sinδ, kPa	
88	2.4	50.4	3.11	≥ 2.20 kPa
94	1.665	51.3	2.13	
Pressure Aging Vessel (PAV) Aged Binder, AASHTO R28				
Dynamic Shear Rheometer, AASHTO T 315				
Test Temperature, °C	G*, kPa	Phase Angle, δ°	G* sinδ, kPa	
19	6401	41.1	4207	≤ 5,000 kPa
16	9399	39	5917	
Bending Beam Rheometer (BBR), AASHTO T313				
Test Temperature, °C				
-12	Stiffness, Mpa		121	≤ 300 Mpa
	m-value		0.339	≥ 0.300
-18	Stiffness, Mpa		277	
	m-value		0.286	
True Grade	93.5 -26.4			
PG Grade	88 -22			

1. DSR Original: T_{max}
   Temperature at which G*/sinδ = 1.00 kPa — 100.8
2. DSR RTFO: T_{max}
   Temperature at which G*/sinδ = 2.20 kPa — 93.5
3. DSR PAV: T_{int}
   Temperature at which G*sinδ = 5,000 kPa — 17.5
4. BBR PAV: T_{min}
   Tempearautre at which S(t) = 300 Mpa — -28.9
   Temperature at which m = 0.300 — -26.4

Table C.2 PG Grading of Virgin Binder Used in Base Lift of Section S9

Test Method			Test Results	Specification
Original Binder				
Rotational Viscosity @ 135°C, AASHTO T 316, PaS				≤ 3 PaS
Dynamic Shear Rheometer AASHTO T 315				
Test Temperature, °C	G*, kPa	Phase Angle δ, °	G* / sinδ, kPa	
64	1.91	84.9	1.91	≥ 1.00 kPa
70	0.94	86.3	0.94	
Rolling Thin Film (RTFO) Aged Binder, AASHTO T 240				
Mass Change, %				≤ 1.00%
Dynamic Shear Rheometer AASHTO T 315				
Test Temperature, °C	G*, kPa	Phase Angle δ, °	G* / sinδ, kPa	
70	2.40	82.4	2.42	≥ 2.20 kPa
76	1.186	84.5	1.19	
Pressure Aging Vessel (PAV) Aged Binder, AASHTO R28				
Dynamic Shear Rheometer AASHTO T 315				
Test Temperature, °C	G*, kPa	Phase Angle δ, °	G* sinδ, kPa	
22	6245	41.9	4169	≤ 5,000 kPa
19	9212	39.3	5837	
Bending Beam Rheometer (BBR) AASHTO T313				
Test Temperature, °C				
-12	Stiffness, Mpa		141	≤ 300 Mpa
	m-value		0.333	≥ 0.300
-18	Stiffness, Mpa		313	
	m-value		0.283	
True Grade	69.5 -26.0			
PG Grade	64 - 22			

1. DSR Original: T_{max}

   Temperature at which G*/sinδ = 1.00 kPa — 69.5

2. DSR RTFO: T_{max}

   Temperature at which G*/sinδ = 2.20 kPa — 70.8

3. DSR PAV: T_{int}

   Temperature at which G*sinδ = 5,000 kPa — 20.4

4. BBR PAV: T_{min}

   Temperature at which S(t) = 300 Mpa — -27.5

   Temperature at which m = 0.300 — -26.0

Table C.3 PG Grading of Virgin Binder Used in Intermediate Lift of Section S9

Test Method			Test Results	Specification
Original Binder				
Rotational Viscosity @ 135°C, AASHTO T 316, PaS			1.444	≤ 3 PaS
Dynamic Shear Rheometer AASHTO T 315				
Test Temperature, °C	G*, kPa	Phase Angle δ, °	G* / sinδ, kPa	
76	1.22	84.1	1.27	≥ 1.00 kPa
82	0.71	76.3	0.73	
Rolling Thin Film (RTFO) Aged Binder, AASHTO T 240				
Mass Change, %			-0.042	≤ 1.00%
Dynamic Shear Rheometer AASHTO T 315				
Test Temperature, °C	G*, kPa	Phase Angle δ, °	G* / sinδ, kPa	
76	2.83	67.9	3.06	≥ 2.20 kPa
82	1.66	70	1.77	
Pressure Aging Vessel (PAV) Aged Binder, AASHTO R28				
Dynamic Shear Rheometer AASHTO T 315				
Test Temperature, °C	G*, kPa	Phase Angle δ, °	G* sinδ, kPa	
22	6383	41.0	4185	≤ 5,000 kPa
19	9350	38.6	5834	
Bending Beam Rheometer (BBR) AASHTO T313				
Test Temperature, °C				
-12	Stiffness, Mpa		135	≤ 300 Mpa
	m-value		0.326	≥ 0.300
-18	Stiffness, Mpa		285	
	m-value		0.282	
True Grade	78.6 -25.5			
PG Grade	76 - 22			

1. DSR Original: T_{max}

   Temperature at which G*/sinδ = 1.00 kPa — 78.6

2. DSR RTFO: T_{max}

   Temperature at which G*/sinδ = 2.20 kPa — 79.6

3. DSR PAV: T_{int}

   Temperature at which G*sinδ = 5,000 kPa — 20.4

4. BBR PAV: T_{min}

   Temperature at which S(t) = 300 Mpa — -28.6

   Temperature at which m = 0.300 — -25.5

Table C.4 PG Grading of Binder Extracted from Mixtures Used in Surface Lift of Section S9

Test, Method			Test Results	Specification
Rolling Thin Film (RTFO) Aged Binder, AASHTO T 240				
Rotational Viscosity @ 135°C, AASHTO T 316, PaS			2.287	≤ 3 PaS
Dynamic Shear Rheometer AASHTO T 315				
Test Temperature, °C	G*, kPa	Phase Angle δ, °	G* / sinδ, kPa	
76	3.45	67.3	3.74	≥ 2.20 kPa
82	2.00	69.5	2.14	
Pressure Aging Vessel (PAV) Aged Binder, AASHTO R28				
Dynamic Shear Rheometer AASHTO T 315				
Test Temperature, °C	G*, kPa	Phase Angle δ, °	G* sinδ, kPa	
22	7607	40.7	4964	≤ 5,000 kPa
19	11060	38.5	6880	
Bending Beam Rheometer (BBR) AASHTO T313				
Test Temperature, °C				
-12	Stiffness, Mpa		124	≤ 300 Mpa
	m-value		0.317	≥ 0.300
-18	Stiffness, Mpa		277	
	m-value		0.279	
True Grade	81.7 -24.7			
PG Grade	76 - 22			

1. DSR RTFO: T_{max}

   Temperature at which G*/sinδ = 2.20 kPa — 81.7

2. DSR PAV: T_{int}

   Temperature at which G*sinδ = 5,000 kPa — 21.9

3. BBR PAV: T_{min}

   Temperature at which S(t) = 300 Mpa — -28.9

   Temperature at which m = 0.300 — -24.7

APPENDIX D - MASTER CURVE DATA

TABLE D1. MEPDG Input values for Dynamic Modulus Testing (Unconfined)

Section-Lift ID	Temp (deg C)	Temp (deg F)	Frequency (Hz)	Shift Factor	Reduced Frequency	E*, (ksi)	E*, (Mpa)
CONTROL-SURFACE	-10.0	14	25	4.035	2.71E+05	2516.5	17356.1
CONTROL-SURFACE	-10.0	14	10	4.035	1.09E+05	2418.3	16679.0
CONTROL-SURFACE	-10.0	14	5	4.035	5.43E+04	2334.7	16102.4
CONTROL-SURFACE	-10.0	14	1	4.035	1.09E+04	2108.1	14539.8
CONTROL-SURFACE	-10.0	14	0.5	4.035	5.43E+03	1996.7	13771.1
CONTROL-SURFACE	-10.0	14	0.1	4.035	1.09E+03	1709.2	11788.0
CONTROL-SURFACE	4.4	40	25	1.984	2.41E+03	1856.1	12801.8
CONTROL-SURFACE	4.4	40	10	1.984	9.63E+02	1686.5	11631.5
CONTROL-SURFACE	4.4	40	5	1.984	4.81E+02	1551.9	10703.6
CONTROL-SURFACE	4.4	40	1	1.984	9.63E+01	1229.4	8479.3
CONTROL-SURFACE	4.4	40	0.5	1.984	4.81E+01	1091.3	7526.5
CONTROL-SURFACE	4.4	40	0.1	1.984	9.63E+00	789.0	5442.0
CONTROL-SURFACE	21.1	70	25	-0.134	1.84E+01	906.1	6249.6
CONTROL-SURFACE	21.1	70	10	-0.134	7.35E+00	742.3	5119.7
CONTROL-SURFACE	21.1	70	5	-0.134	3.68E+00	629.1	4338.8
CONTROL-SURFACE	21.1	70	1	-0.134	7.35E-01	409.1	2821.8
CONTROL-SURFACE	21.1	70	0.5	-0.134	3.68E-01	334.0	2303.5
CONTROL-SURFACE	21.1	70	0.1	-0.134	7.35E-02	202.3	1395.4
CONTROL-SURFACE	37.8	100	25	-2.024	2.37E-01	292.2	2015.5
CONTROL-SURFACE	37.8	100	10	-2.024	9.46E-02	219.3	1512.8
CONTROL-SURFACE	37.8	100	5	-2.024	4.73E-02	175.5	1210.5
CONTROL-SURFACE	37.8	100	1	-2.024	9.46E-03	104.0	717.2
CONTROL-SURFACE	37.8	100	0.5	-2.024	4.73E-03	83.3	574.3
CONTROL-SURFACE	37.8	100	0.1	-2.024	9.46E-04	50.9	350.9
CONTROL-SURFACE	54.4	130	25	-3.722	4.74E-03	83.3	574.7
CONTROL-SURFACE	54.4	130	10	-3.722	1.90E-03	62.6	431.9
CONTROL-SURFACE	54.4	130	5	-3.722	9.48E-04	50.9	351.1
CONTROL-SURFACE	54.4	130	1	-3.722	1.90E-04	32.7	225.6
CONTROL-SURFACE	54.4	130	0.5	-3.722	9.48E-05	27.6	190.1
CONTROL-SURFACE	54.4	130	0.1	-3.722	1.90E-05	19.4	134.0
KRATON-SURFACE	-10.0	14	25	4.320	5.22E+05	2616.6	18046.4
KRATON-SURFACE	-10.0	14	10	4.320	2.09E+05	2545.7	17558.0
KRATON-SURFACE	-10.0	14	5	4.320	1.04E+05	2486.0	17146.1
KRATON-SURFACE	-10.0	14	1	4.320	2.09E+04	2325.3	16037.4
KRATON-SURFACE	-10.0	14	0.5	4.320	1.04E+04	2246.1	15491.2
KRATON-SURFACE	-10.0	14	0.1	4.320	2.09E+03	2038.6	14060.5
KRATON-SURFACE	4.4	40	25	2.124	3.32E+03	2101.7	14495.6
KRATON-SURFACE	4.4	40	10	2.124	1.33E+03	1974.5	13618.4
KRATON-SURFACE	4.4	40	5	2.124	6.64E+02	1871.8	12910.0
KRATON-SURFACE	4.4	40	1	2.124	1.33E+02	1615.1	11139.2
KRATON-SURFACE	4.4	40	0.5	2.124	6.64E+01	1498.6	10335.9
KRATON-SURFACE	4.4	40	0.1	2.124	1.33E+01	1222.5	8431.7

Section-Lift ID	Temp (deg C)	Temp (deg F)	Frequency (Hz)	Shift Factor	Reduced Frequency	E*, (ksi)	E*, (Mpa)
KRATON-SURFACE	21.1	70	25	-0.143	1.80E+01	1274.5	8790.1
KRATON-SURFACE	21.1	70	10	-0.143	7.19E+00	1117.8	7709.6
KRATON-SURFACE	21.1	70	5	-0.143	3.60E+00	1001.9	6910.0
KRATON-SURFACE	21.1	70	1	-0.143	7.19E-01	749.7	5170.9
KRATON-SURFACE	21.1	70	0.5	-0.143	3.60E-01	651.5	4493.2
KRATON-SURFACE	21.1	70	0.1	-0.143	7.19E-02	453.8	3130.1
KRATON-SURFACE	37.8	100	25	-2.167	1.70E-01	554.1	3821.5
KRATON-SURFACE	37.8	100	10	-2.167	6.81E-02	447.9	3089.5
KRATON-SURFACE	37.8	100	5	-2.167	3.41E-02	377.7	2605.1
KRATON-SURFACE	37.8	100	1	-2.167	6.81E-03	247.3	1705.6
KRATON-SURFACE	37.8	100	0.5	-2.167	3.41E-03	204.1	1408.0
KRATON-SURFACE	37.8	100	0.1	-2.167	6.81E-04	129.2	890.9
KRATON-SURFACE	54.4	130	25	-3.985	2.59E-03	189.1	1303.9
KRATON-SURFACE	54.4	130	10	-3.985	1.04E-03	145.7	1004.8
KRATON-SURFACE	54.4	130	5	-3.985	5.18E-04	119.4	823.5
KRATON-SURFACE	54.4	130	1	-3.985	1.04E-04	75.5	520.4
KRATON-SURFACE	54.4	130	0.5	-3.985	5.18E-05	62.2	429.1
KRATON-SURFACE	54.4	130	0.1	-3.985	1.04E-05	40.6	279.9
KRATON-BASE	-10.0	14	25	4.058	2.86E+05	2793.7	19267.9
KRATON-BASE	-10.0	14	10	4.058	1.14E+05	2718.1	18746.5
KRATON-BASE	-10.0	14	5	4.058	5.71E+04	2652.3	18292.6
KRATON-BASE	-10.0	14	1	4.058	1.14E+04	2467.3	17016.9
KRATON-BASE	-10.0	14	0.5	4.058	5.71E+03	2372.6	16364.2
KRATON-BASE	-10.0	14	0.1	4.058	1.14E+03	2116.7	14598.7
KRATON-BASE	4.4	40	25	1.995	2.47E+03	2245.5	15487.3
KRATON-BASE	4.4	40	10	1.995	9.88E+02	2091.0	14422.0
KRATON-BASE	4.4	40	5	1.995	4.94E+02	1964.0	13545.4
KRATON-BASE	4.4	40	1	1.995	9.88E+01	1640.8	11316.5
KRATON-BASE	4.4	40	0.5	1.995	4.94E+01	1493.3	10299.4
KRATON-BASE	4.4	40	0.1	1.995	9.88E+00	1147.7	7915.7
KRATON-BASE	21.1	70	25	-0.134	1.83E+01	1279.9	8827.2
KRATON-BASE	21.1	70	10	-0.134	7.34E+00	1085.3	7485.5
KRATON-BASE	21.1	70	5	-0.134	3.67E+00	944.0	6510.6
KRATON-BASE	21.1	70	1	-0.134	7.34E-01	649.5	4479.3
KRATON-BASE	21.1	70	0.5	-0.134	3.67E-01	541.5	3734.7
KRATON-BASE	21.1	70	0.1	-0.134	7.34E-02	340.6	2349.4
KRATON-BASE	37.8	100	25	-2.035	2.31E-01	476.3	3284.9
KRATON-BASE	37.8	100	10	-2.035	9.22E-02	364.9	2516.7
KRATON-BASE	37.8	100	5	-2.035	4.61E-02	295.4	2037.2
KRATON-BASE	37.8	100	1	-2.035	9.22E-03	177.2	1222.2
KRATON-BASE	37.8	100	0.5	-2.035	4.61E-03	141.8	977.9
KRATON-BASE	37.8	100	0.1	-2.035	9.22E-04	85.5	589.5
KRATON-BASE	54.4	130	25	-3.743	4.52E-03	140.9	971.8
KRATON-BASE	54.4	130	10	-3.743	1.81E-03	105.3	726.3

Section-Lift ID	Temp (deg C)	Temp (deg F)	Frequency (Hz)	Shift Factor	Reduced Frequency	E*, (ksi)	E*, (Mpa)
KRATON-BASE	54.4	130	5	-3.743	9.04E-04	85.0	586.0
KRATON-BASE	54.4	130	1	-3.743	1.81E-04	53.3	367.5
KRATON-BASE	54.4	130	0.5	-3.743	9.04E-05	44.4	305.9
KRATON-BASE	54.4	130	0.1	-3.743	1.81E-05	30.4	209.6
CONTROL-INTERMEDIATE	-10.0	14	25	4.037	2.72E+05	2808.7	19371.7
CONTROL-INTERMEDIATE	-10.0	14	10	4.037	1.09E+05	2737.7	18881.9
CONTROL-INTERMEDIATE	-10.0	14	5	4.037	5.44E+04	2676.4	18459.2
CONTROL-INTERMEDIATE	-10.0	14	1	4.037	1.09E+04	2506.0	17283.7
CONTROL-INTERMEDIATE	-10.0	14	0.5	4.037	5.44E+03	2419.5	16687.1
CONTROL-INTERMEDIATE	-10.0	14	0.1	4.037	1.09E+03	2186.7	15081.6
CONTROL-INTERMEDIATE	4.4	40	25	1.984	2.41E+03	2307.3	15913.5
CONTROL-INTERMEDIATE	4.4	40	10	1.984	9.64E+02	2167.4	14948.4
CONTROL-INTERMEDIATE	4.4	40	5	1.984	4.82E+02	2052.2	14154.0
CONTROL-INTERMEDIATE	4.4	40	1	1.984	9.64E+01	1757.5	12121.2
CONTROL-INTERMEDIATE	4.4	40	0.5	1.984	4.82E+01	1621.4	11182.5
CONTROL-INTERMEDIATE	4.4	40	0.1	1.984	9.64E+00	1295.7	8936.7
CONTROL-INTERMEDIATE	21.1	70	25	-0.134	1.84E+01	1426.8	9840.4
CONTROL-INTERMEDIATE	21.1	70	10	-0.134	7.35E+00	1240.8	8557.6
CONTROL-INTERMEDIATE	21.1	70	5	-0.134	3.68E+00	1102.4	7603.4
CONTROL-INTERMEDIATE	21.1	70	1	-0.134	7.35E-01	802.0	5531.5
CONTROL-INTERMEDIATE	21.1	70	0.5	-0.134	3.68E-01	686.2	4733.1
CONTROL-INTERMEDIATE	21.1	70	0.1	-0.134	7.35E-02	458.6	3163.1
CONTROL-INTERMEDIATE	37.8	100	25	-2.025	2.36E-01	617.7	4260.5
CONTROL-INTERMEDIATE	37.8	100	10	-2.025	9.45E-02	490.1	3380.2

Section-Lift ID	Temp (deg C)	Temp (deg F)	Frequency (Hz)	Shift Factor	Reduced Frequency	E*, (ksi)	E*, (Mpa)
CONTROL-INTERMEDIATE	37.8	100	5	-2.025	4.72E-02	406.9	2806.2
CONTROL-INTERMEDIATE	37.8	100	1	-2.025	9.45E-03	256.7	1770.3
CONTROL-INTERMEDIATE	37.8	100	0.5	-2.025	4.72E-03	208.7	1439.7
CONTROL-INTERMEDIATE	37.8	100	0.1	-2.025	9.45E-04	128.6	886.7
CONTROL-INTERMEDIATE	54.4	130	25	-3.723	4.73E-03	208.8	1440.1
CONTROL-INTERMEDIATE	54.4	130	10	-3.723	1.89E-03	158.4	1092.5
CONTROL-INTERMEDIATE	54.4	130	5	-3.723	9.46E-04	128.6	886.9
CONTROL-INTERMEDIATE	54.4	130	1	-3.723	1.89E-04	80.3	554.0
CONTROL-INTERMEDIATE	54.4	130	0.5	-3.723	9.46E-05	66.3	457.1
CONTROL-INTERMEDIATE	54.4	130	0.1	-3.723	1.89E-05	43.9	302.7
CONTROL-BASE	-10.0	14	25	3.618	1.04E+05	2739.1	18891.4
CONTROL-BASE	-10.0	14	10	3.618	4.15E+04	2649.4	18272.8
CONTROL-BASE	-10.0	14	5	3.618	2.08E+04	2571.4	17734.8
CONTROL-BASE	-10.0	14	1	3.618	4.15E+03	2353.1	16229.2
CONTROL-BASE	-10.0	14	0.5	3.618	2.08E+03	2242.2	15464.7
CONTROL-BASE	-10.0	14	0.1	3.618	4.15E+02	1946.5	13425.2
CONTROL-BASE	4.4	40	25	1.779	1.50E+03	2186.9	15083.1
CONTROL-BASE	4.4	40	10	1.779	6.01E+02	2018.8	13923.8
CONTROL-BASE	4.4	40	5	1.779	3.00E+02	1881.1	12973.7
CONTROL-BASE	4.4	40	1	1.779	6.01E+01	1534.3	10581.9
CONTROL-BASE	4.4	40	0.5	1.779	3.00E+01	1378.3	9506.1
CONTROL-BASE	4.4	40	0.1	1.779	6.01E+00	1020.6	7039.3
CONTROL-BASE	21.1	70	25	-0.120	1.90E+01	1274.7	8791.6
CONTROL-BASE	21.1	70	10	-0.120	7.59E+00	1071.2	7388.3
CONTROL-BASE	21.1	70	5	-0.120	3.79E+00	923.7	6371.0
CONTROL-BASE	21.1	70	1	-0.120	7.59E-01	619.0	4269.0
CONTROL-BASE	21.1	70	0.5	-0.120	3.79E-01	508.8	3509.0
CONTROL-BASE	21.1	70	0.1	-0.120	7.59E-02	307.8	2122.9
CONTROL-BASE	37.8	100	25	-1.815	3.83E-01	510.2	3518.7
CONTROL-BASE	37.8	100	10	-1.815	1.53E-01	386.1	2663.1
CONTROL-BASE	37.8	100	5	-1.815	7.66E-02	308.8	2129.5
CONTROL-BASE	37.8	100	1	-1.815	1.53E-02	178.3	1229.8
CONTROL-BASE	37.8	100	0.5	-1.815	7.66E-03	139.9	964.7

Section-Lift ID	Temp (deg C)	Temp (deg F)	Frequency (Hz)	Shift Factor	Reduced Frequency	E*, (ksi)	E*, (Mpa)
CONTROL-BASE	37.8	100	0.1	-1.815	1.53E-03	80.1	552.4
CONTROL-BASE	54.4	130	25	-3.337	1.15E-02	161.3	1112.5
CONTROL-BASE	54.4	130	10	-3.337	4.60E-03	117.0	806.9
CONTROL-BASE	54.4	130	5	-3.337	2.30E-03	92.0	634.5
CONTROL-BASE	54.4	130	1	-3.337	4.60E-04	54.0	372.4
CONTROL-BASE	54.4	130	0.5	-3.337	2.30E-04	43.6	301.0
CONTROL-BASE	54.4	130	0.1	-3.337	4.60E-05	28.0	193.0

TABLE D2 Confined Master Curve Data

Section-Lift ID	Temp (deg C)	Temp (deg F)	Frequency (Hz)	Shift Factor	Reduced Frequency	E*, (ksi)	E*, (Mpa)
CONTROL-SURFACE	-10.0	14	25	3.882	1.90E+05	2574.6	17756.8
CONTROL-SURFACE	-10.0	14	10	3.882	7.62E+04	2472.4	17051.9
CONTROL-SURFACE	-10.0	14	5	3.882	3.81E+04	2383.8	16441.4
CONTROL-SURFACE	-10.0	14	1	3.882	7.62E+03	2139.5	14756.2
CONTROL-SURFACE	-10.0	14	0.5	3.882	3.81E+03	2018.0	13918.0
CONTROL-SURFACE	-10.0	14	0.1	3.882	7.62E+02	1704.3	11754.8
CONTROL-SURFACE	4.4	40	25	1.908	2.02E+03	1899.4	13099.9
CONTROL-SURFACE	4.4	40	10	1.908	8.09E+02	1716.8	11840.5
CONTROL-SURFACE	4.4	40	5	1.908	4.05E+02	1572.5	10845.8
CONTROL-SURFACE	4.4	40	1	1.908	8.09E+01	1232.3	8499.4
CONTROL-SURFACE	4.4	40	0.5	1.908	4.05E+01	1090.3	7519.9
CONTROL-SURFACE	4.4	40	0.1	1.908	8.09E+00	790.4	5451.7
CONTROL-SURFACE	21.1	70	25	-0.129	1.86E+01	939.1	6477.2
CONTROL-SURFACE	21.1	70	10	-0.129	7.44E+00	776.2	5353.8
CONTROL-SURFACE	21.1	70	5	-0.129	3.72E+00	666.2	4595.0
CONTROL-SURFACE	21.1	70	1	-0.129	7.44E-01	458.8	3164.1
CONTROL-SURFACE	21.1	70	0.5	-0.129	3.72E-01	389.6	2687.1
CONTROL-SURFACE	21.1	70	0.1	-0.129	7.44E-02	269.3	1857.5
CONTROL-SURFACE	37.8	100	25	-1.947	2.83E-01	365.3	2519.4
CONTROL-SURFACE	37.8	100	10	-1.947	1.13E-01	295.7	2039.8
CONTROL-SURFACE	37.8	100	5	-1.947	5.65E-02	253.6	1748.9
CONTROL-SURFACE	37.8	100	1	-1.947	1.13E-02	182.8	1260.8
CONTROL-SURFACE	37.8	100	0.5	-1.947	5.65E-03	161.3	1112.3
CONTROL-SURFACE	37.8	100	0.1	-1.947	1.13E-03	125.5	865.8
CONTROL-SURFACE	54.4	130	25	-3.580	6.57E-03	165.6	1142.1
CONTROL-SURFACE	54.4	130	10	-3.580	2.63E-03	142.2	980.5
CONTROL-SURFACE	54.4	130	5	-3.580	1.31E-03	128.2	884.3
CONTROL-SURFACE	54.4	130	1	-3.580	2.63E-04	105.0	724.0
CONTROL-SURFACE	54.4	130	0.5	-3.580	1.31E-04	97.8	674.8
CONTROL-SURFACE	54.4	130	0.1	-3.580	2.63E-05	85.8	591.7
KRATON-SURFACE	-10.0	14	25	4.299	4.97E+05	2677.8	18469.1
KRATON-SURFACE	-10.0	14	10	4.299	1.99E+05	2607.2	17982.0
KRATON-SURFACE	-10.0	14	5	4.299	9.95E+04	2546.7	17564.8
KRATON-SURFACE	-10.0	14	1	4.299	1.99E+04	2380.7	16419.8
KRATON-SURFACE	-10.0	14	0.5	4.299	9.95E+03	2297.6	15846.8
KRATON-SURFACE	-10.0	14	0.1	4.299	1.99E+03	2077.7	14329.6
KRATON-SURFACE	4.4	40	25	2.113	3.24E+03	2148.4	14817.2
KRATON-SURFACE	4.4	40	10	2.113	1.30E+03	2013.1	13884.7
KRATON-SURFACE	4.4	40	5	2.113	6.49E+02	1903.7	13130.0
KRATON-SURFACE	4.4	40	1	2.113	1.30E+02	1631.1	11250.0
KRATON-SURFACE	4.4	40	0.5	2.113	6.49E+01	1508.6	10405.1
KRATON-SURFACE	4.4	40	0.1	2.113	1.30E+01	1223.4	8437.9
KRATON-SURFACE	21.1	70	25	-0.142	1.80E+01	1281.0	8835.0

Section-Lift ID	Temp (deg C)	Temp (deg F)	Frequency (Hz)	Shift Factor	Reduced Frequency	E*, (ksi)	E*, (Mpa)
KRATON-SURFACE	21.1	70	10	-0.142	7.20E+00	1122.1	7738.9
KRATON-SURFACE	21.1	70	5	-0.142	3.60E+00	1006.7	6943.0
KRATON-SURFACE	21.1	70	1	-0.142	7.20E-01	763.2	5263.7
KRATON-SURFACE	21.1	70	0.5	-0.142	3.60E-01	671.3	4629.9
KRATON-SURFACE	21.1	70	0.1	-0.142	7.20E-02	491.6	3390.8
KRATON-SURFACE	37.8	100	25	-2.156	1.75E-01	584.5	4031.5
KRATON-SURFACE	37.8	100	10	-2.156	6.98E-02	488.6	3369.9
KRATON-SURFACE	37.8	100	5	-2.156	3.49E-02	426.0	2938.2
KRATON-SURFACE	37.8	100	1	-2.156	6.98E-03	310.8	2143.9
KRATON-SURFACE	37.8	100	0.5	-2.156	3.49E-03	272.6	1880.1
KRATON-SURFACE	37.8	100	0.1	-2.156	6.98E-04	204.7	1411.7
KRATON-SURFACE	54.4	130	25	-3.965	2.71E-03	260.1	1794.0
KRATON-SURFACE	54.4	130	10	-3.965	1.08E-03	220.7	1522.3
KRATON-SURFACE	54.4	130	5	-3.965	5.42E-04	196.2	1353.5
KRATON-SURFACE	54.4	130	1	-3.965	1.08E-04	153.3	1057.5
KRATON-SURFACE	54.4	130	0.5	-3.965	5.42E-05	139.5	962.3
KRATON-SURFACE	54.4	130	0.1	-3.965	1.08E-05	115.3	795.4
KRATON-BASE	-10.0	14	25	4.100	3.15E+05	2863.2	19747.4
KRATON-BASE	-10.0	14	10	4.100	1.26E+05	2789.8	19241.5
KRATON-BASE	-10.0	14	5	4.100	6.29E+04	2724.4	18790.0
KRATON-BASE	-10.0	14	1	4.100	1.26E+04	2534.3	17478.8
KRATON-BASE	-10.0	14	0.5	4.100	6.29E+03	2434.4	16790.0
KRATON-BASE	-10.0	14	0.1	4.100	1.26E+03	2159.1	14891.4
KRATON-BASE	4.4	40	25	2.015	2.59E+03	2289.9	15793.8
KRATON-BASE	4.4	40	10	2.015	1.04E+03	2121.9	14634.6
KRATON-BASE	4.4	40	5	2.015	5.18E+02	1983.1	13677.3
KRATON-BASE	4.4	40	1	2.015	1.04E+02	1632.3	11258.0
KRATON-BASE	4.4	40	0.5	2.015	5.18E+01	1475.0	10173.2
KRATON-BASE	4.4	40	0.1	2.015	1.04E+01	1118.3	7713.2
KRATON-BASE	21.1	70	25	-0.136	1.83E+01	1241.3	8561.3
KRATON-BASE	21.1	70	10	-0.136	7.31E+00	1045.8	7213.0
KRATON-BASE	21.1	70	5	-0.136	3.66E+00	908.7	6267.2
KRATON-BASE	21.1	70	1	-0.136	7.31E-01	638.0	4400.0
KRATON-BASE	21.1	70	0.5	-0.136	3.66E-01	544.0	3752.2
KRATON-BASE	21.1	70	0.1	-0.136	7.31E-02	376.3	2595.6
KRATON-BASE	37.8	100	25	-2.056	2.20E-01	483.6	3335.3
KRATON-BASE	37.8	100	10	-2.056	8.79E-02	392.2	2704.7
KRATON-BASE	37.8	100	5	-2.056	4.39E-02	336.2	2318.9
KRATON-BASE	37.8	100	1	-2.056	8.79E-03	241.7	1667.2
KRATON-BASE	37.8	100	0.5	-2.056	4.39E-03	212.9	1468.7
KRATON-BASE	37.8	100	0.1	-2.056	8.79E-04	165.3	1140.0
KRATON-BASE	54.4	130	25	-3.781	4.14E-03	210.7	1453.3
KRATON-BASE	54.4	130	10	-3.781	1.65E-03	181.3	1250.7
KRATON-BASE	54.4	130	5	-3.781	8.27E-04	163.9	1130.6

Section-Lift ID	Temp (deg C)	Temp (deg F)	Frequency (Hz)	Shift Factor	Reduced Frequency	E*, (ksi)	E*, (Mpa)
KRATON-BASE	54.4	130	1	-3.781	1.65E-04	135.0	931.3
KRATON-BASE	54.4	130	0.5	-3.781	8.27E-05	126.2	870.7
KRATON-BASE	54.4	130	0.1	-3.781	1.65E-05	111.5	768.8
CONTROL-INTERMEDIATE	-10.0	14	25	4.116	3.27E+05	2878.7	19854.1
CONTROL-INTERMEDIATE	-10.0	14	10	4.116	1.31E+05	2810.0	19380.7
CONTROL-INTERMEDIATE	-10.0	14	5	4.116	6.54E+04	2749.4	18962.7
CONTROL-INTERMEDIATE	-10.0	14	1	4.116	1.31E+04	2575.7	17764.9
CONTROL-INTERMEDIATE	-10.0	14	0.5	4.116	6.54E+03	2485.4	17141.9
CONTROL-INTERMEDIATE	-10.0	14	0.1	4.116	1.31E+03	2237.7	15433.4
CONTROL-INTERMEDIATE	4.4	40	25	2.023	2.64E+03	2352.3	16223.6
CONTROL-INTERMEDIATE	4.4	40	10	2.023	1.06E+03	2200.8	15178.9
CONTROL-INTERMEDIATE	4.4	40	5	2.023	5.28E+02	2075.5	14315.0
CONTROL-INTERMEDIATE	4.4	40	1	2.023	1.06E+02	1756.0	12111.3
CONTROL-INTERMEDIATE	4.4	40	0.5	2.023	5.28E+01	1610.3	11106.5
CONTROL-INTERMEDIATE	4.4	40	0.1	2.023	1.06E+01	1270.7	8764.1
CONTROL-INTERMEDIATE	21.1	70	25	-0.136	1.83E+01	1385.3	9554.3
CONTROL-INTERMEDIATE	21.1	70	10	-0.136	7.31E+00	1195.4	8245.0
CONTROL-INTERMEDIATE	21.1	70	5	-0.136	3.65E+00	1058.5	7300.8
CONTROL-INTERMEDIATE	21.1	70	1	-0.136	7.31E-01	775.8	5350.8
CONTROL-INTERMEDIATE	21.1	70	0.5	-0.136	3.65E-01	672.5	4638.6
CONTROL-INTERMEDIATE	21.1	70	0.1	-0.136	7.31E-02	478.8	3302.2
CONTROL-INTERMEDIATE	37.8	100	25	-2.065	2.15E-01	602.0	4151.7
CONTROL-INTERMEDIATE	37.8	100	10	-2.065	8.62E-02	495.8	3419.5
CONTROL-INTERMEDIATE	37.8	100	5	-2.065	4.31E-02	428.6	2955.9

Section-Lift ID	Temp (deg C)	Temp (deg F)	Frequency (Hz)	Shift Factor	Reduced Frequency	E*, (ksi)	E*, (Mpa)
CONTROL-INTERMEDIATE	37.8	100	1	-2.065	8.62E-03	310.1	2138.7
CONTROL-INTERMEDIATE	37.8	100	0.5	-2.065	4.31E-03	272.5	1879.5
CONTROL-INTERMEDIATE	37.8	100	0.1	-2.065	8.62E-04	208.4	1437.5
CONTROL-INTERMEDIATE	54.4	130	25	-3.797	3.99E-03	268.8	1853.9
CONTROL-INTERMEDIATE	54.4	130	10	-3.797	1.60E-03	229.7	1584.1
CONTROL-INTERMEDIATE	54.4	130	5	-3.797	7.99E-04	206.0	1421.0
CONTROL-INTERMEDIATE	54.4	130	1	-3.797	1.60E-04	165.9	1144.4
CONTROL-INTERMEDIATE	54.4	130	0.5	-3.797	7.99E-05	153.5	1058.4
CONTROL-INTERMEDIATE	54.4	130	0.1	-3.797	1.60E-05	132.2	911.7
CONTROL-BASE	-10.0	14	25	3.651	1.12E+05	2805.8	19351.5
CONTROL-BASE	-10.0	14	10	3.651	4.47E+04	2716.7	18736.9
CONTROL-BASE	-10.0	14	5	3.651	2.24E+04	2637.5	18190.7
CONTROL-BASE	-10.0	14	1	3.651	4.47E+03	2409.9	16620.9
CONTROL-BASE	-10.0	14	0.5	3.651	2.24E+03	2292.0	15808.2
CONTROL-BASE	-10.0	14	0.1	3.651	4.47E+02	1974.6	13618.7
CONTROL-BASE	4.4	40	25	1.794	1.56E+03	2225.8	15351.3
CONTROL-BASE	4.4	40	10	1.794	6.23E+02	2044.5	14100.8
CONTROL-BASE	4.4	40	5	1.794	3.11E+02	1895.9	13075.9
CONTROL-BASE	4.4	40	1	1.794	6.23E+01	1526.2	10525.9
CONTROL-BASE	4.4	40	0.5	1.794	3.11E+01	1363.7	9405.3
CONTROL-BASE	4.4	40	0.1	1.794	6.23E+00	1004.7	6929.6
CONTROL-BASE	21.1	70	25	-0.121	1.89E+01	1248.7	8612.0
CONTROL-BASE	21.1	70	10	-0.121	7.57E+00	1045.8	7213.2
CONTROL-BASE	21.1	70	5	-0.121	3.78E+00	903.7	6232.7
CONTROL-BASE	21.1	70	1	-0.121	7.57E-01	624.4	4306.3
CONTROL-BASE	21.1	70	0.5	-0.121	3.78E-01	528.3	3643.5
CONTROL-BASE	21.1	70	0.1	-0.121	7.57E-02	358.6	2473.4
CONTROL-BASE	37.8	100	25	-1.831	3.69E-01	525.0	3621.1
CONTROL-BASE	37.8	100	10	-1.831	1.48E-01	420.5	2900.2
CONTROL-BASE	37.8	100	5	-1.831	7.38E-02	356.5	2458.7
CONTROL-BASE	37.8	100	1	-1.831	1.48E-02	248.8	1716.2
CONTROL-BASE	37.8	100	0.5	-1.831	7.38E-03	216.3	1492.2
CONTROL-BASE	37.8	100	0.1	-1.831	1.48E-03	163.2	1125.7
CONTROL-BASE	54.4	130	25	-3.367	1.07E-02	233.1	1607.4
CONTROL-BASE	54.4	130	10	-3.367	4.30E-03	195.4	1347.9

Section-Lift ID	Temp (deg C)	Temp (deg F)	Frequency (Hz)	Shift Factor	Reduced Frequency	E*, (ksi)	E*, (Mpa)
CONTROL-BASE	54.4	130	5	-3.367	2.15E-03	173.3	1195.4
CONTROL-BASE	54.4	130	1	-3.367	4.30E-04	137.2	946.1
CONTROL-BASE	54.4	130	0.5	-3.367	2.15E-04	126.4	871.6
CONTROL-BASE	54.4	130	0.1	-3.367	4.30E-05	108.5	748.2